Determination of free indium concentration and lability degree of indium complexes using electroanalytical techniques

Marjan Heidarkhan Tehrani

Universitat de Lleida

TESI DOCTORAL

Determination of free indium concentration and lability degree of indium complexes using electroanalytical techniques

Marjan Heidarkhan Tehrani

Memòria presentada per optar al grau de Doctor per la Universitat de Lleida
Programa de Doctorat en *Electrochemisty. Science and Technology*.

Directors
Josep Galceran
Encarna Companys

Tutor
Josep Galceran

2018

Dedication

I would like to dedicate this dissertation to my loving parents, grandparents, and my brother, Ashkan, for their undeniable support and encouragement throughout my studies.

Acknowledgements

There are many people whom I owe thanks for their help during these four years of my PhD studies at the University of Lleida (UdL).

I would like to express my appreciations:

Foremost to my supervisors, Drs, Josep Galceran and Encarna Companys for all of their guidance, assistance and kindnesses. It is through their strength that I have accomplished this undertaking.

To Dr Jaume Puy, Vice Rector of Research at the University of Lleida, not only for his advices on my research, but for his support during these years.

To Drs, Jose Salvador the Head of Chemistry Department, Calin David, Carlos Rey, Dolors Morlans, Gemma Villorbina, the secretary of the department of Chemistry , Olga Raich, and to the people in the Organic Chemistry Laboratory for their assistance.

To my dear friend, Dr Angela Dago, for her valuable helps in some parts of the project. She was always there when I needed her to give me a hand. I have many great memories with her which will always remain in my mind.

To all of my friends, Alexandra, Martin, Federico, Pepita, Antonio, Merche, Paulo, Nancy, Erika, Silvia, Olalla, Holly, Mireia, Sara, David, Romeral, Maria, Mariluz, Mauri, Abel, Adriana, Laura, Tania, Catherin, Bea, Mary, Jordi, Nuria, Karla, Francesco, Judit, Harry and Esther, without you, I would not have had as much fun, nor would I have been able to carry on!

And finally thanks to the University of Lleida (UdL), specially to the department of doctorate, the Spanish Ministry MINECO, the center for research in Agrotechnology (AGROTECNICO) and to the Generalitat de Catalonia for providing me a PhD grant (AGAUR) during all these years.

Abstract

Indium is a trivalent amalgamating element and one of the rare metals in the earth crust. It has a vast application interest in the industry (e.g. alkali batteries, solar cells, electronic displays, etc.). Such a high applicability of indium implies that its eventual leakage to the environment is unavoidable and various ecotoxicological and health problems (e.g. lung, liver and kidney diseases, etc.) could appear.

Hence, there is a strong need to find proper techniques in order to determine free concentration of indium and parameters indicating the availability of indium complexes in different media.

In this thesis, we have proposed that the electroanalytical techniques Absence of Gradients and Nernstian Equilibrium Stripping (AGNES) and Accumulation Under Diffusion Limited Conditions (ADLC) could be proper choices. Free concentration of indium from pH 3 to around 6 has been measured. A new calibration for indium has been implemented and speciation measurements in solutions with nitrilotriacetic acid and oxalate ligands have been carried out successfully. ADLC has been applied to calculate the lability degree of indium oxalate and indium hydroxide compounds. This information is a guideline for adequate deposition times in AGNES experiments. AGNES has been successfully used to determine even picomolar concentration of free indium in precipitated solutions. The dissolution of In_2O_3 nanoparticles in synthetic solutions including seawater has been investigated. Results in background electrolyte solution from pH 2 to 4, have revealed that AGNES measurements at each pH have been significantly lower than the predictions of NIST 46.7 expectation assuming that solubility was ruled by $In(OH)_3$, consistent with the less hydrated phases exhibiting lower solubilities.

Resumen

El indio es un elemento que forma amalgamas y uno de los metales raros en la corteza terrestre. Tiene un gran interés aplicativo en la industria (por ejemplo baterías alcalinas, paneles solares, pantallas electrónicas, etc.). Tan alta aplicabilidad del indio implica que alguna filtración final al medio ambiente es inevitable y podrían aparecer diversos problemas ecotoxicológicos y de salud (por ejemplo, enfermedades pulmonares, hepáticas, renales, etc.).

Por lo tanto, es muy necesario encontrar técnicas adecuadas para determinar concentraciones libres de indio y parámetros que indiquen la disponibilidad de complejos de este elemento en diferentes medios.

En esta tesis, proponemos que las técnicas electroanalíticas *Absence of Gradients and Nernstian Equilibrium Stripping* (AGNES) y *Accumulation under Diffusion Limited Conditions* (ADLC) podrían ser elecciones adecuadas. Se han medido concentraciones libres de indio en sistemas con pH desde 3 hasta 6. Se ha implementado una nueva calibración para indio y las medidas de especiación en soluciones con ligandos ácido nitrilotriacético y oxalato han permitido elegir entre conjuntos alternativos de constantes de estabilidad. Se ha aplicado ADLC para calcular el grado de labilidad de oxalatos e hidróxidos de indio. Esta información es una guía para encontrar tiempos de deposición adecuados en los experimentos AGNES, llegando incluso a determinar en -soluciones precipitadas- concentraciones picomolares de indio libre. Se ha investigado la disolución de nanopartículas de In_2O_3 en disoluciones sintéticas, incluida el agua de mar. Los resultados en disolución con electrolito de fondo con pH de 2 hasta 4 han revelado que las medidas de AGNES a cada pH son significativamente más bajas que las predicciones de NIST 46.7 si se supone que la solubilidad se rige por $In(OH)_3$. Esto es consistente con el hecho que fases menos hidratadas exhiben solubilidades menores.

Resum

L'indi és un element que forma amalgames i un dels metalls rars en l'escorça terresre. Té un gran interès aplicat a la indústria (per exemple bateries alcalines, panells solars, pantalles electròniques, etc.). Unes aplicacions tan vastes impliquen que l'indi arribarà finalment al medi ambient i podrien sorgir diversos problemes ecotoxicològics i de salut (per exemple, malalties pulmonars, hepàtiques, renals, etc.).

Per tant, cal trobar tècniques escaients per a determinar concentracions lliures d'indi (III) i paràmetres que indiquin la disponibilitat dels complexos d'indi en diferents medis. En aquesta tesi, proposem que les tècniques electroanalítiques *Absence of Gradients and Nernstian Equilibrium Stripping* (AGNES) i *Accumulation under diffusion limited conditions* (ADLC) podrien ser bones opcions. S'han mesurat concentracions lliures d'indi en sistemes amb pH des de 3 fins a 6. S'ha implementat un nou calibratge per a indi i les mesures en dissolucions amb els lligands àcid nitrilotriacètic i oxalat han servit per a triar entre conjunts alternatius de constants d'estabilitat. S'ha aplicat ADLC per a calcular el grau de labilitat de l'oxalat d'indi. Aquesta informació fou una orientació per a trobar temps de deposició adequats en experiments d'AGNES que fins i tot arribaren -en dissolucions precipitades- a concentracions picomolars d'indi lliure. S'ha investigat la dissolució de nanopartícules d'In_2O_3 en medis sintètics, inclosa l'aigua de mar. Els resultats amb electròlit de fons en dissolucions amb pH des de 2 fins a 4, han revelat que les mesures d'AGNES a cada pH són significativament menors que les predites per NIST 46.7 suposant que la solubilitat fos regida pel $In(OH)_3$. Això és consistent amb el fet que fases menys hidratades presenten menors solubilitats.

Table of Contents

Chapter 5. Dissolution of indium (III) oxide nanoparticles

List of figures

List of tables

List of symbols and abbreviations

Latin symbols

Symbol	Description	Units
A	Electrode surface area	m^2
a_i	Activity of ion *i*	none
c^*_{M}	Bulk concentration of metal ion M	mol L^{-1} or mol m^{-3}
$c^*_{M^0}$	Reduced metal concentration in the amalgam	mol L^{-1} or mol m^{-3}
$c_{T,i}$	Total concentration of species *i* in the solution	mol L^{-1} or mol m^{-3}
$D_{M^{n+}}$	Diffusion coefficient for the metal ion in solution	m^2s^{-1}
D_{M^0}	Diffusion coefficient of the reduced metal inside the amalgam	m^2s^{-1}
E	Potential	V
E_{calib}	**Potential** used in the calibration	V
$E^{0'}$	Formal standard potential of the redox couple	V
E_1	Deposition potential	V
$E_{1,a}$	The potential applied in the first sub-stage of AGNES 2P	V
$E_{1,b}$	The potential applied in the second sub-stage of AGNES 2P	V
E_2	Stripping potential	V
E_{const}	Constant potential	V
E_i	Initial potential	V
E_J	Liquid junction potential	V
E_M	Membrane potential	V
E_b	Base potential	V
E_{peak}	DPP peak potential	V
E_d	Potential applied during the deposition period	V
E_{pa}	Potential of the anodic peak	V
E_{pc}	Potential of the cathodic peak	V
F	Faraday constant	C mol^{-1}
I	Current	A

Symbol	Description	Units
I_{∞}	Residual current by the end of the second stage in AGNES-I or AGNES-Q	A
I_{l}	Current under diffusion limited conditions	A
I_{s}	Constant oxidizing current	A
I_{ox}	Current due to oxidants	A
I_{cap}	Capacitive current	A
I_j	Faradaic intensity currents	A
J_i	Flux of specie *i*	mol m^{-2} s^{-1}
J_{labile}	Flux of system if all complexes were fully labile	mol m^{-2} s^{-1}
J_{free}	Flux of the free metal	mol m^{-2} s^{-1}
K'	Conditional stability constant	none
K_{sp}	Solubility product	none
L	Free macromolecular site, ligand	none
M	Metal	none
M^{n+}	Free metal ion	none
M^{0}	Reduced metal inside the amalgam	none
$\left[\mathrm{M}^{n+}\right]$	Free metal ion concentration	mol L^{-1} or mol m^{-3}
ML	Complexed metal in solution	none
$\left[\mathrm{ML}\right]$	Complexed metal concentration	mol L^{-1}
n	Number of electrons involved in an electrode reaction	none
Q	Charge	C
R	Gas constant	J K^{-1} mol^{-1}
R	Reference solution	none
r_0	Radius of the spherical electrode	m
T	Temperature	K
t_1	Deposition time in AGNES 1P	s
t_2	Stripping time in AGNES 1P or 2P	s
$t_{1,\mathrm{a}}$	Duration of the first sub-stage in AGNES 2P	s
$t_{1,\mathrm{b}}$	Duration of the second sub-stage in AGNES 2P	s
t_{d}	Deposition period	s

Symbol	Description	Units
t_p	Pulse period	s
V_{Hg}	Volume of the mercury drop	cm^3
v	Linear potential scan rate	V/s
Y	Concentration gain (in general or aimed by the end of the first stage of AGNES, Y_1)	none
Y_{calib}	Concentration gain applied in calibration	none
Y_1	Concentration gain applied in AGNES 1P during the deposition stage	none
Y_2	Concentration gain applied in AGNES-I or AGNES-Q during the stripping stage	none
$Y_{1,a}$	Concentration gain in the first sub-stage of AGNES 2P	none
$Y_{1,b}$	Concentration gain in the second sub-stage of AGNES 2P	none
z_i	Charge of specie *i*	none

Greek symbols

Greek symbols	Description	Unit
α	1-Index to denote the test solution 2- Index to indicate the conditions of the experiments for ADLC	none
β	Index to denote the internal filling solution	none
γ_i	Activity coefficient of the specie *i*	none
δ	Diffusion layer thickness	m
ε	Normalized diffusion coefficient	none
η_Q	Proportionality factor between charge and amalgamated metal concentration at the electrode surface	C L mol^{-1}
η	Proportionality factor between faradaic current and amalgamated metal concentration at the electrode surface	A L mol^{-1}
μ	Ionic strength	mol L^{-1}
ξ	Lability degree	none
τ	Transition time in SCP	s
τ^*_M	Limiting transition time in absence of Ligand in SCP	A
τ^*_{M+L}	Limiting transition time in presence of Ligand in SCP	A

Abbreviations and acronyms

Abbreviation	Description
AAS	Atomic Absorption Spectrometry
AdSV	Adsorptive Stripping Voltammetry
ADLC	Accumulation under Diffusion Limited Conditions
AE	Auxiliary Electrode
AGNES	Absence of Gradients and Nernstian Equilibrium Stripping
AGNES-1P	AGNES one pulse: only one potential pulse in the deposition stage
AGNES-2P	AGNES two pulses: two potential pulses in the deposition stage
AGNES-I	In this variant of AGNES, In^0 is reoxidized under diffusion limited conditions, then the current is measured
AGNES-Q	In this variant of AGNES, the stripped charge is measured during a stripping time (t_2) at constant re-oxidation potential (E_2)
AGNES-SCP	In this variant of AGNES, during the transition time τ, a constant oxidizing current I_s is applied
AGNES-LSV	In this version of AGNES, the stripping current is recorded when the potential is being scanned at a constant rate
ASV	Anodic Stripping Voltammetry
BiFE	Bismuth-Film Electrode
BLM	Biotic Ligand Model
CV	Cyclic Voltammetry
CPE	Cloud Point Extraction
DPP	Differential Pulse Polarography
DPV	Differential Pulse Voltammetry
DMT	Donnan Membrane Technique
DLLE	Dispersive Liquid Liquid Extraction
DLL-SFODME	Dispersive Liquid-Liquid-Solidified Floating Organic Drop Micro Extraction
EAAS	Electrothermal Atomic Absorption Spectrometry
EDTA	Ethylenediaminetetraacetic acid
FAAS	Flame Atomic Absorption Spectrometry
FIAM	Free Ion Activity Model
FIP	Flow Injection Potentiometry
FO-LADS	Fiber Optic linear Array Detection Spectrometry
GC	Gas Chromatography
GFAAS	Graphite Furnace Atomic Absorption Spectroscopy
GPES	General Purpose Electrochemical System: software to control the Autolab potentiostat
HMDE	Hanging Mercury Drop Electrode
ICP	Inductively Coupled Plasma
ICP-MS	Inductively Coupled Plasma-Mass Spectrometry
ICP-OES	Inductively Coupled Plasma Optical Emission Spectrometry
ISE	Ion Selective Electrode

Abbreviation	Description
ITO	Indium Tin Oxide
LCD	Liquid Crystal Display
LSV	Linear Stripping Voltammetry
LLME	Liquid Liquid Micro Extraction
MS	Mass Spectrometry
MES	2-(N-morpholino)ethanesulfonic acid
MDE	Mercury Drop Electrode
MFE	Mercury Film Electrode
NPP	Normal Pulse Polarography
NOVA	Software package to control the Autolab potentiostat
NIST 46.7	Database of stability constants (from the National Institute of Standards and Technology) used by default in the speciation program VMINTEQ 3.1
NTA	Nitrilotriacetic Acid
NP	Nanoparticle
OES	Optical Emission Spectrometry
PVC	Polyvinyl chloride
PDCA	Pyridinedicarboxylic acid
PGSTAT	Potentiostatic mode
RDE	Rotating Disk Electrode
RT	Resin titration technique
RES	Reticuloendothelial system
SWASV	Square Wave Anodic Stripping Voltammetry
SWV	Square Wave Voltammetry
SMDE	Static Mercury Drop Electrode
SCE	Saturated Calomel Electrode
SCP	Stripping Chronopotentiometry
SSCP	Scanned Stripping Chronopotentiometry
TEM	Transmission Electron Microscopy
UME	Ultra Microelectrode
VMINTEQ	Speciation software Visual MINTEQ
WE	Working Electrode

Chapter 1: Introduction

1.1. Chemical behavior of indium

Indium has the atomic number 49, and it is placed under Ga and above Tl in the periodic table, with the configuration [Kr] $4d^{10}$ $5s^2$ $5p^1$. In its neutral state, its orbitals d are completely full, so, when indium donates its three electrons to be reduced to In^{3+}, one comes from the orbital p and two from the orbital s.[1] Some other times, if it donates only one electron from orbital p, it will become In^+. Many researchers have devoted their attention to the reduction and oxidation of indium ions and indium metal.[2]

1.1.1. Indium (0)

Main group metals do not usually form complexes with neutral molecules such as CO, PF_3 and C_2H_6, but, in contrast, p-block metals (metals whose orbital d is fully occupied) such as indium have such a tendency.[3] For instance, let us consider $In(CO)_2$ which is the main product of some indium experiments.[3] The structure is shown in figure 1-1. Based on the IR-spectrum and on Density Functional Theory calculations, it is seen that there is a tight angle C–In– C (almost 60 degrees) and In– C≡ O arms are in a special position (bent outward), so that two carbon atoms are getting close to each other. Such a special geometry provides optimum overlap between the vacant np orbital of indium with π -orbitals of carbon-oxygen bond.

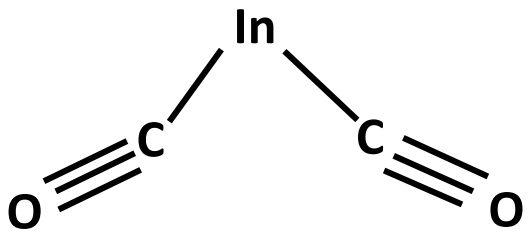

Figure 1-1: Structure of $In(CO)_2$. Adapted from [3]

1.1.2. Indium (I)

In the group 13, it is very uncommon to have +1 oxidation state except for thallium. Hence we can understand that indium (I) compounds are not very long lasting and accordingly are not very usual in nature.[3]

As we said previously, the configuration of indium is [Kr] $4d^{10}$ $5s^2$ $5p^1$, so in case of In^+ the resulting structure will be [Kr] $4d^{10}$ $5s^2$. The high energy of the two electrons that are in orbital s makes such compounds to be ready for oxidization. Such an oxidation

could be done by H^+ (aq), or, in the absence of oxidizing agent, could follow from the disproportionation of indium (0).[3]

Possible explanations of the extremely low abundance of In^+ in the environment could be: the extremely low solubility of indium (I) halide complexes in aqueous solutions and the oxidation or disproportionation of *in-situ* generated indium (I).[4]

1.1.3. Indium (II)

In general, it has been indicated that it is very rare to have even electron oxidation states such as 2+ in group 13,[3] which means that indium (II) is not very common in the nature. It has been reported that there are experimental evidences that demonstrate that mononuclear indium (II) species are intermediates or disproportionation products of indium (I) compounds.[3,5] The standard reduction potential for In(II)/In(I) is around -0.23V, while for In(III)/In(II) this value is almost -0.65 V.[3]

Many years ago, the equilibrium reaction between In^{3+}(aq) and In^0(s) was studied and it was indicated that probably both In^+ and In^{2+} exists in the equilibrium.[2] However some years later, the results of another investigation turned to reject the existence of In^{2+} which was indicated previously.[2] Then, other researchers such as Clark *et al.*[6] and Biederman *et al.*[7] tried to shed light on the electrochemical reactions of indium metal and its ions in the solution. Both of them were only able to identify In^+ during their experiments. So, any evidence for the existence of In^{2+} still remained uncertain.

Further investigations revealed that, although the exact nature of In^{2+} is unknown,[3,8] indium with such a oxidation state (In^{2+}) is one of the species of indium and exists in the electron transfer process. Polarographic studies demonstrated that the process of reduction proceeds in a succession of one electron reduction steps.[2,9,10] For instance, Lovrecek *et al.* [9] indicated that, in indium sulfate solution at pH=2.5, when the current density was lower than 2.5×10^{-3} A cm^{-2}, instead of the direct reaction $In^{3+} + 3e^- \rightleftharpoons In^0$ what happened was in fact

$$In^{3+} \underset{-e}{\overset{+e}{\rightleftharpoons}} In^{2+} \underset{-e}{\overset{+e}{\rightleftharpoons}} In^{+} \underset{-e}{\overset{+e}{\rightleftharpoons}} In^{0} \qquad (1\text{-}1)$$

It was also indicated that at lower current densities (<2.5×10^{-3} A cm^{-2}), the reaction below was the rate determining step for both anodic and cathodic polarization:

$$In^{3+} \underset{-e}{\overset{+e}{\rightleftharpoons}} In^{2+} \qquad (1\text{-}2)$$

1.1.4. In^{3+}

Since In^{+} and In^{2+} are not very common in the nature, most works in the literature devoted attention to study the chemical affinity of In^{3+}. For instance, some reports have focused on the hydrolysis of In^{3+} [7,11,12] or on studying precipitation of indium hydroxide.[13] Also, in some other cases, they have concentrated not only on studying the hydrolysis of In^{3+}, but also on the hydrolysis of other metal ions to give a more complete view about the process of hydrolysis.[14] A relatively recent investigation focused on comparing the chemistry of In^{3+} with that of its neighbors in the periodic table (Al^{3+} and Ga^{3+}). Interestingly, it was demonstrated that although $InCl_3$ complexes were more stable than those of Al^{3+} and Ga^{3+}, indium's mononuclear hydroxide complexes were not as strong as the mononuclear ones of aluminum and gallium.[15,16]

Indium metal dissolves in mineral acids and produces In^{3+} ions which forms $[In(H_2O)_6]^{3+}$ in aqueous solutions with a constant In^{3+}-OH_2 distance of 0.214 nm.[14,15] $[In(H_2O)_6]^{3+}$ can be hydrolysed to $In(H_2O)_5(OH)^{2+}$ and $In(H_2O)_4(OH)_2^{+}$, before any electron-transfer process or any other reactions occur. It was reported that, when the concentration of indium is less than 0.001 mol L^{-1}, the main products of the hydrolysis (at pH values lower than 5) are ions $In(OH)^{2+}$ and $In(OH)_2^{+}$.

Hydrolysis constants of In^{3+} in solutions containing KNO_3 0.1 mol L^{-1} are organized in the table 1-1. K_{h1}, K_{h2} and K_{h3} represent the conditional hydrolysis constants. Reactions associated to K_{h1}, K_{h2} and K_{h3} are defined respectively as equations (1-3), (1-4) and (1-5) below;

$$In^{3+} + H_2O \rightleftharpoons InOH^{2+} + H^{+} \quad (1\text{-}3)$$

$$In^{3+} + 2H_2O \rightleftharpoons In(OH)_2^{+} + 2H^{+} \quad (1\text{-}4)$$

$$In^{3+} + 3H_2O \rightleftharpoons In(OH)_3 + 3H^{+} \quad (1\text{-}5)$$

It is reported that In^{3+} is one of the ions that has a tendency to form complexes with hard ligands such as OH^{-}, F^{-} and organic ligands which will bind with indium through oxygen or acetate.[15] In a recently published work,[15] several disagreements between some previous reports about hydrolysis constants of $InOH^{2+}$, $In(OH)_2^{+}$ and $In(OH)^0_3$ were identified. It was demonstrated that the 0.5 log unit of difference in estimated hydrolysis constants of such indium complexes reported in some previous works [11,12] was probably due to experimental errors.[15]

The problem of determining hydrolysis constants worsens when higher mononuclear hydrolysis species ($In(OH)_2^+$, $In(OH)_3^0$, $In(OH)_4^-$) or polynuclear hydroxides of In^{3+} have to be considered.[15]

Table 1-1: Conditional hydrolysis constants of In^{3+} in solutions that contained KNO_3 0.1 mol L^{-1}. This table is adapted from previous literatures.[15,17]

Ion	Determination condition	pK_{h1} $In(OH)^{2+}$	pK_{h2} $In(OH)_2^+$	pK_{h3} $In(OH)_3^0$	Source
In^{3+}	25^0C, 0.1 mol L^{-1} KNO_3	4.35	8.43	13.04	[18]
In^{3+}	25^0C, 0.1 mol L^{-1} KNO_3	4.31	9.35	-	[15]
In^{3+}	25^0C, 0.1 mol L^{-1} KNO_3	3.88	8.52	12.31	[17]

Figure 1-2 represents that predominance diagram of indium hydroxide and indium chloride complexes, while figure 1-3 shows the one of indium hydroxide and indium fluoride complexes. As can be seen in figure 1-2, indium hydroxide complexes at pH more than 7 predominate over chloride complexes, while as can be seen in figure 1-3, indium hydroxide complexes predominate over the ones of fluorides at more basic values (above pH 8). This means that at pH values higher than 8, indium hydroxide complexes ($In(OH)_3^0$ and $In(OH)_4^-$) predominate over both chloride and fluoride complexes. Also figure 1-2 demonstrates that in the region of the pH from around 4 to 5, $InOHCl^+$ complexes predominate over $In(OH)_2^+$. In the case of figure 1-3 at pH of approximately 5, with a fluoride concentration more than 10^{-3} mol L^{-1} and 10^{-5} mol L^{-1}, fluoride complexes predominate over indium hydroxide complexes and free In^{3+} ion.

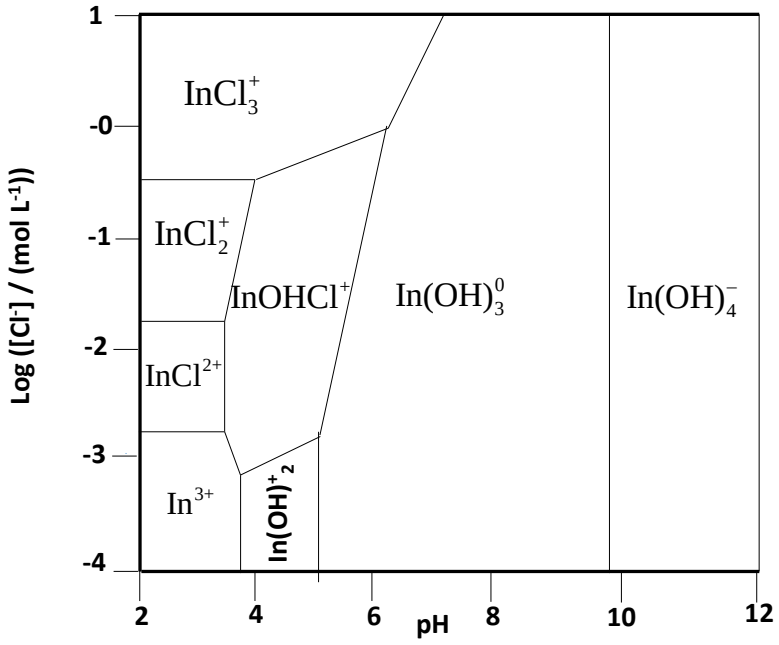

Figure 1-2: Predominance diagram at 1 bar and 25ºC of chloride, hydroxide and hydroxychloride complexes of In3+ as a function of log[Cl-] and pH. This figure is adapted from.[15]

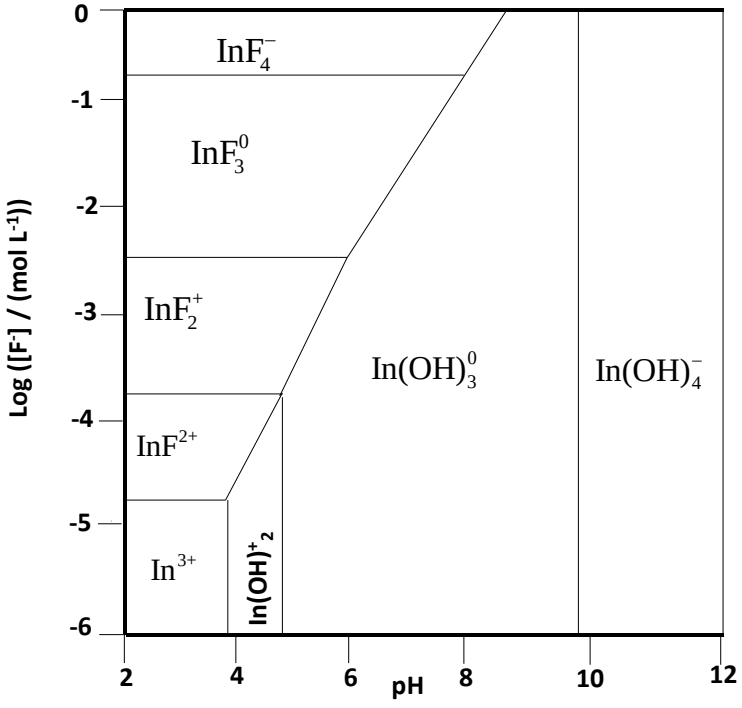

Figure 1-3: Predominance diagram of fluoride and hydroxide complexes of In^{3+} at 25⁰C and 1 bar. This figure is adapted from.[15]

Figure 1-4 illustrates the solubility of $In(OH)_3(s)$ in pure water at 25^0C. As can be seen in this figure, the minimum for the solubility of the system is wide (in the pH range from $\sim$ 4.5 up to $\sim$ 8.5), with the total dissolved concentration around $10^{-7.3}$ mol L^{-1}.

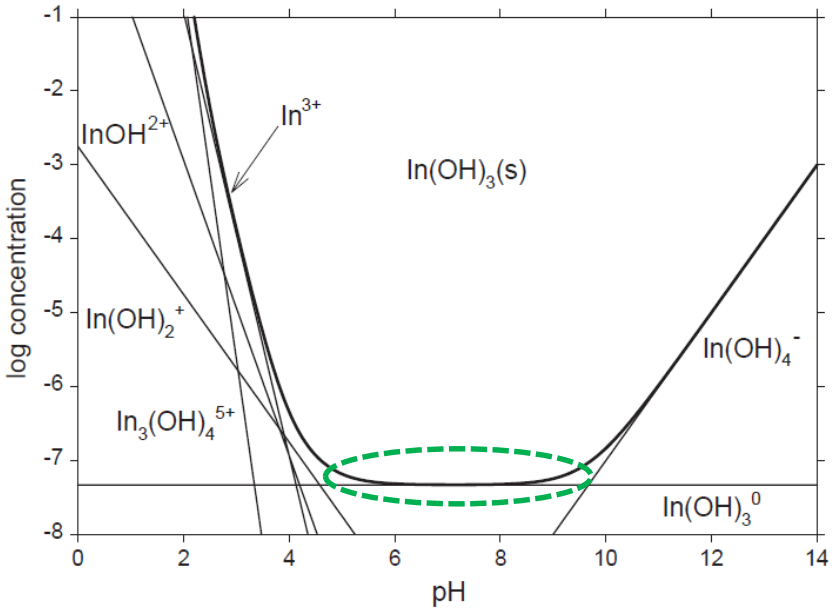

Figure 1-4: Solubility of $In(OH)_3(s)$ vs. pH at 25⁰C and zero ionic strength. The lines show the concentration (in mol L^{-1}) of individual In^{3+} species in equilibrium with $In(OH)_3(s)$ and the curve indicates the total solubility. The green dashed circle shows the wide range of the minimum for the solubility of the system. This figure is adapted from [15]

This means that the more stable solid phases are formed, the lower will become the solubility. Hence it is apparent that to be able to transport more quantities of indium, it could be better to be in acidic conditions or to have strong complexes.

1.2. Uses and production of indium

Indium has been used widely in many applications such as in alkali batteries and in producing alloy compounds that are binary (Al-In, Bi-In, Pb-In), ternary (Al-Sb-In, Cd-Sn-In), quaternary (Cd-Ge-Sn-In) and quinary (Cd-Ge-Sn-Zn-In). Some of the indium alloys, for instance InSb, InP, InN and InGaAs, are used in optoelectronic and magnetoresistive materials and also as anodic substances for lithium batteries.[2] Many years ago, indium was used as an additive to steel alloys in order to produce resistant thermometers, optical instruments or component of metallic anticorrosion coating.[19] Recently, it is being widely used in high technology industries. In fact indium can be labelled as one of the technology-critical elements (TCE)[1].[20] Some indium alloys have conductive properties and are utilized as semiconductors, infrared detectors, high efficiency photovoltaic devices and high speed transistors.[19] One of the most widely used

[1] Technology-critical elements (TCE) are elements such as (Nb, Ta, Te, In, Ga, Ge and TI) that are increasingly being used in modern technology.[20]

compounds of indium is indium tin oxide (ITO). It has been indicated that above 75% of total indium consumption arises from ITO.[21] ITO is a mixture of In_2O_3 and tin-oxide (SnO_2) in a ratio of 90:10 (wt:wt) which can be utilized as coating for plasma displays, solar cells, electroluminescent lamps, cathode ray tubes, energy efficient windows, gas sensors, aircraft, automobile windshields, LEDs (Light Emitting Diodes)[1,22] and LCD (Liquid Crystal Display) screens.[19] In fact these panels of LCDs are utilized in cell phones, Cd/DVD devices, flat panel displays, computers and all kind of devices with a display surface which is covered with a thin film of indium.[19,23,24]

These vast applications of indium compounds justify that the world production of indium has been increased over these past 30 years. It has been suggested that the interest of using indium compounds will become considerably apparent during the next few years.[1]

Countries with the largest indium production are China, Korea, Japan, Canada, Belgium, France, Russia and Peru. The estimated world refinery production of indium of these countries during the year 2015 in tons were 350, 195, 70, 70, 20, 41, 4 and 9 respectively. Hence, the summation of all of these productions during the year 2015 was around 759,000 kg.[25]

Also, according to a recent report, since late 1980 refined indium production has grown year by year.[26] For instance, the value of refined indium in 1980 was reported around 70 tons, and increased dramatically to 570 tones as a total primary production of indium during the year 2010.[26] Another investigation revealed that in 2013 the primary refined production of indium was around 770 tons and the second refined production of this metal in the mentioned year was approximately 610 tons. From this reported value (610 tons), 510 tons (84%) were produced nearby or in manufacturing centres in Japan, South Korea and China. In fact, these amounts (510 tons) are probably recovered from spent ITO sputtering targets that are mostly used in the production of flat panel displays (see section executive summary in the reference[27]). Accordingly, such wide productions and high usages of indium compounds can demonstrate that it is important to study the chemistry of indium that might be introduced to the environment.

1.3. Toxicity of indium

Up to now very little is known about the toxicity of indium and there are many concerns about health problems of some of its compounds.[19]

In principle, when it comes to study their toxicities, it is also important to take into account the duration of the exposure and what organ of the body is being affected.[28,29]

One of the compounds that could cause significant health problems is ITO, whose inhalation not only might result in lung damages, skin problems such as irritations and serious burns, but also eye illnesses.[19]

For instance, shockingly, it was reported that more than 700 workers in Japanese indium factories were diagnosed with lung disease as a matter of inhaling indium. Additionally, in another paper it was reported that a very young indium worker who suffered from interstitial pneumonia, despite of several treatments, died because of inhalation of ITO.[1] Due to high levels of indium in his blood serum, it was concluded that indium dissolution from ITO particles can damage the liver and enlarge the spleen.[1] Also it has been indicated that oral ingestion of ITO can cause problems in gastrointestinal tract.[19]

Moreover, pulmonary toxicity has been reported for other indium compounds, as an example, exposure to indium arsenide (InAs) [30,31] and indium phosphide (InP) [30,32] can cause several health problems such as lung inflammation, interstitial fibrosis, emphysema, etc. On the other hand, the effects of being exposed to indium oxide was also investigated in those reports. A report,[24] which was focused on the chemical information profile for ITO, supported the conclusion of another work[1] about the harmful effects of indium oxide exposition to rats and rabbits. It was observed that diseases such as pneumonia, early fibrosis in the lungs, hyperplasia in lung lymph nodes, dystrophic changes in livers, kidneys and hearts appeared in the body of the animals that were exposed to indium-oxide. Additionally, the existence of ITO compounds in seawater could have harmful effect on bacteria that are found in marine environment as well.[1,33]

Beside the mentioned compounds of indium, $InCl_3$ is also toxic for several aquatic species such as *Americamysis bahia*, *Brachionus plicatilis*, *Artemia salina*, *Sillago japonica* [29] and *Tilapia larvae.*[34] Not only this compound is toxic as said for aquatic species, but also it is harmful for humans. In fact, being exposed to $InCl_3$ might cause significant health problems such as lung inflammation, hyperplasia, interstitial fibrosis, pneumonia and emphysema.[1]

Moreover, in another research the effect of injecting both In_2O_3 and $InCl_3$ compounds into the tail vein of mice was investigated. The results showed that In_2O_3 was 40 times more toxic than $InCl_3$. Such a high toxicity of In_2O_3 is really concerning. It has been

reported that serious damages in the organs of the reticuloendothelial system (RES)[2] appeared due to the absorption of In_2O_3 compounds. It was indicated that these compounds were accumulated in liver, spleen and bone marrow and were mostly excreted in the feces.[28] It was also revealed that, although $InCl_3$ was less toxic than In_2O_3, such compounds caused acute tubular necrosis of the kidneys and were excreted mainly in the urine.[28]

In another study it was reported that the half-life of In_2O_3 in rats was around 10 days, while in one of the recent studies it was demonstrated that indium might remain in the human body for about 8 years.[35,36] All these investigations convince us that it is extremely crucial to devote more time to find safer ways to work with such compounds and prevent their leakage to the environment.

The Department of Health and Human Services of the National Institute for Occupational Safety and Health (NIOSH) in the United States has recommended the maximum exposure limits for indium in air to be around 0.1 mg/m^3,[37] but still no limitations have been indicated in case of oral inhalation of indium and, more importantly, there has been no standard rule published to know how much should be the proper level of indium concentration in drinking water.[1,35]

Accordingly, toxicity of indium and its compounds must be considered as an important issue.

1.4. Indium in the environment

The average concentration of indium in the earth crust is almost the same as the concentration of silver and mercury, which is around 52 $\mu g/kg$[1] and also it is approximately half of that of arsenic and three orders of magnitude less than the concentration of lead.

Two of the main sources of indium in the nature are zinc and lead-zinc ores. In 2007 approximately 600 metric tons of purified indium were produced from those ores. Indium percolates, from zinc and lead-zinc wastes that contain hydrochloric or sulfuric acid, to the environment.[1] Additionally, indium can be enriched in cassiterite ores and in rare sulfide ores such as sphalerite, chalcopyrite and stannite.[15]

[2] In Pathology, (RES) are types of monocyte cells that have the ability to protect the body by ingesting harmful foreign particles. Such a mechanism of protection is called phagocytosis.[69]

Total indium concentrations in natural waters have been reported to be, generally, extremely low, around 0.1 ng/kg.[1] For instance according to previous reports, total concentrations of indium in the Pacific and Atlantic oceans were in the range of 0.06 to 0.15 pmol/kg and 0.6 to 1.5 pmol/kg, respectively, while in the river and estuarine waters were approximately in the range 0.01 to 15 pmol/kg.[38] A recent review[1] reported concentrations of indium in oceans from 0.006 to 0.5 ng L^{-1} and from 0.13 to 15 pg L^{-1} for some freshwaters. The concentration of dissolved indium[39] could reach 6 to 29 μg/L in streams influenced by acid mine drainage (pH around 3).

Total concentrations of indium measured near mining and smelting areas were very high.[1] In natural sediments this concentration was approximately 0.05 mg/kg, while high indium concentrations up to 75 mg/kg were measured in river sediments near smelters.[40] Additionally, according to another study, an average concentration of indium in coal is 100 μg/kg and its concentration in petroleum can vary from 1 μg/kg up to about 20 μg/kg.[1]

To explain the concentrations of indium in atmosphere, we can briefly take into account two groups of fluxes: inputs to the atmosphere and outputs from atmosphere.[1] Dusts, ocean sea spray and volcanic emissions are natural sources that can introduce indium to the atmosphere.[1] Almost 0.04 ton/year[41] is the amount of global indium dust flux and this value is approximately the same in case of ocean sea spray.[42] And more importantly volcanic emissions can cause a global flux of indium to be around 0.01-21 tons/year[43] which could result from a fractionation of the more volatile elements, such as indium.[1,44] Industrial inputs to the atmosphere which can be due to fossil fuel combustion, mining, smelting, semiconductor and electronics manufacture, and incineration are also important in releasing huge amounts of indium into the atmosphere. Approximately, 300 tons of indium are released annually to the atmosphere from coal-burning, 600 tons/year from mining and smelting emissions. Global releases from semiconductors and electronic devices are presently smaller. The total input of indium into the atmosphere is around 1000 tons/year.[1]

On the other hand, human activities play an important role in the increase of indium concentration in the environment. As an example, industrial inputs could be extremely high and many researchers have indicated that anthropogenic sources might have significant effect,[45,46] causing an increase in concentration of indium in the environment. Hence these anthropogenic sources might be mentioned as a main source of indium input into the ocean.[1]

1.5. Speciation of indium

Many investigators have studied hydroxide complexes of indium.[7,11,12] These hydroxide complexes have been described in section 1.1. Recently it has been indicated that un-hydrolyzed In^{3+} ion is only predominant at pH values lower than 4 at 25°C or in presence of very high concentrations of F^- or Cl^-.[1,15] The stability constant of complexes that In^{3+} forms with Iminodiacetic acid (IDA), tartaric acid, aspartic acid, maleic acid, oxalic acid and picolinic acid have been studied some years ago.[47] Also some investigations have been devoted their attention on complexes of indium with acetylaceton, benzylacetone, malonic acid and phthalic acid.[48] Another report performed potentiometric titrations to study the behavior of oxalic acid and indium oxalate at higher concentrations of the ligands to understand its stoichiometry and complexation.[49] In another investigation it was indicated that indium has higher complexation constant for small organic molecules than Cu^{2+}, Pb^{2+} and Zn^{2+}, but lower than Hg^{2+}.[1,50] So, all of these studies can show that still there is a need to devote more investigations to study speciation of indium-complexes deeper in various media.

1.6. Analytical methods for the determination of indium

Many techniques have been applied to determine total and free concentrations of indium in different samples. Up to now few studies has been focused on determining trace concentration of indium. [51] These studies involves using spectrometric[38,52–58] and electroanalytical techniques.[19,51,59–68]

Tables 1-2 and 1-3 show various spectrometric and voltammetric techniques which were respectively used for determining total concentration of indium.

Table 1-2: Spectrometric techniques which were applied to determine total concentration of indium in various samples.

Spectrometric techniques	Combined with the technique	Some comments	Source
Flame Atomic Absorption Spectrometry (FAAS)	Preconcentration technique: Cloud Point Extraction (CPE)	To be able to preconcentrate target ions such as gallium, indium and thallium, Triton X-114 was used as a non-ionic surfactant. This method was not affected by interferences and such a property made this technique to be appropriately used to determine concentration of the mentioned target ions in sediments and mobile-phones liquid-crystal display samples.	52

Spectrometric techniques	Combined with the technique	Some comments	Source
Electrothermal Atomic Absorption Spectrometry (EAAS)	-	A sensitive method to determine total concentration of indium by Graphite Furnace Atomic Absorption Spectrometry (GFAAS) using a L'vov platform coated with tungsten. This method was successfully used to determine indium concentration in aluminum-rod samples.	53
EAAS	Dispersive Liquid-Liquid-Solidified Floating Organic Drop Micro Extraction (DLL-SFODME)	This method was used to preconcentrate indium–1-(2-pyridylazo)-2-naphthol complex in 25 μL of 1-undecanol and was applied successfully to extract and determine indium in water and standard samples.	54
Inductively Coupled Plasma Optical Emission Spectrometry (ICP-OES)	Complexation and separation technique	In this method, the ligand 2-(5-bromo-2-pyridylazo)-5-diethylaminophenol (5-Br-PADAP) was used to form a complex and non-ionic surfactant (*t*-octylphenoxy-polyethoxyethanol). Triton X-100 was utilized for the separation step. Satisfactory results were observed in determining concentration of gallium and indium in urine and lake water.	55
ICP-OES and (5-Br-PADAP)[3] Spectrometry	-	The comparison of the results obtained from two techniques revealed that ICP-OES is more suitable option for determining indium concentration in the solutions than (5-Br-PADAP) Spectrometry technique.	56
Inductively Coupled Plasma Mass Spectrometry (ICP-MS)	- Isotope dilution technique - Using Y as Internal Standard	The two methods consisted in the application of the flow injection ICP-MS technique, one using isotope dilution technique ^{113}In enriched spike and the other one utilizing natural yttrium which was present in the sample as an internal standard. These methods resulted in the determination of picomolar concentrations of indium in Pacific and Atlantic ocean seawater.	38
ICP-MS	Concentration and separation technique	Different target ions including indium were concentrated and separated from major ions in the seawater by using 8-hydroxyquinoline chelating ion exchange resin (TSK-8HQ). Picomolar concentrations of target ions were measured.	57
Fiber Optic linear Array Detection Spectrometry (FO-LADS)	Dispersive Liquid Liquid Micro Extraction (DLLME)	Ligand PAN[4] was used to form a complex and a cloudy solution. Then (FO-LADS) was utilized to determine concentration of the enriched analyte in the sediment phase of the water samples and standard alloys.	58

[3] (5-Br-PADAP) stands for 2-(5-bromo-2-pyridylazo)- 5-diethylaminophenol [56]
[4] PAN stands for 1-(2-pyridylazo)-2-naphthol

Table 1-3: Voltammetric techniques which were applied to determine total concentration of indium in various samples.

Voltammertic techniques	Some comments	Source
Differential Pulse Polarography (DPP)	DPP was developed to determine trace concentration of indium in standard alloys, synthetic and biological samples. In this technique the ligand PAN was used. Such measurements were done in the pH range 6.5-11.5.	59
Adsorptive Stripping Voltammetry (AdSV)	Bismuth electrode was used to determine trace concentration of indium in natural water samples. Additionally cupferron was utilized as a complex agent to form In(III)-cupferron complex.	19
AdSV	In(III) was complexed with 2′,3,4′-5,7-pentahydroxyflavone (morin) and static mercury drop electrode was used with the technique AdSV. In this investigation samples of jarosite[5] which contains high quantities of indium were used.	65
AdSV	The complex of indium ion with xylenol orange was absorbed on the surface of the Hanging Mercury Drop Elecetrode (HMDE). Indium was determined in the real samples such as water, alloy and jarosite (zinc ore).	66
AdSV	LLME[6] and Anodic Stripping Voltammetry (ASV) were coupled to determine traces concentrations of cadmium, lead, thallium and indium. This method was applied to determine concentration of each single metal in presence of large amounts of interfering metals.	67
Anodic Potential-Step Stripping Voltammerty (APSSV)	The technique (APSSV) was tried for determining various metal ions. Results were compared with the ones of ASV. It was concluded that, when it comes to determine concentrations of metal ions that their electron transfer is irreversible, APSSV is more sensitive than ASV. However, the APSSV technique was founded to be difficult to provide precise analysis of ion mixtures with the proximate anodic peak potentials.	60
Square Wave Anodic Stripping Voltammetry (SWASV)	Indium was determined in presence of lead and cadmium using the Bismuth-film electrode (BiFEs). It was concluded that redox process of cadmium and lead were more reversible than the case of indium on the BiFEs. Also it was revealed that peaks of indium and cadmium were better separated on a BiFE than on a Mercury Film Electrode (MFE).	62
SWASV	Indium and gallium were determined using the technique SWASV at mercury, bismuth and mixed mercury-bismuth thin-film electrodes, which were generated *in situ* on the surface of glassy carbon rotating disk electrode. Two competitions for the surface site of the glassy carbon electrode was observed. One was the contest between indium and bismuth and the other one was the rivalry between gallium and mercury.	68

[5] Jarosite is an industrial residue from the refinement of zinc ore
[6] LLME stands for Liquid Liquid Micro Extraction.

Voltammertic techniques	Some comments	Source
Differential Pulse Anodic Stripping Voltammetry (DPASV)	A sensor array was formed by a combination of *ex-situ* antimony film deposited on a screen printed carbon nanofiber-modified electrode (*ex-situ*-SbSPCNFE) to determine thallium and indium ions in water. Concurrent determination of thallium (I) and indium (III) in the spiked tap water was also satisfactory in comparison to ICP-MS measurements.	61

Several proposals for measuring free indium concentrations (i.e. the free concentrations of the hexaaquo complex) have been reported, including Ion Selective Electrodes [63,64] or molecularly imprinted polymer sensors,[51] but their limit of quantification (around 10^{-7} mol L^{-1}) is still relatively modest. Table 1-4 explains more details about the investigations that are mentioned above in case of measuring free indium concentration.

Table 1-4: Indium selective sensors which were applied to determine free concentration of indium in various samples.

Selective sensors	Some comments	Source
Solid sensor selective to In (III)	All-solid sensor which was selective for In(III) was developed and then Flow Injection Potentiometry FIP was used to determine indium in alloys.	63
Indium (III) selective Polyvinyl Chloride (PVC) sensor	Polyvinyl Chloride membrane sensor with the property of being sensitive to indium (III) was used. Utilizing such sensors provided satisfactory results in partially non-aqueous media. Finally the quantitative application of the sensor was investigated by analyzing synthetic seawater solution with the technique AAS.	64
Highly selective molecularly imprinted sensors	This technique successfully analyzed In^{3+}. This investigation was performed in real samples such as sphalerite, blast furnace dust, ground water and silver powder.	51

So, up to now, no investigation was found to be focused on measuring free In^{3+} concentration in mixtures of ligands. This justifies the interest of another technique, Absence of Gradients and Nernstian Equilibrium Stripping (AGNES) to measure free indium concentration.

Now, we can specify some advantages and disadvantages of the most common techniques that we mentioned above.

ICP-MS is one of the most used techniques to determine total indium concentration in environmental samples, but one difficulty of this technique is that a sample preconcentration step is previously needed to remove other ions that might interfere with the target one and to be within the detectable range.[1]

Regarding preconcentration techniques such as solvent extraction, we have to indicate that most of the times there is a need to evaporate the solution. This process might cause interferences in the measurements due to the formation of complicated complexes.

FAAS techniques are also problematic when it comes to use them for determining indium. In fact, in these techniques some ions such as tellurium, tin, silicon, and particles containing sulfate can interfere with indium.[51]

Stripping methods such as Anodic Stripping Voltammetry techniques (ASV), Adsorptive Stripping Voltammetry (AdSV) and Polarographic techniques[19] can be indicated as powerful ones for determining trace concentrations of metals in various environmental samples, especially for the case of indium. Simplicity, being not expensive, fast responses with high sensitivity are the main advantages of ASV and AdSV techniques.[19] However, they can rarely access directly to the free ion concentration. More details about potentiometric, polarographic and voltammetric techniques will be discussed in detail in chapter 2.

1.7. Objectives and outline of this thesis

The objective of the present thesis is to study the speciation of indium with voltammetric techniques. The capability of the electroanalytical technique AGNES (Absence of Gradients and Nernstian Equilibrium Stripping) to determine low concentrations of free indium in different media, different ligands and pH values is examined for the first time. The application of the technique named Accumulation under Diffusion Limited Conditions (ADLC) to calculate the lability degree of indium-oxalate complexes is another novelty of this project. ADLC results can improve the ability of AGNES to determine extremely low free concentrations of indium in precipitated solutions (solutions that are in equilibrium with precipitated $In(OH)_3$).

Then, finally, we aim to apply AGNES to study the kinetics and dissolution of indium nanoparticles (In_2O_3) in dispersions containing KNO_3 and synthetic seawater solutions. This thesis is organized into 5 more chapters (besides this one):

Chapter 2 firstly gives a brief description about the electroanalytical techniques often used in speciation studies, i.e. potentiometry and voltammetry, and then focuses on the techniques that are predominantly applied in this thesis, AGNES and ADLC.

Chapter 3 presents the application of AGNES technique to the determination of free indium concentration in solution. In particular, speciation of free indium in In-NTA and In-Oxalate mixtures at pH around 3 using AGNES is assessed.

Chapter 4 shows how ADLC can be used to determine the lability degree of indium oxalate complexes and how these results can provide a guideline to determine low concentrations of free indium in solutions that are in equilibrium with precipitated $In(OH)_3$ in the pH range 4 to 6.

Chapter 5 sheds light on kinetics and thermodynamic features of the dissolution of indium nanoparticles (In_2O_3) in solutions that contain KNO_3 0.1 mol L^{-1} from pH 2 to 5 and in synthetic seawater solutions at pH around 8.

Chapter 6 presents the general conclusions from the results of this thesis.

1.8. References

(1) White, S. J. O.; Hemond, H. F. The Anthrobiogeochemical Cycle of Indium: A Review of the Natural and Anthropogenic Cycling of Indium in the Environment. *Crit. Rev. Environ. Sci. Technol.* **2012**, *42* (2), 155–186.

(2) Chung, Y. H.; Lee, C. W. Electrochemical Behaviors of Indium. *J. Electrochem. Sci. Technol.* **2012**, *3* (1), 1–13.

(3) Pardoe, J. A. J.; Downs, A. J. Development of the Chemistry of Indium in Formal Oxidation States Lower than +3. *Chem. Rev.* **2007**, *107* (1), 2–45.

(4) Tuck, D. G. Critical Evaluation of Equilibrium Constants in Solution Part A : Stability Constants of Metal Complexes. Critical Survey of Stability Constants of Complexes of Indium. *Pure Appl. Chem.* **1983**, *55* (9), 52.

(5) Tuck, G. Gallium and Indium Dihalides: A Classic Structural Problem. *Polyhedron* **1990**, *9* (2/3), 377–386.

(6) Clark, R. J.; Griswold, E.; Kleinberg, J. Some Observations on Lower Halides of

Indium. *Am. Chem. Soc.* **1958**, *80* (18), 4764–4767.

(7) Biedermann, G.; Ferri, D. On the Polynuclear Hydrolysis of Indium Ion; In^{3+}. *Acta Chem. Scand.* **1982**, *A* (36), 611–622.

(8) Tuck, D. G.; Yang, M. K. Co-Ordination Compounds of Indium. Part IX. Indium (III)–dithiolate Complexes. *Chem. Soc. A Inorganic, Phys. Theor.* **1971**, No. 0, 214–219.

(9) Lovrecek, B.; Markovac, V. Studies of the Electrochemical Kinetics of Indium I. Kinetics of Deposition and Dissolution in the Indium+ Indium Sulfate System. *Electrochem. Soc.* **1962**, *109* (8), 727–731.

(10) Visco, R. . An Intermediate in the Electrochemical Oxidation of Indium Metal. *Electrochem. Soc.* **1965**, *112* (9), 932–937.

(11) Lasztity, S. Determination of the Hydrolysis Constants of indium(III) Ions by Liquid Ion Exchange and Tracer Indication. *Radiochem. Radioanal. Lett.* **1977**, *29* (4), 215–221.

(12) Hemmes, P.; D. Rich, L.; L. Cole, D.; M. Eyring, E. Kinetics of the Hydrolysis of Aqueous Indium (III) and gallium(III) Perchlorates. *Phys. Chem.* **1970**, *74* (15), 2859–2862.

(13) Moeller, T. Contributions to the Chemistry of Indium. III. An Electrometric Study of the Precipitation of Hydrous Indium Hydroxide. *J. Am. Chem. Soc.* **1941**, *63* (10), 2625–2628.

(14) Biedermann, G.; Li, N.; Yu, J. Studies on the Hydrolysis of Metal Ions. Part 34. The Hydrolysis of the Indium (III) Ion, in 3 M Na+ Cl - Medium. *Acta Chem. Scand.* **1961**, *15*, 555–564.

(15) Wood, S. A.; Samson, I. M. The Aqueous Geochemistry of Gallium, Germanium, Indium and Scandium. *Ore Geol. Rev.* **2006**, *28* (1), 57–102.

(16) Baes, C. F.; Mesmer, R. E. *The Hydrolysis of Cations*, Second Edi.; Krieger Publishing Company: Malabar, Florida, USA, 1986.

(17) Alekseev, V. G.; Myasnikova, E. N.; Nikol'skii, V. M. Hydrolysis Constants of Al^{3+}, Ga^{3+}, and In^{3+} Ions in 0.1 M KNO_3 Solution. *Russ. J. Inorg. Chem.* **2013**, *58* (12), 1593–1596.

(18) Smith, R. .; Martell, A. .; Motekaitis, R. NIST Crititically Selected Stability Constants of Metal Complexes Database. Gaithersburg, MD 2003.

(19) Wasąg, J.; Grabarczyk, M. Adsorptive Stripping Voltammetry of In(III) in the Presence of Cupferron Using an in Situ Plated Bismuth Film Electrode. *Anal. Methods* **2016**, *8* (17), 3605–3612.

(20) Cobelo García, A.; Filella, M. Electroanalytical Techniques for the Quantification of Technology-Critical Elements in Environmental Samples. *Curr. Opin. Electrochem.* **2017**, *3* (1), 78–90.

(21) Brun, N. R.; Christen, V.; Furrer, G.; Fent, K. Indium and Indium Tin Oxide Induce Endoplasmic Reticulum Stress and Oxidative Stress in Zebrafish (Danio Rerio). *Environ. Sci. Technol.* **2014**, *48* (19), 11679–11687.

(22) Lison, D.; Laloy, J.; Corazzari, I.; Muller, J.; Rabolli, V.; Panin, N.; Huaux, F.; Fenoglio, I.; Fubini, B. Sintered Indium-Tin-Oxide (ITO) Particles: A New Pneumotoxic Entity. *Toxicol. Sci.* **2009**, *108* (2), 472–481.

(23) Alfantazi, A. M.; Moskalyk, R. R. Processing of Indium: A Review. *Miner. Eng.* **2003**, *16* (8), 687–694.

(24) *Chemical Information Profile for Indium Tin Oxide*; National Toxicology program: Research Triangle Park, North Carolina, USA, 2009.

(25) Indium production by country (kilograms) http://www.indexmundi.com/en/commodities/minerals/indium/indium_t3.html (accessed Feb 12, 2017).

(26) Gibson, C.; Hayes, T. *Indium and Gallium Overview*; Edison investment research, 2011.

(27) Lokanc, M.; Eggert, R.; Redlinger, M. *The Availability of Indium: The Present, Medium Term, and Long Term*; National renewable energy laboratory (NREL): Colorado, USA, 2015.

(28) Castronovo, F. P. J.; Wagner, H. N. J. Comparative Toxicity and Pharmacodynamics of Ionic Indium Chloride and Hydrated Indium Oxide. *J. Nucl. Med.* **1973**, *14* (9), 677–682.

(29) Onikura, N.; Akiko, N.; Katsuyuki, K. Acute Toxicity of Thallium and Indium toward Brackish-Water and Marine Organisms. *J. Fac. Agri. Kyusbu Univ* **2008**, No. 53, 467–469.

(30) Yamazaki, K.; Tanaka, A.; Hirata, M.; Omura, M.; Makita, Y.; Inoue, N.; Sugio, K.; Sugimachi, K. Long Term Pulmonary Toxicity of Indium Arsenide and Indium Phosphide Instilled Intratracheally in Hamsters. *J. Occup. Health* **2000**, *42* (4),

169–178.

(31) Tanaka, A. Toxicity of Indium Arsenide, Gallium Arsenide, and Aluminium Gallium Arsenide. *Toxicol Appl Pharmacol* **2004**, *198* (3), 405–411.

(32) Tanaka, A.; Hirata, M.; Omuru, M.; Inoue, N.; Uneno, T.; Homma, T.; Sekizawa, K. Pulmonary Toxicity of Indium-Tin Oxide and Indium Phosphide after Intratracheal Instillations into the Lung of Hamsters. *Occup Heal.* **2002**, *44* (2), 99–102.

(33) Blaise, C.; Gagné, F.; Férard, J. F.; Eullaffroy, P. Ecotoxicity of Selected Nano-Materials to Aquatic Organisms. In *Environmental Toxicology*; 2008; Vol. 23, pp 591–598.

(34) Lin, H. C.; Hwang, P. P. Acute and Chronic Effects of Indium Chloride ($InCl_3$) on Tilapia (*Oreochromis Mossambicus*) Larvae. *Bull. Environ. Contam. Toxicol.* **1998**, *61* (1), 123–128.

(35) Andersen, J. C. Ø.; Cropp, A.; Paradise, D. C. Solubility of Indium-Tin Oxide in Simulated Lung and Gastric Fluids: Pathways for Human Intake. *Sci. Total Environ.* **2017**, *579*, 628–636.

(36) Amata, A.; Chonan, T.; Omae, K.; Nodera, H.; Terada, J.; Tatsumi, K. High Levels of Indium Exposure Relate to Progressive Emphysematous Changes: A 9-Year Longitudinal Surveillance of Indium Workers. *Thorax* **2015**, *70* (11), 1040–1046.

(37) Barsan, M. E. *Pocket Guide to Chemical Hazards*; Columbia Parkway, USA, 2007.

(38) Alibo, D. S.; Amakawa, H.; Nozaki, Y. Determination of Indium in Natural Waters by Flow Injection Inductively Coupled Plasma Mass Spectrometry. *Proc. Indian Acad. Sci. Planet. Sci.* **1998**, *107* (4), 359–366.

(39) White, S. J. O.; Hussain, F. A.; Hemond, H. F.; Sacco, S. A.; Shine, J. P.; Runkel, R. L.; Walton-Day, K.; Kimball, B. A. The Precipitation of Indium at Elevated pH in a Stream Influenced by Acid Mine Drainage. *Sci. Total Environ.* **2017**, *574*, 1484–1491.

(40) Bougriet, A.; Proix, N.; Billon, G. Environmental Impacts of Heavy Metal Discharges from a Smelter in *Deûle*-Canal Sediments (Northern France): Concentration Levels and Chemical Fractionation. *Water Air Soil Pollut* **2007**, *180* ((1-4)), 83–95.

(41) Rudnick, R. L.; Gao, S. Composition of the Continental Crust. *Treatise on*

Geochemistry **2003**, *3*, 1–64.

(42) Klee, R. J.; Graedel, T. E. Elemental Cycles: A Status Report on Human or Natural Dominance. *Annu. Rev. Environ. Resour.* **2004**, *29* (1), 69–107.

(43) Matsumoto, A.; Hinkley, T. K. Trace Metal Suites in Antarctic Pre-Industrial Ice Are Consistent with Emissions from Quiescent Degassing of Volcanoes Worldwide. *Earth Planet. Sci. Lett.* **2001**, *186* (1), 33–43.

(44) Hinkley, T. K.; Lamothe, P. J.; Wilson, S. A.; Finnegan, D. L.; Gerlach, T. M. Metal Emissions from Kilauea, and a Suggested Revision of the Estimated Worldwide Metal Output by Quiescent Degassing of Volcanoes. *Earth Planet. Sci. Lett.* **1999**, *170* (3), 315–325.

(45) Obata, H.; Alibo, D. S.; Nozaki, Y. Dissolved Aluminum, Indium, and Cerium in the Sea of Japan and the Sea of Okhotsk: Comparison to the Marginal Seas of the Western North Pacific. *J. Geophys. Res.* **2007**, *112* (C12), 1–10.

(46) Obata, H.; Nozaki, Y.; Alibo, D. S.; Yamamoto, Y. Dissolved Al, In, and Ce in the Eastern Indian Ocean and the Southeast Asian Seas in Comparison with the Radionuclides 210Pb and 210Po. *Geochim. Cosmochim. Acta* **2004**, *68* (5), 1035–1048.

(47) Pingarron Carrazon, J. M.; Gallego Andreu, R.; Sanchez Batanero, P. Potentiometric Determination of Stability Constants of Complexes Formed by indium(III) and Different Chelating Agents. *Bull. Soc. Chim. Fr.* **1984**, No. 3–4, 115–122.

(48) Sarin, R.; Munshi, K. N. Physicochemical Investigation on Complexes of Indium (III) with Ligands Containing Oxygen as Donor Atoms. *J. indian Chem. Soc.* **1977**, *54* (7), 659–666.

(49) Kebede, T.; Sailaja, B. B. V; Rao, G. N.; Rao, M. S. P. Chemical Speciation of Oxalato Complexes of indium(III). *Chem. Speciat. Bioavailab.* **2010**, *22* (4), 241–246.

(50) Martell, A. E.; Smith, R. M. *Critical Stability Constants*; Springer: Boston, MA, USA, 1982.

(51) Zhang LM, Li JP, Zeng Y, Meng LH, F. C. Highly Selective Molecularly Imprinted Polymer Sensor for Indium Detection Based on Recognition of In-Alizarin Complexes. *Electroanalysis* **2015**, *27* (7), 1758–1765.

(52) Mortada, W. I.; Kenawy, I. M.; Hassanien, M. M. A Cloud Point Extraction Procedure for Gallium, Indium and Thallium Determination in Liquid Crystal Display and Sediment Samples. *Anal. Methods* **2015**, *7* (5), 2114–2120.

(53) Dianjie, M. A.; Kamoto, Y. O.; Umamaru, T. K.; Wamoto, E. I. Determination of Indium in Aluminum Alloy by Electrothermal Atomic Absorption Spectrometry with a Tungsten-Coated L ' Vov Platform Tube. *Anal. Sci.* **1999**, *15* (2), 193–195.

(54) Ashrafzadeh Afshar, E.; Taher, M. A.; Fazelirad, H.; Naghibzadeh, M. Application of Dispersive Liquid–liquid–solidified Floating Organic Drop Microextraction and ETAAS for the Preconcentration and Determination of Indium. *Anal. Bioanal. Chem.* **2017**, *409* (7), 1837–1843.

(55) Liu, H. M.; Jiang, J. K.; Lin, Y. H. Simultaneous Determination of gallium(III) and indium(III) in Urine and Water Samples with Cloud Point Extraction and by Inductively Coupled Plasma Optical Emission Spectrometry. *Anal. Lett.* **2012**, *45* (14), 2096–2107.

(56) Sun, Y.; Chang, M.; Yu, H.; Zhou, R.; Guo, R.; Yun, H.; Hu, R. Determination of In^{3+} in Solution by ICP-OES and 5-Br-PADAP Spectrophotometry. *J. Chem. Pharm. Res.* **2014**, *6* (5), 150–154.

(57) Orians, K. J.; Boyle, E. A. Determination of Picomolar Concentrations of Titanium, Gallium and Indium in Sea Water by Inductively Coupled Plasma Mass Spectrometry Following an 8-Hydroxyquinoline Chelating Resin Preconcentration. *Anal. Chim. Acta* **1993**, *282* (1), 63–74.

(58) Kazemi, E.; Shokoufi, N.; Shemirani, F. Indium Determination and Preconcentration Using Fiber Optic Linear Array Detection Spectrometry Combined with Dispersive Liquid-Liquid Micro Extraction. *J. Anal. Chem.* **2011**, *66* (10), 924–929.

(59) Taher MA. Differential Pulse Polarography Determination of Indium after Column Preconcentration with [1-(2-Pyridylazo)-2-Naphthol]-Naphthalene Adsorbent or Its Complex on Microcrystalline Naphthalene. *Talanta* **2000**, *52* (2), 301–309.

(60) Komatsu, M. Potential-Step Anodic Stripping Voltammetry. *Bull. Chem. Soc. Jpn.* **1973**, *46* (6), 1670–1674.

(61) Pérez-Ràfols, C.; Serrano, N.; Díaz-Cruz, J. M.; Ariño, C.; Esteban, M. Simultaneous Determination of Tl(I) and In(III) Using a Voltammetric Sensor

Array. *Sensors Actuators, B Chem.* **2017**, *245*, 18–24.

(62) Charalambous, A.; Economou, A. A Study on the Utility of Bismuth-Film Electrodes for the Determination of In(III) in the Presence of Pb(II) and Cd(II) by Square Wave Anodic Stripping Voltammetry. *Anal. Chim. Acta* **2005**, *547* (1), 53–58.

(63) Abbas, M. N.; Amer, H. S. A Solid-Contact indium(III) Sensor Based on a Thiosulfinate Ionophore Derived from Omeprazole. *Bull. Korean Chem. Soc.* **2013**, *34* (4), 1153–1159.

(64) Gupta, V. K.; Hamdan, A. J.; Pal, M. K. Comparative Study on 2-Amino-1,4-Naphthoquinone Derived Ligands as Indium (III) Selective PVC-Based Sensors. *Talanta* **2010**, *82* (1), 44–50.

(65) Farias, P. A.; Martin, C. M.; Ohara, A. K.; Gold, J. S. Cathodic Adsorptive Stripping Voltammetry of Indium Complexed with Morin at a Static Mercury Drop Electrode. *Anal. Chim. Acta* **1994**, *293* (1–2), 29–34.

(66) Benvidi, A.; Ardakani, M. . Subnanomolar Determination of Indium by Adsorptive Stripping Differential Pulse Voltammetry Using Factorial Design for Optimization. *Anal. Lett.* **2009**, *42* (15), 2430–2443.

(67) Labuda, J.; Vaničková, M. Anodic Stripping Voltammetry with Mercury Electrodes in Extracts of Cadmium, Lead, Thallium and Indium Diethyldithiocarbamate Complexes and Analysis of Mixtures. *Anal. Chim. Acta* **1988**, *208*, 219–230.

(68) Medvecký, Ľ.; Briančin, J. Possibilities of Simultaneous Determination of Indium and Gallium in Binary InGa Alloys by Anodic Stripping Voltammetry in Acetate Buffer. *Chem. Pap. Acad. Sci.* **2004**, *58* (2), 93–100.

(69) Baas, J.; Senninger, N.; Elser, H. The Reticuloendothelial System. An Overview of Function, Pathology and Recent Methods of Measurement. *Z. Gastroenterol.* **1994**, *32* (2), 117–123.

Chapter 2: Electroanalytical techniques

2.1. Electroanalytical techniques

The aim of this chapter is to gather some background information about electroanalytical techniques and their use to determine metal speciation.

2.1.1. Suitability of electroanalytical techniques for metal speciation

The term speciation indicates a set of chemical forms in which an element distributes in a living system or in the environment. In an aquatic system, chemical species can be classified as:[1,2]

1) Particulate (>1μm)

2) Incorporated to colloidal particles (1nm-1μm)

3) Dissolved species (≤1 nm), which includes free metal ions, complexes with anthropogenic and natural ligands, and also simple inorganic complexes.

Monitoring metals which might cause health problems is significantly important and sometimes just total metal concentrations would not provide sufficient information.[1]

Two models, the Free Ion Activity Model (FIAM)[3] and the Biotic Ligand Model (BLM) [4], are based on the common key point that free metal ion is the only directly bioavailable species. These models suffer from some limitations.[5] Both are based on a direct (linear) relationship between free ion concentration and the surface bound metal, but this relationship is only reasonable when the species are at equilibrium.[5] This equilibrium is, perhaps, valid for metal ions equilibrating with microorganisms and inorganic ligands in water. So, it seems that these models probably would not be applicable for more complex media such as soil, sediments and biofilms, or when heterogeneous ligands like humic substances exist.[5] When the metal is transported from the bulk to the biological surface, it might undergo many dissociation and association reactions.[5] This property is not included in FIAM/ BLM. In fact what has been assumed in these two models is that the transport of metal species is not limiting.[5] But in reality, some transport happens both directly and through the dissociation of the labile complexes. So, still there is a need to develop techniques which should provide more trustable information about speciation of metals,[6–8] which can be harmonized within the current understanding of the environmental functioning.

Up to now, many analytical techniques have been developed to study the speciation of metals[9] in aquatic solutions, such as potentiometry (e.g. using ion selective electrodes),

voltammetry and spectroscopic techniques.[4] Some examples of spectroscopic techniques that were used in speciation measurements are hyphenated techniques (e.g. Gas Chromatography- Inductively Coupled Plasma- Mass Spectrometry, GC-ICP-MS) that were applied to analyse organometallic elements[10,11] and X-ray Spectroscopic techniques.[9] But the major drawback of spectrometric techniques such as Graphite Furnace Atomic Absorption Spectrometry (GFAAS) and Inductively Coupled Plasma-Mass Spectrometry (ICP-MS) is that, although they can be applied for large number of elements, they are all very expensive and are used to determine the total concentration of the metals.[2] So, in principle, these techniques cannot be directly applied for speciation measurements.[1] Hence, to make them applicable for such an aim, they must be coupled with separation and extraction procedures and this coupling increases the risks of contamination during the sample storage or handling. Additionally, the cost of sample analysis with these techniques is often high.[2]

In contrast, voltammetric techniques are suitable for speciation measurements. They are low cost, and when applied *in situ* they have minimum probability of sample change or contamination by reagents and losses by adsorption on containers.[2] Stripping techniques can be considered as very indicated because of the low detection limits. Anodic Stripping Voltammetry (ASV) is the most popular one and has the property of determining labile fractions that have sometimes been correlated with the bioavailable fraction of the metal.[12,13]

2.1.2. Potentiometric techniques

Potentiometry measures the potential difference between two electrodes, without affecting the solution relevantly. Two electrodes are used, one is called the reference electrode with a constant potential, while the other one is the working or indicator electrode which responds to the analyte activity. In the simplest case, the analyte is an "electroactive species", that is, part of a galvanic cell. These electroactive species can donate or accept electrons at an electrode surface.[14]

2.1.2.1. Ion selective electrodes (ISE)

The common Ion selective electrodes belong to the potentiometric techniques. These electrodes respond selectively to one specific ion. Figure 2-1 represents a classical potentiometric setting which includes indicator electrode (I), reference electrode (R) and potentiometer device (PM).

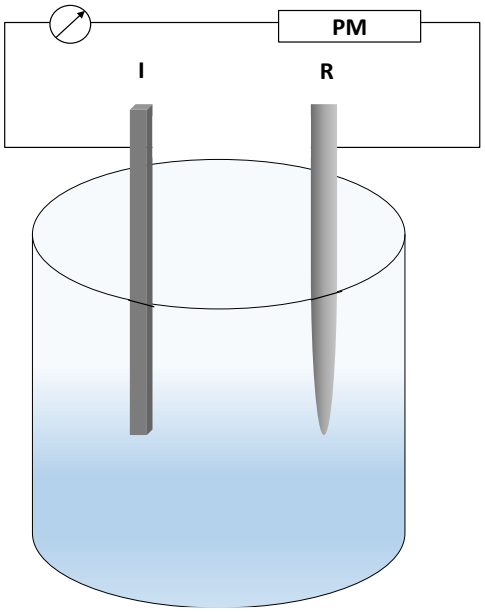

Figure 2-1: Basic representation of a classical potentiometry. I= indicator electrode; R=reference electrode; PM= potentiometer device. This figure is adapted from reference [15].

These electrodes are one of the most important groups of chemical sensors.[16] Many articles and reports describing their applications and the methodology have been written about such electrodes.[17–20]

In case of an ion selective electrode, the measured electromotive force (E_{emf}) of a cell depends on the potential across the interface of the sample and the membrane phase.[21] As can be seen in equation (2-1), E_{emf} is a sum of potentials:[21]

$$E_{emf} = E_{const} + E_J + E_M \tag{2-1}$$

In this equation E_{const} is a constant potential, E_M is the potential of the membrane and E_J is the potential of the liquid junction at the sample/bridge electrolyte interface. [21] When two non-similar electrolytes are in contact, a voltage difference, which is called liquid junction potential (E_J) develops at their interfaces. Sometimes this junction potential can cause limitations in the accuracy of the direct potentiometry measurements, because the exact contribution of the junction to the measured voltage most of the times is not clear .[14]

Equation (2-2) can be used to relate E_M with the composition of the sample and the internal filling

$$E_M = -\frac{RT}{z_i F} \ln \frac{a_i^{\beta}}{a_i^{\alpha}} \tag{2-2}$$

In this equation, a_i^{β} and a_i^{α} stand for the activity of substance *i* in a phase β and α, respectively, additionally z_i represents the charge of species *i*.[22] Phase α and phase β correspond to the test solution (the sample) and internal filling solution of the electrode, respectively. If the activities of specie *i* is kept constant in one phase, then the membrane potential can be calculated with a Nernstian-like equation and the ion activity in the other phase (see page 74, chapter 2 section 2.4.1 of the reference[22]).

Ion selective electrodes are immersed in a solution and respond to the activity of the free analyte, not the complexed ones. A potential difference will appear between the electrodes or membranes as a result of a charge imbalance or movements of ions. The crucial factor in an ideal Ion selective electrode is to have a special membrane that is sensitive and capable to bind to the needed specific ion.[14]

Now, we can briefly see different types of ISE.

2.1.2.1.1. *Glass membranes*

They consist of a glass bulb membrane with a wire of Ag inside it. This bulb separates the internal filling solution (HCl 0.1 mol L^{-1}) and an Ag/AgCl electrode from the solution. This Ag/AgCl is utilized as a reference electrode which is connected to the wire of Ag.[22,23] This tiny glass membrane is immersed inside the target solution. One of the common usages of such electrodes are pH electrodes. The glasses used in these electrodes are mostly amorphous silicon dioxides with embedded oxides of alkali metals.

Although the pH sensing ability of the glass electrode provides information about the activity of hydronium H^+ in water and can be used for measuring the pH of the solutions, there are some problems to take into account while using these electrodes.

As an example, in solutions that have high concentrations of alkali metals, while the activity of H^+ is very small, the equilibration is more difficult. Besides that, strong alkaline solutions or solution containing fluoride might damage these electrodes. Additionally the electrode might be affected by the absorption of certain proteins on its surface. Moreover noble metals such as Ag^+ and Cu^+ could also damage the electrode by being reduced and deposited on the surface of the electrode.[23]

2.1.2.1.2. *Crystalline membrane*

Electrodes based on crystalline membranes are called solid state ion selective electrodes. Their structure is based on inorganic crystals. One common kind is the fluoride

electrode which employs a crystal of LaF_3 doped with Eu^{2+} (doping means adding a small amount of Eu^{2+} as a replacement of La^{3+}). Other frequent types are AgCl, AgBr, AgI, Ag_2S, CuS, CdS and PbS. For instance, Ag_2S responds to Ag^+ and S^{2-} .[14] Generally the surface of these electrodes tends to respond to ions or species that form almost insoluble precipitates (see section 2.4.3 in [22]).

2.1.2.1.3. *Liquid-based ion-selective electrodes*

Typically, the membrane that is placed at the bottom of these electrodes is made from polyvinyl chloride and is impregnated with an ion exchanger and the plasticizer dioctyl sebacate.[14] Figure 2-2 shows a liquid-based ion-selective electrode that is immersed in an analyte solution and how it works. The inside of the electrode has cations (C^+ (aq)) and anions (B^-(aq)) and the outside of the electrode is immersed in the analyte solution which contains C^+(aq) and A^-(aq) and many other ions. Essentially, it does not matter what exactly are A^-, B^- and other ions. The voltage across the ion-selective membrane is measured using two reference electrodes, which are usually Ag|AgCl. When the activity of C^+ is modified, the voltage measured between the two reference electrodes will change as well. One of the important issues in this figure is the ligand L, which is called ionophore. This ligand is not soluble outside the membrane and can selectively bind to the target ion, for instance if we consider a potassium ion selective electrode, L could be a ligand such as valinomycin. This ligand is a natural antibiotic and carries K^+ across the membrane of the cell. Also we can assume that C^+ and R^- are K^+ and tetraphenylborate $(C_2H_5)_4B^-$, respectively. L has a high affinity for C^+ and low affinity for R^-, so this means that in an optimal electrode L should only bind to C^+, but in reality the ionophores of ion selective electrodes have a tendency to bind with some other cations. This might cause some interferences when the aim is to measure C^+. Inside the membrane we have a complex LC in equilibrium with C^+. Also, some excess of L exists inside the membrane. C^+ can pass through the outer surface of the membrane and enter the analyte solution and cause excess positive charge inside the solution. Taking into account that in an ideal electrode R^- and A^- are insoluble (or very poorly soluble) in aqueous and organic phase (membrane) respectively, then the diffusion of C^+ and its entrance in aqueous solution will provide an imbalanced charge and an electric potential difference will result. It is also important to take into account that the diffusion of C^+ cannot be sustained for ever. In fact relatively few C^+ ions can pass across the membrane because each C^+ tends to stay close to an R^- in the membrane (for electroneutrality), so after a certain potential

difference is generated it can block more diffusion of C^+.[14] As can be seen in figure 2-2, the indicator electrode and the reference electrode are both immersed in the solution and the cell is connected to the potentiometer device. One problem that might appear with these electrodes is that some special types of them work in a specific region of concentrations. As an example, the response of the Pb^{2+}- selective electrode might be levelled off at a concentration of an analyte around 10^{-6} mol L^{-1}. Lower free concentrations (~ 10^{-11} M) have been reached by using a metallic buffer solution as inner electrolyte. Also, generally, it has been reported that leakage of a target ion from the internal filling solution through the ion-exchange membrane can limit the sensitivity of these electrodes [14]

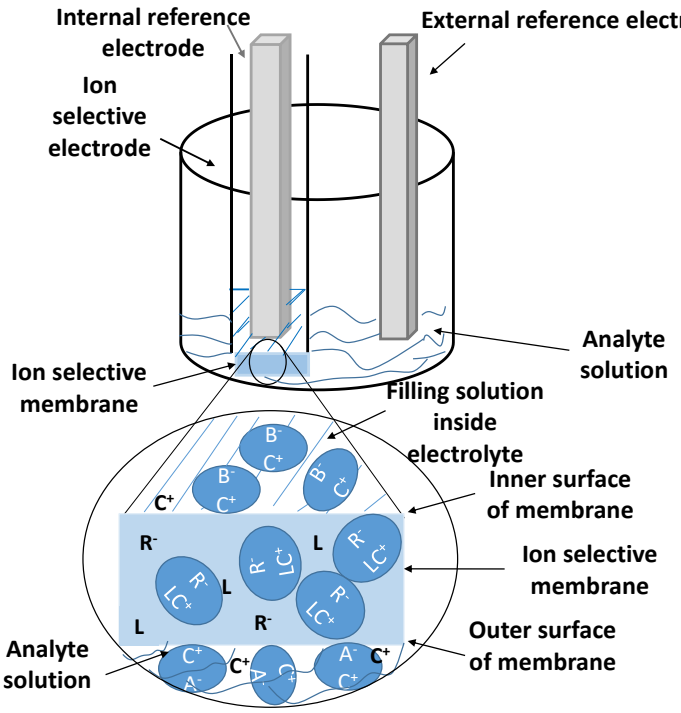

Figure 2-2: Ion selective electrode placed in an aquatic solution, C^+, L^+, R^-, A^- and LC represent the analyte cation, ligand, hydrophobic anion, analyte anion and complex, respectively (adapted from [14]).

Now, we turn to evaluate the attempts[24,25,14,16–23] to measure free concentration of indium with ISE (see chapter 1, section 1.6, table 1-3).

Two main characteristics of In-ISE are the selected ionophore and polymeric membrane. In a recent published work,[25] it was concluded that the decline in the sensitivity of their polymeric membrane could be related to the limited lipophilicity and chemical stability of ionophores. Such a deterioration in the sensitivity of this polymer could result from the leakage of the ionophore from the membrane. As indium (III)-ionophore chelates are compounds with high lipophilicity, their leakage should be

minimal. This membrane could be used for a long time (3.5 months) without any drift in the potentials if it is stored in 0.01 mol L^{-1} In^{3+} when it is not being used. Additionally, it was found that there is a limitation of pH range, the safe pH values in presence of indium (III) selective PVC based sensors needs to be in the range 4.5 up to 7.5.[25] It has been indicated that this could result from the interference of H^+ at acidic pH values (pH= 1-3) and of OH^- at basic pH values (higher to pH 8) in the aqueous solutions.[25]

In another work, the effect of membrane composition on the potentiometric response of the coated graphite indium (III) sensors using 10^{-7}- 10^{-2} mol L^{-1} indium $InCl_3$ at pH 5.4 was studied. In fact they claimed that they measured the concentration mentioned above, but they did not comment on the expected concentration under these condictions. They revealed that sensors with the solid contact had a good performance with the Nernstian slope 19.09 mV/decade, a linear range 3×10^{-7} to 1×10^{-2} and a Lower Detection Limit of 1×10^{-7} mol L^{-1} for In(III) was achieved.[24]

2.1.2.2. Zero current potentiometry

Zero current potentiometry is a potentiometric technique where the ceasing of flow of current indicates the end point.

In fact at equilibrium conditions the net current is zero and the electrode potential is related to the bulk concentrations of oxidized (c_O^*) and reduced form (c_R^*) of the redox couple, as prescribed by Nernst equation.[22]

$$E = E^{0'} + \frac{RT}{nF}\ln\frac{c_O^*}{c_R^*} \qquad (2\text{-}3)$$

2.1.2.3. Constant current potentiometry

The end point of constant current potentiometries can be determined directly as a result of a large change in the electrode potential.[15]

This technique is mostly practical for redox titrations where one of the couples is irreversible i.e. in cases that equilibrium on the surface of the electrode would not be achieved very fast.[15] Constant current potentiometry has been developed in variants such as Stripping Chronopotentiometry (SCP),[26,27] Stripping Chronopotentiometry at Scanned deposition Potential (SSCP) [28] and Potentiometric Stripping Analysis (PSA).[29]

In all constant current potentiometry variants, the evolution of potential is recorded while a fixed current is prescribed. Figure 2-3 represents current voltage curves for two redox couples (a) and (b), one behaved irreversible (b) while the other one is reversible

(a). As can be seen in this figure, for practically zero currents, the potentials are almost close to each other, but, then, as the current increases they start to diverge one from another. This divergence is not always the same; in some cases it can be even more than that.

Thermodynamically, a process can be categorized as reversible if just an infinitesimal reversal in a driving force can cause the direction of the process to be changed. Also we need to take into account that the concept of "electrochemical reversibility" is different, as it is a kinetic concept related to the inability of the concentrations and potential to meet electrochemical equilibrium (i.e. Nernst law is not applicable). More explanations about reversibility or irreversibility are discussed in the section 2.1.3.4. in this chapter.

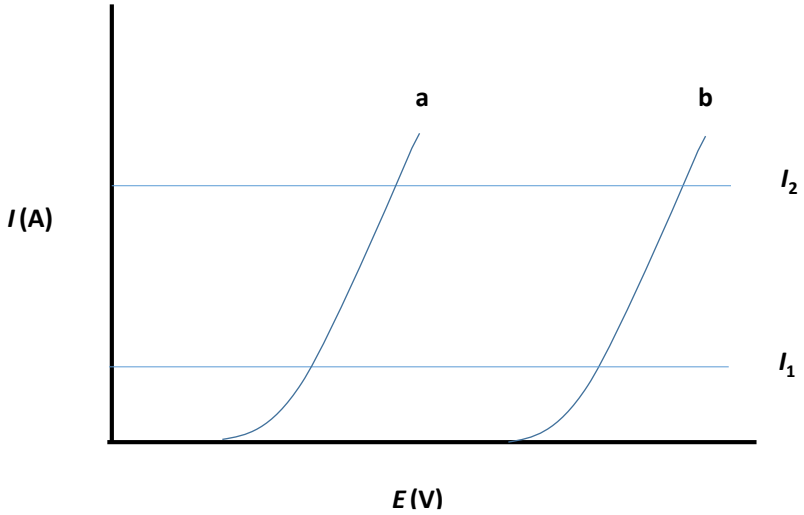

Figure 2-3: Current potential curves, a) reversible and b) irreversible couple. Constant current I_2 presents better separation of potentials than I_1, Adapted from [15] .

2.1.3. Voltammetric techniques

In voltammetric techniques, the current *I* which flows between the working electrode (WE) and the Auxiliary electrode (AE) is recorded. This current is measured as a result of the oxidation or reduction of the target element and is plotted as a function of the potential, *E*, which is imposed on the WE and expressed with respect to that of a reference electrode.[2] The reduction and oxidation of the species at the surface of the working electrode not only generates current, but it also requires a mass transfer of the various species to/from the surface of the electrode.[30] Voltammetry, especially with mercury electrodes, is one of the powerful techniques for analysing both inorganic and organic analytes with high reproducibility and low detection and quantification limits.[31]

Additionally we can consider voltammetry as one of the versatile techniques that can be used for various fields of research and, mainly, it has been used for quantitative

analysis of trace metals at µg/L levels or less [32–40] For instance, table 2-1 gathers some of the applications of voltammetry techniques in biochemistry.

Table 2-1: Some voltammetric techniques used in biochemistry

Voltammetric techniques	The aims	Source
Square wave voltammetry (SWV)[7], Differential pulse voltammetry (DPV) and Cyclic Voltammetry (CV)	To spot changes in the oxidation signal of tyrosine (Tyr)[8]	[41]
Adsorptive Transfer Stripping Voltammetry (AdTSV)[9], DPV and Alternating Current Voltammetry (ACV)[10]	To detect DNA hybridization effect	[42]
(SWV)	To measure the oxidation signal of Homocysteine (HCys)[11]	[43]

2.1.3.1. Indicator electrodes used in voltammetry

In this section, we will present different types of indicator electrodes, such as the Ultra microelectrode (UME), the Rotating disk electrode (RDE) and the Mercury drop electrode (MDE). Additionally we will describe their applications, advantages and disadvantages.

2.1.3.1.1. *Ultra microelectrodes (UME)*

The small surface of UME, which are less than 50 µm in radius, leads to steady-state diffusion-controlled currents.[15] They also include electrodes with micrometre length in one direction with millimetre length in another direction. The use of these electrodes can help to understand mass transport at the electrode surface better, since it can be seen that

[7] Square wave Voltammetry (SWV) is usually applied at stationary electrodes such as HMDE and was invented by Ramaley and Krause.[22]
[8] Tyrosine (Tyr) or 4-hydroxyphenylalanine is one of the 22 amino acids that cells use for synthesizing proteins.[80]
[9] In the technique Adsorptive Transfer Stripping Voltammetry (AdTSV), target molecule is strongly absorbed on the electrode surface at an open electrode circuit, then by using a rinsing buffer the electrode is washed and thereafter is transferred to the supporting electrolyte.[81]
[10] Alternating Current Voltammetry (ACV), is one of the powerful techniques used for quantitative evaluation of the mechanisms of electrodes.[82]
[11] Homocysteine (HCys) is an intermediate of methionine metabolism in which at it high levels could result in vascular disease and antherothrombosis.[83]

such a transport might be diverse from planar diffusion normal to the electrode surface and, rather, consists in two or three dimensional diffusion.[44] Advantages of using these electrodes can be mentioned as follows:[15,44]

1- Steady-state or quasi-steady state can be observed even in absence of supporting electrolyte. This can be obtained even in non-polar or resistive solutions with high accuracy of measurements.

2- The current-potential curves provide rapid measurements.

3- Using these electrodes can enhance the opportunity of studying fast reactions of electroactive species.

In some cases, to perform quantitative measurements in aqueous solutions, it might be convenient to increase the size of the microelectrodes, even up to a point where such a condition is no longer suitable. For instance, some authors have suggested to use radii larger than 4 mm radius, to avoid contributions of edge effect that comes from radial contributions[45] and these electrodes are clearly macroelectrodes.

2.1.3.1.2. *Rotating disk electrode (RDE)*

This electrode is one of the hydrodynamic working electrodes which consists of the electrode disk (commonly platinum wires) fixed in a rod of isolating material.

Through three transport phenomena molecules can arrive to the surface of these electrodes: convection, migration and diffusion. Convection is the movement of bulk fluids which could happen as a result of using physical means such as stirring and boiling. Migration occurs when an ion is attracted or repulsed by a charged surface. And diffusion takes place when atoms or ions move from a region with high concentration to a region with low concentration. Among these three ways of ion transport, in the case of RDE, convection is the most relevant phenomena. Now let us simplify the effect of convection by considering that increasing the rotation rate implies reducing the diffusion layer. As can be seen in the figure 2-4 if the applied potential is high enough, the analyte will arrive to the surface of the electrode and react very fast, so the concentration of the analyte will become almost close to the zero. The higher is the difference between the concentration of the analyte in bulk solution and the concentration of the analyte at the surface of the electrode, the higher is the rate of arrival of the diffusing analyte from the bulk solution to the surface of the electrode [14] The diffusion layer will be decreased if the disk electrode spins faster and consequently the diffusion current will be higher.[14]

In the figure below, the symbol δ represents the thickness of the layer. From this figure we see that we are assuming that the analyte arrives to the layer just by diffusion.

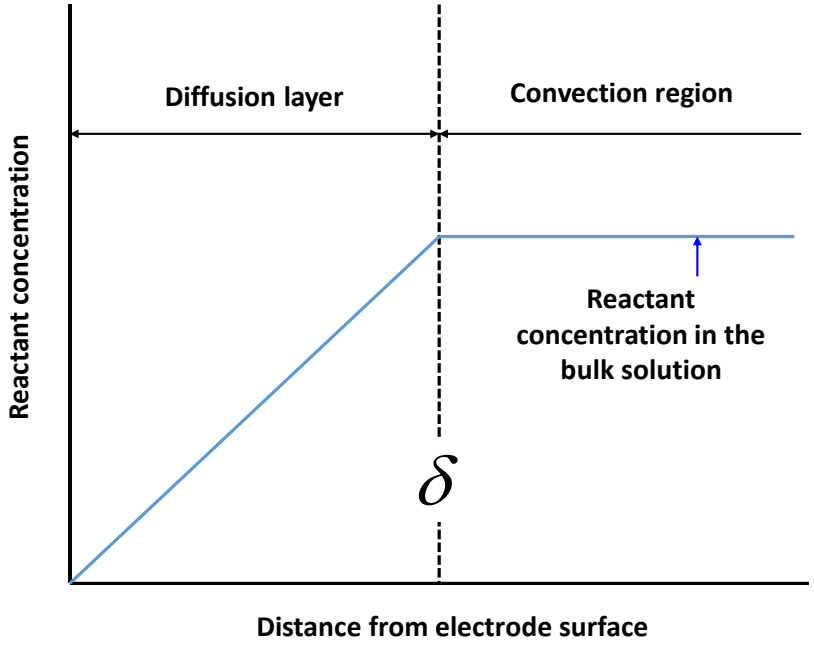

Figure 2-4: Schematic concentration profile of an analyte close to the surface of the RDE when the potential is high enough to reduce the concentration of an analyte to 0 at the surface of the electrode. This figure is adapted from reference [14].

$$\text{Current} \propto \text{rate of diffusion} \propto [C]^{*} - [C]^{0} \qquad (2\text{-}4)$$

In the equation above, the symbol $\propto$ means that the current is proportional to the rate of diffusion and to the difference between the concentrations. $[C]^{*}$ stands for the concentration of analyte in the bulk solution while $[C]^{0}$ reflects the concentration of analyte at electrode surface.

Hence, in a case that the rate of reaction is sufficiently fast and the applied potential is high enough, the equation will change:

$$\text{Diffusion current} \propto [C]^{0} \qquad (2\text{-}5)$$

The advantage of the RDEs is that they have a very simple structure which includes a rotating disk imbedded in a rod of insulating material[22] and, also, the rapid rotation of these disks supplies fresh analyte to the surface of electrode very fast.[14] Indeed, the reduction of the thickness of diffusion layer can increase the fluxes and consequently lower the LOD that could be achieved.

At high rotation of the disk, two factors are important: the configuration of the insulating material and the arrangement of the disk embedded in it. At high rotations, turbulences and spiral formations might appear and this can cause problems during the measurements. Also it is crucial to be sure that there is no leakage of the solution between the electrodes and the insulating material. [22]

2.1.3.1.3. Mercury drop electrodes (SMDE and HDME)

The invention of the Static Mercury Drop Electrode (SMDE) was one of the important factors that caused polarography to develop (see chapter 7 in [22]). This electrode is designed in a way that after the voltage and current are measured, the drop is dislodged by a drop knocker and falls down from the tip of the capillary. Then, the electronically-controlled valve remains open for 30-100 ms and during this short period of time a new drop is formed (see figure below).

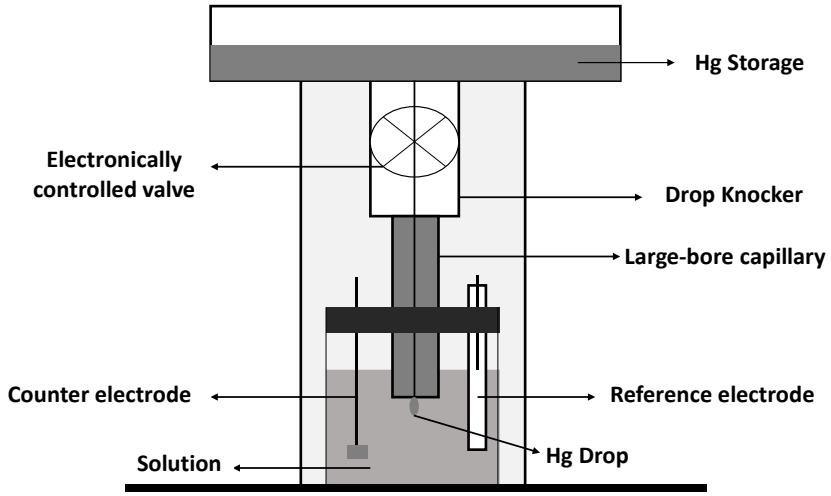

Figure 2-5: Schematic diagram of the static mercury drop electrode. Adapted from [22]

SMDE can serve as Hanging Mercury Drop Electrode (HMDE). The difference is that in SDME the drop falls down consistently after each measurement, while in HMDE the whole potential program is applied in a unique drop.[22]

Now let us consider their applications, advantages and disadvantages.

These electrodes have been applied widely in the reduction of organic and inorganic electroactive compounds.[46] SDME has been used in pulse polarographic techniques (polarography is a subclass of voltammetry), and electrocapillary studies (that follow the study of changes in interfacial tension of the dropping mercury electrode as the electrode

potential varies), while HMDE electrodes have been applied [47] in stripping analysis (explained in section 2.1.3.3.) and cyclic voltammetry (discussed in section 2.1.3.4.).

Special properties of dropping mercury electrodes such as their renewable electrode surface and wide cathodic potential range, made polarography techniques useful for determining different species. When SMDE is used, the continuous formation of the drop prevents any difficulties that might arise through the progressive passivation process on the surface of the electrode. In fact it has been reported that at negative potential regions (0.0 to -1.8V vs. Saturated Calomel Electrode (SCE)) passivation of some metals often occurs, therefore the electrode surface of solid electrodes needs to be regenerated periodically, but with SMDE or HDME each new drop is a new surface. Additionally the accumulation of some metals (such as Ni, Cu and Fe) on the surface of solid electrodes can affect the measurements, causing a decrease in the overvoltage of hydrogen (large hydrogen overvoltage exists in mercury electrodes) and increase the background current.[48] Hydrogen overvoltage can be explained as the difference of the potential between a reversible hydrogen electrode and an electrode in the same solution. In such a situation H_2 is being formed from hydrogen ions. In other words, we can say that hydrogen overvoltage is related to the fact that H^+ (despite being in negative potentials), due to some kinetic limitation at the Hg electrode, does not becomes H_2 at this surface.[49]

The other advantages of the mercury electrode is its simplicity and trustable results which could be more apparent if the capillary is placed in a correct position and its maintenance is proper enough.[47] The main disadvantage of the SMDE electrodes is its high consumption of the mercury and higher charging current, so for these reasons HMDE electrodes are more used. In fact, not only HDME electrodes are capable of eliminating such problems, but also can provide other positive points such as increasing the reproducibility of the results, and decreasing the possibility of adsorbing electrolytic accumulations of analytes on the surface of electrode. Nevertheless, there exists the risk of operator poisoning (as a result of using mercury) and sometimes the drops are dislodged out of the proper time.[46] Hence, it is important to take care while working with these electrodes and to find a way to overcome the problems mentioned above.

2.1.3.2. Pulse techniques

These techniques are aimed to reduce the detection limits of voltammetry measurements. In fact, the limit of quantification can be reduced to 10^{-8} mol L^{-1} as a result of increasing the ratio between faradaic and non-faradaic currents.[47] Here we will discuss

two variants of pulse polarography: Normal Pulse Polarography (NPP) and Differential Pules Polarography (DPP).

2.1.3.2.1. *Normal Pulse Polarography (NPP)*

This technique has been widely used to determine low concentrations of metals in environmental samples [22] and it is based on series of pulses. During the first step ($t<t_0$), the base potential (E_b) is sufficiently positive to prevent any electrochemical reaction. During most of the life of each mercury drop, the electrode is kept at the base potential (E_b) in which partial electrolysis does not appear.[22] At t_0 the potential changes to the new value E_i which is applied during the time t_p (about 50 ms). Next successive drops have new potentials E_i increasingly negative which can cause a very intensive reduction of the electroactive species at the electrode.[50] τ is the time at which the current will be measured (slightly before the end of the drop life) and (for DPP) τ' is the time of a measurement at the end of the base potential period.[22] Figure 2-6 supports this explanation.

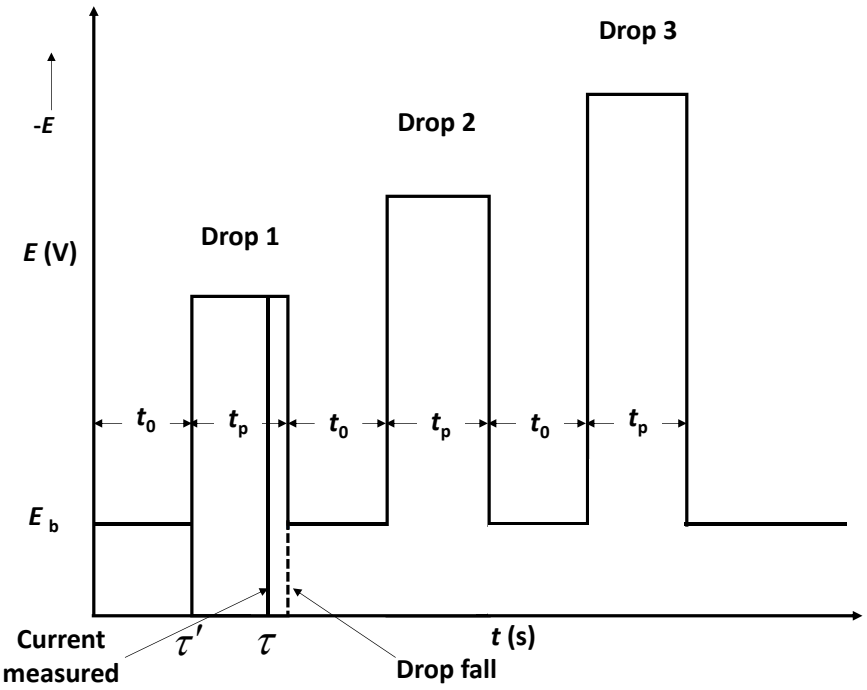

Figure 2-6: Potential program for three drops in a normal pulse polarographic experiment. Adapted from references [22,50]

Figure 2-7 is a schematic representation of an NPP polarogram where the abscissae axis is inverted for a case without electrodic absorption. I_l stands for limiting current which happens when there is no variation in the current although the potential becomes more negative. Diffusion limited conditions occur when the potential is very reductive

and the concentration of the electroactive species drops to zero at the surface of the electrode. During this process the current is regulated by the diffusion of the electroactive species across the solution.[50]

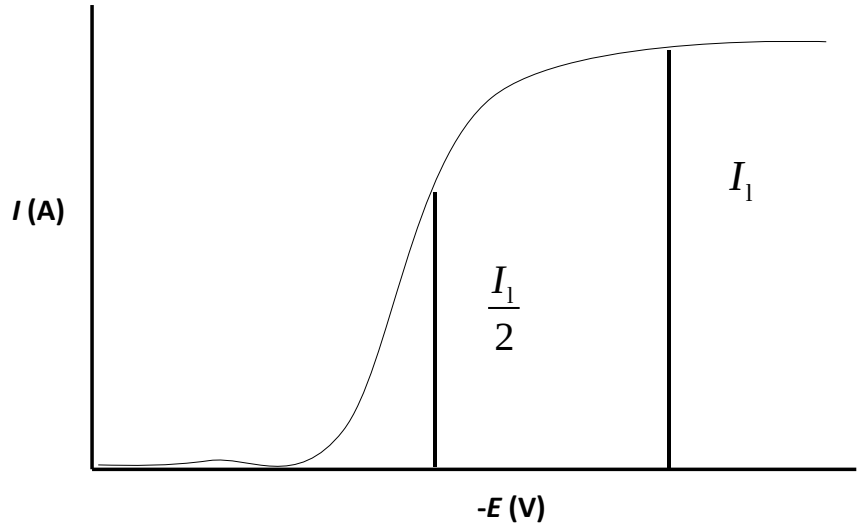

Figure 2-7: Typical wave in one NPP experiment after discounting the capacitive current. The figure is adapted from the reference [50].

2.1.3.2.2. *Differential Pulse Polarography (DPP)*

Differential pulse polarography is a polarographic technique (i.e. based on the use of a static mercury drop as working electrode) whose potential program is a series of separated potential steps.[22,51] Figure 2-8 shows that the potential program is a combination of a linear ramp with a superimposed square wave. During the life of each drop, two potentials are applied: the base potential E_b during a time denoted t_0 (first pulse) and the potential $E_b + \Delta E$ during a time $t_p = t_d - t_0$ (second pulse or pulse width). The polarogram takes, for each drop, the $E_b + \Delta E$ potential as abscissa while, for ordinate, it takes the difference between two current samples: one immediately before the time t_0 and the other just before the end of the drop lifetime (t_d).

In uncomplicated systems (i.e. just metal ions and background electrolyte with negligible complexation), the height of the peak is proportional to the free metal ion concentration (which is also the total metal concentration), but such proportionality vanishes -in general- when the metal is complexed. Relatively cumbersome mathematical expressions are needed to describe the differential pulse polarogram, even in cases without electrodic adsorption.

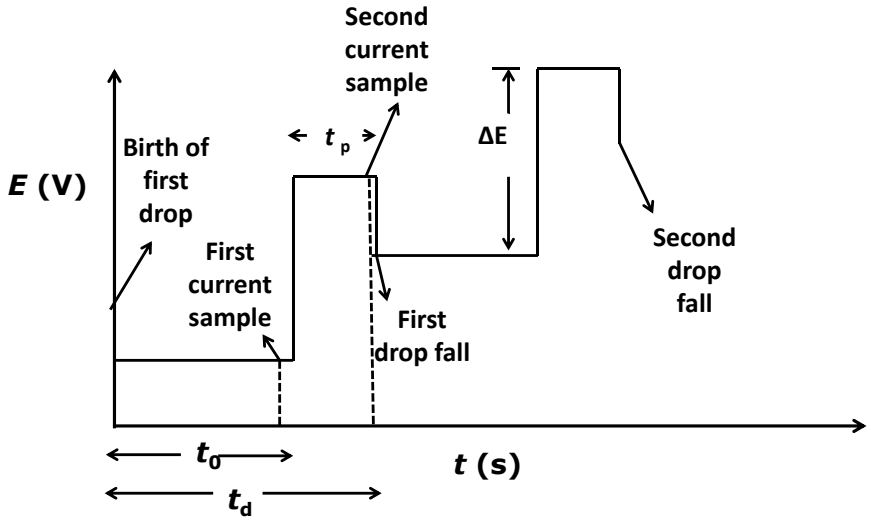

Figure 2-8: Potential program for two drops in a differential pulse polarographic experiment. Adapted from reference [22].

Assuming a reversible redox couple and planar electrode, the peak potential (Epeak) or position of the maximum of the polarogram can be computed (see page 295, section 7.3 equation (7.3.30) in 22) with

$$E_{\text{peak}} = E^{0'} + \frac{RT}{nF}\ln\sqrt{\frac{D_{M^0}}{D_{M^{n+}}}} - \frac{\Delta E}{2} \qquad (2\text{-}6)$$

where E°' is the standard formal potential of the redox couple, R is the gas constant, T is the temperature, n is the number of exchanged electrons, F is the Faraday constant, D_{M^0} is the diffusion coefficient for the reduced metal inside the amalgam, $D_{M^{n+}}$ is the diffusion coefficient for the free metal ion in solution and ΔE is the modulation amplitude (or pulse height).

DPP is an ancillary technique for AGNES because the gain can be computed from E_{peak} for several analytes (Zn, Cd, Pb, Sn).

Complexation of the electroactive metal (with ligands including OH^-) changes the position of the DPP peak and its height. So, in the particular case of indium, a low pH (such as 3) is convenient to avoid an impact on E_{peak} due to the formation of indium hydroxides.[52] DPP will be used in chapter 3, sections 3.3.2 and 3.4.1.

2.1.3.3. Anodic Stripping Voltammetry (ASV)

In stripping techniques three steps could be observed.

- Deposition.
- Rest period.
- Stripping.

Essentially, in this technique there should be a long deposition stage to pre-accumulate the analyte, followed by a short stripping stage to measure the current.

ASV is one of the most used methods among stripping techniques in voltammetry. In this process, metals will be electroplated on the surface of the electrode (or inside the amalgam electrode) during a relatively long deposition step. Convection and diffusion with stirring can help the ions to reach the surface of the electrode, where they will be reduced and preconcentrated. The needed time for the deposition step can be controlled from the minimum 0.5 min (for the concentration of the metal around 10^{-7} M) up to 20 min (for the concentration of the metal around 10^{-10} M).[47]

When the potential is scanned anodically, the stripping step can be applied in various forms such as linear, pulse, square wave or staircase.[47] Along the anodic scan, the amalgamated metals will be re-oxidized and stripped out of the electrode.

Figure 2-9 represents a schematic view of an Anodic Stripping Voltammogram of an indium solution using the deposition time 30 s (which is related to the ASV presented in figure 5-1 in chapter 5). a) Represents the deposition step, E_d is the applied potential -1.30 V and during this step indium is electroplated at the surface of the electrode (from where it diffuses inside the amalgam). Then the stirrer will be turned off and the rest period (b) will start. In the rest period the solution will be allowed to become quiescent and the concentration of indium inside the amalgam becomes more stable. A typical time for this period is t_w = 5 s. Thereafter the process will be continued to the stripping step (c), in which the linear scanning of the potential will start from negative potentials to the more positive ones. The time that is needed for scanning is represented with t_s (e.g. 15 s). E_p is the peak potential (which is close to -0.51 V for indium) and I_p is the peak current.

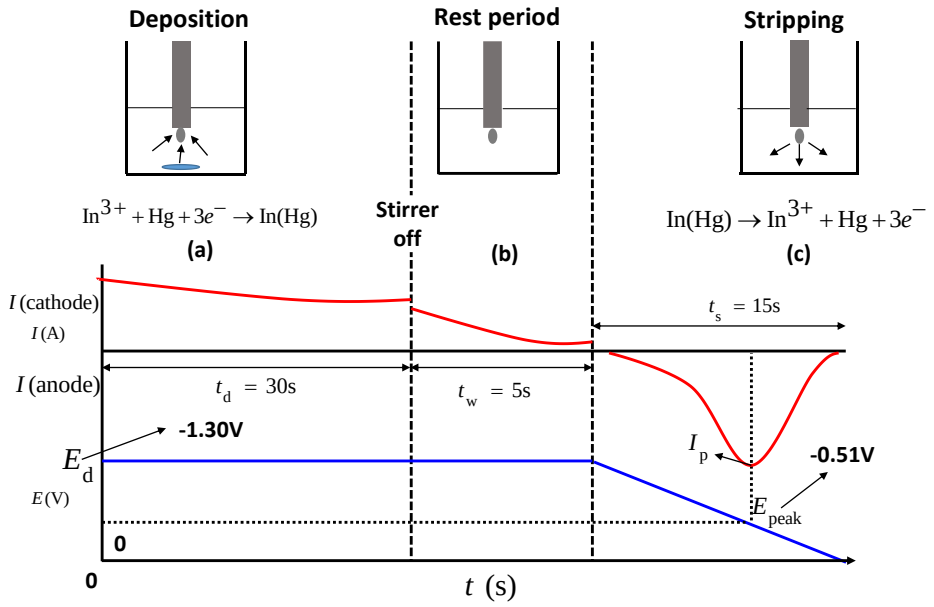

Figure 2-9: Schematic representation of the three steps of Anodic Stripping Voltammogram. The input program (blue graph) is related to figure 5-1 in chapter 5 using the deposition time (t_d) 30 s. a) Deposition step, b) Rest period (when the stirrer is off) and c) Stripping step. E_d is the potential applied in the deposition step which is equal to -1.3 V and E_{peak} represents the peak potential around -0.51 V. t_w stands for waiting period which is equal to 5 s and t_s represents scan time which is 15 s. The measured I_{peak}= 2.5×10^{-6} A. This figure is adapted from reference [22].

The peak current can, for simple systems, be calculated using the equation below.

$$I_p = 2.72\times10^5 n^{3/2} A D^{1/2} v^{1/2} \left[M^0\right] \quad (2\text{-}7)$$

Symbols *A* and *D* represent the area and the diffusion coefficient, respectively and, *v* (in V/s) is the potential scan rate during the stripping process .[47]

ASV can be categorized as one of the most useful methods for determining ions, but there are some issues needed to be taken into account when ASV is performed. For instance, overlapping stripping peaks can derive from the similarity in oxidation potentials of some metals such as Pb, Tl, Cd, Sn or Bi, Cu and Sb. Also adsorption of surface-active organic compounds on the mercury electrode is another negative point, since this can impact on the metal deposition and reoxidation. Moreover, it is important to indicate that the position and size of the peak can be affected when intermetallic compounds such as ZnCu are present.[47] In chapter 5, sections 5.4.1., 5.4.6. and 5.4.7. ASV results for solutions containing indium are presented and discussed.

2.1.3.4. Cyclic Voltammetry (CV)

Potential sweep methods are widely used to study electrode processes. One of the variants is Cyclic Voltammetry (CV), where the sweep direction is inverted at a certain chosen potential.

The applied potential is varying within time in a symmetrical saw-tooth wave form[53] as shown in figure 2-10.

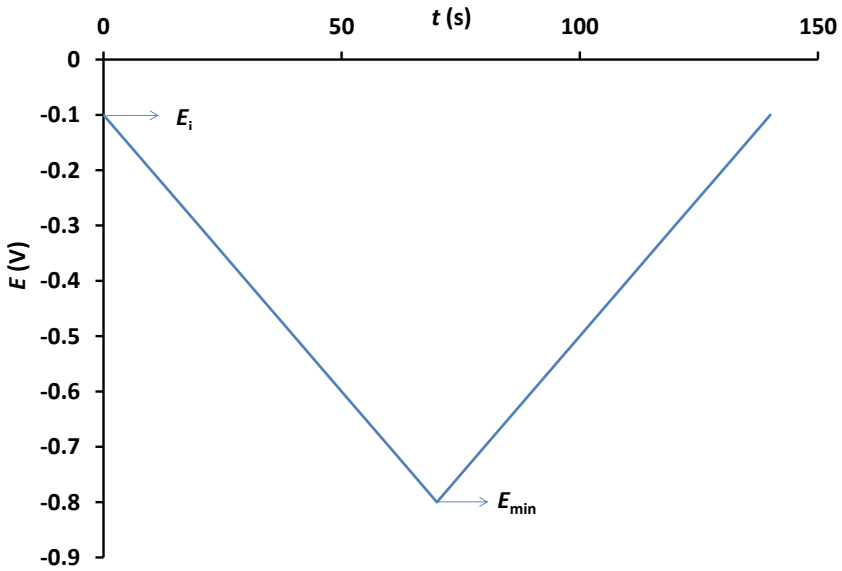

Figure 2-10: Variation of the applied potential with time in cyclic voltammetry, showing the initial potential, E_i = -0.100 V, and the return potential E_{min}= -0.800 V. Adapted from reference [53].

In this technique, as can be seen in figure 2-11, the resulting current is recorded over the whole cycle of forward and reverse sweeps. Indium species reduced in a forward scan of each cycle can be re oxidized in the reverse scan, hence two (cathodic and anodic) peaks appear which can be identified with the reduction and oxidation processes, respectively. E_{pc} represents the cathodic potential while E_{pa} stands for anodic potential. More details about the calculations will be discussed in chapter 3, sections 3.3.2. and 3.4.1.

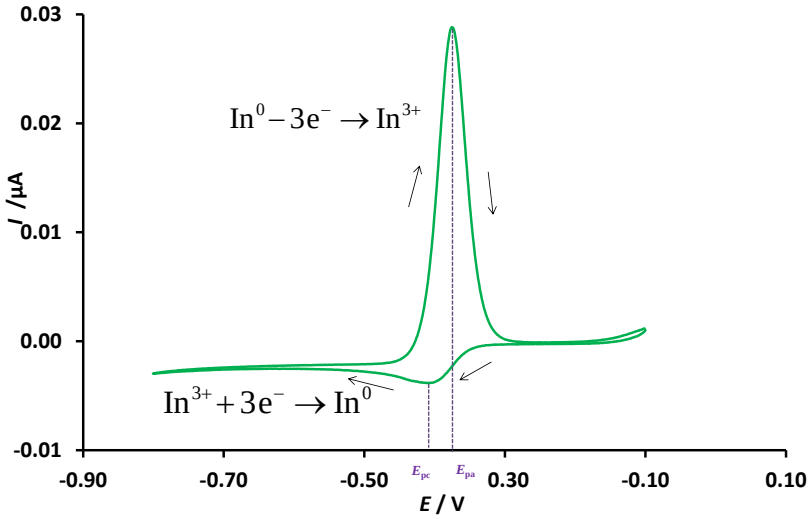

Figure 2-11: Cyclic voltammogram applied to a solution with indium. $c_{T,In}$=1.00 µmol L^{-1} at pH=3 between -0.1V and -0.8V, scan rate 10 mV/s.

2.2. Instrumentation used for experiments

Voltammetric measurements were carried out with Autolab µAUTOLAB type III , PGSTAT10 and PGSTAT101 potentiostats attached to Metrohm 663 VA Stands. All experiments were performed using GPES 4.9.007 (Eco Chemie) and NOVA 1.11 (Metrohm Autolab) softwares.

As can be seen in figure 2-12, the working electrode was a Metrohm Hanging Mercury Drop Electrode (HMDE). Glassy carbon was used as the auxiliary electrode and the reference electrode was double-junction Ag/AgCl/3 mol L^{-1} KCl with KNO_3 0.1 mol L^{-1} in the salt bridge. A glass jacketed cell was used in all the experiments and thermostated at 25.0°C.

A glass combined electrode (Crison, 5209) was attached to an Orion Dual Star ion analyzer (Thermo) and introduced into the cell to measure and, accordingly, control the pH.

Figure 2-12: Voltammetric cell with stirrer, double-junction Ag/AgCl/3mol L^{-1} KCl, Metrohm Hanging Mercury Drop (HMDE) and Glassy carbon were used as reference, working and auxiliary electrodes, respectively.

Figure 2-13 shows a glass cell, Autolab potentiostat and Metrohm polarographic stand all contected to the computer and ready to start the experiment.

Before starting the experiments, purging with purified water-saturated nitrogen N_2 (purity > 99.999%) was necessary not only to spare a large signal from oxygen reduction, but also to avoid dramatic pH increases close to the electrode surface which would lead to indium hydrolysis.[54,55]

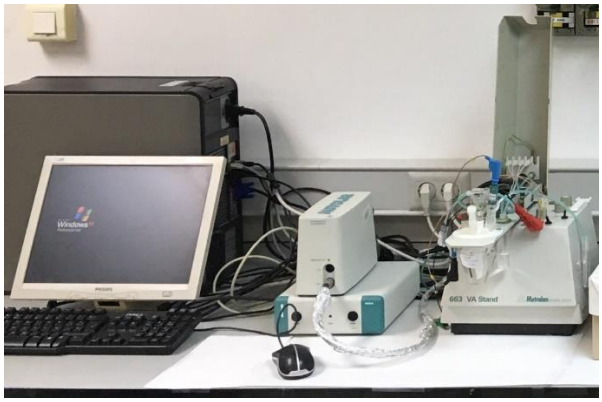

Figure 2-13: Equipment used for the measurements including glass cell, Autolab potentiostat and Metrohm polarographic Stand.

2.3. Techniques developed in this thesis

2.3.1. AGNES

AGNES (Absence of Gradients and Nernstian Equilibrium Stripping) is an electroanalytical technique that, up to now, has been used -with mercury electrodes- to determine free concentrations of amalgamating elements such as Zn, Cd and Pb in various samples.[34,35,56–58]

2.3.1.1. Fundamentals of AGNES

AGNES is a stripping technique consisting of two stages with specific goals. We detail here its principles and implementation considering indium as the target analyte.

2.3.1.1.1. *First stage: Absence of Gradients in the concentration profiles and Nernstian Equilibrium at the electrode surface*

The aim of this deposition stage is to reach a special situation of equilibrium, where two conditions have to be fulfilled: i) Absence of Gradients in the concentration profiles and ii) Nernstian equilibrium at the electrode surface. The deposition is due to the reaction:

$$In^{3+} + 3e^- \rightarrow In^0(Hg) \qquad (2\text{-}8)$$

About condition i): Absence of Gradients. Figure 2-14 shows a schematic representation of the desired concentration profiles. As can be seen in this figure, in the mercury electrode we want a uniform concentration of reduced indium and a flat concentration profile of free indium cation in the solution.

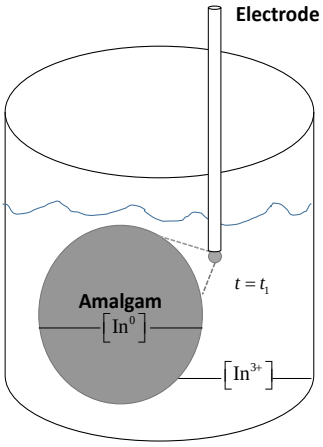

Figure 2-14: Profiles aimed at the end of the first step ($t=t_1$).

About condition ii): Nernstian equilibrium for the redox couple (e.g. In^{3+}/In^0, in this work). The concentrations of the oxidized and re-oxidized species of indium at the electrode must fulfil Nernst equation, which can be written as:

$$E = E^0 + \frac{RT}{3F} \ln \frac{a_{In^{3+}}}{a_{In^0}} \qquad (2\text{-}9)$$

where E^0 is the standard redox potential and a_j is the activity of species j. When equilibrium is reached, Nernst equation can be re-written in terms of concentrations as

$$Y = \frac{\left[\mathrm{In}^{0}\right]}{\left[\mathrm{In}^{3+}\right]} = \exp\left[-\frac{3F}{RT}\left(E_1 - E^{0'}\right)\right] \qquad (2\text{-}10)$$

where Y is the gain or preconcentration factor, which represents the proportionality between the reduced indium concentration in the amalgam and its free form in the solution. E_1 is the deposition potential associated to the gain Y and $E^{0'}$ stands for the formal redox potential.

There are several ways to reach the two equilibrium conditions (i and ii). The simplest one is the 1P strategy, where the same potential E_1 is applied all along the first stage, while waiting for as long time (t_1) as needed to achieve the goal of the two equilibrium conditions. Figure 2-15 shows a scheme of the 1P strategy. Usually, the potential E_1 is just a few millivolts more negative than the standard redox potential of the couple, so that moderate gains are aimed, because larger gains require longer deposition times.

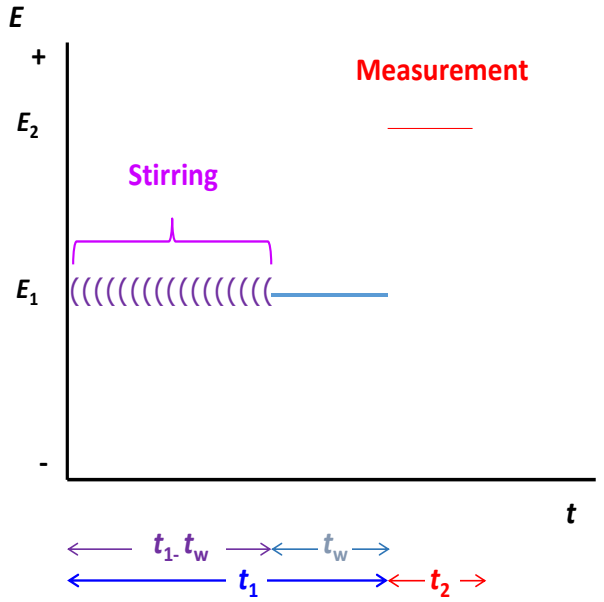

Figure 2-15: Representation of the simplest potential program (i.e. using one potential pulse, 1P) for the first stage. E_1 is the deposition potential associated to the concentration gain Y. In the variant AGNES-I, E_2 corresponds to a potential for a re-oxidation under diffusion limited conditions. t_w is the duration of the period of no stirring at the end of the deposition time.

Alternatively, especially for large Y, one may use the refined strategy "2 pulses" (or 2P). In this methodology, two potentials: $E_{1,a}$ and $E_{1,b}$ are applied in two sub-stages of the deposition stage, see figure 2-16. In the first sub-stage $E_{1,a}$ (prescribing diffusion limited conditions for deposition, which might be associated to an aimed gain $Y_{1,a}$ which will never be attained) is applied during $t_{1,a}$. In the second sub-stage, the potential $E_{1,b}$

(corresponding to the desired gain *Y*) is applied during $t_{1,b}$ (which could be called "relaxation time").

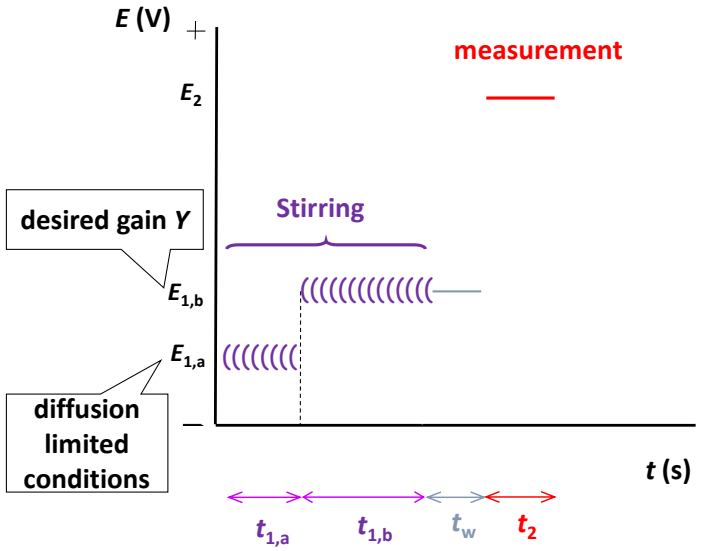

Figure 2-16: Schematic representation of the potential and stirring program using two potential sub-steps in the first stage (AGNES-2P). The total deposition time t_1 is the summation of the first potential step time $t_{1,a}$, the second potential $t_{1,b}$ and the waiting time t_w.

To enhance mass transport, stirring is activated along most of the deposition stage. See table 2-2 with the specification of the periods where stirring is on.

Table 2-2: Combination of parameters for the two strategies available for the first stage (1 Pulse and 2 Pulses) of AGNES.

a: Parameters for 1P

	Stage	Time	Stirring	Potential	Gain
1 *P*	Deposition	t_1-t_w	On	E_1	Y=Y_1
		t_w	Off	E_1	Y=Y_1
	Stripping	t_2	Off	E_2	Y_2

b: Parameters for 2P

	Stage	Time	Stirring	Potential	Gain
2 *P*	Deposition	$t_{1,a}$	On	$E_{1,a}$	$Y_{1,a}$
		$t_{1,b}$	On	E_1	Y=$Y_{1,b}$
		t_w	Off	E_1	Y=$Y_{1,b}$
	Stripping	t_2	Off	E_2	Y_2

After the application of the first sub-stage in 2P, three situations can arise: undershoot, equilibrium or overshoot. The undershoot appears when the number of moles accumulated during the first sub-stage (i.e. throughout the time $t_{1,a}$) is less than those needed for equilibrium. The overshoot appears when the number of moles is greater than those needed. Using the 2P strategy there is a reduction of the deposition time (with respect to the 1P strategy) that might even reach a factor of ten, if $t_{1,a}$ is optimally chosen. Figure 2-17 shows how a large overshoot can be spotted in the currents recorded during the first stage of a 2P experiment.

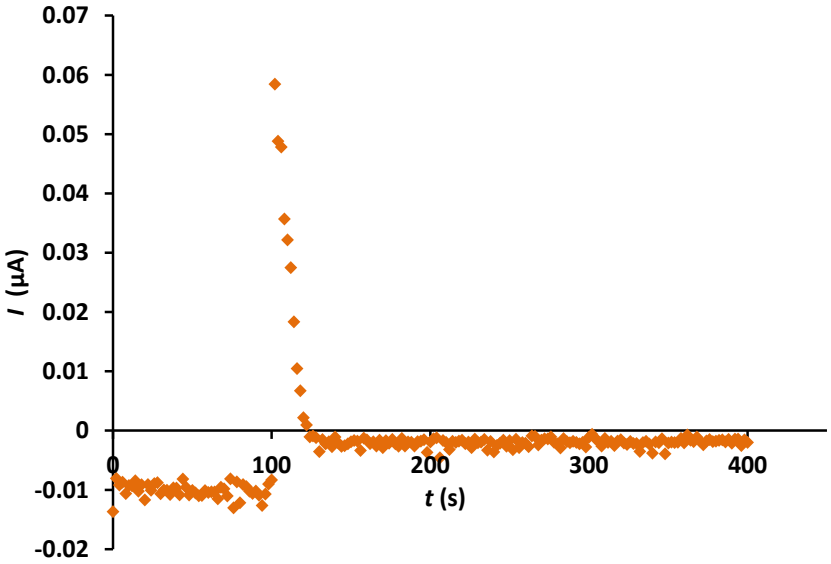

Figure 2-17: Currents recorded during the first stage of a 2P experiment. $Y_{1,a} = 10^{10}$; $Y=50$; $t_{1,a}=100$ s; $t_{1,b}=300$ s; $c_{T,In}=4.97\mu mol\ L^{-1}$, $c_{T,Ox}=69\mu mol\ L^{-1}$ *and pH=3.00.*

To check whether a given $t_{1,a}$ produces overshoot, undershoot or equilibrium in our system, one can compare experiments with various $t_{1,b}$. See figure 2-18. If experiments with longer $t_{1,b}$ produce higher analytical responses (in the stripping stage), one concludes that the applied $t_{1,a}$ has been too short (i.e. undershoot). If longer $t_{1,b}$ produce lower analytical responses, one concludes that the applied $t_{1,a}$ has been too long (i.e. overshoot).

Regardless of which strategy (1P or 2P) is adopted for the first stage, it is convenient to use small electrodes, as the required deposition time increases with the size of the electrode.[59] So, drop size 1 -the smallest in our stand- is selected to reach to the equilibrium faster. Its approximate radius is 141 µm.

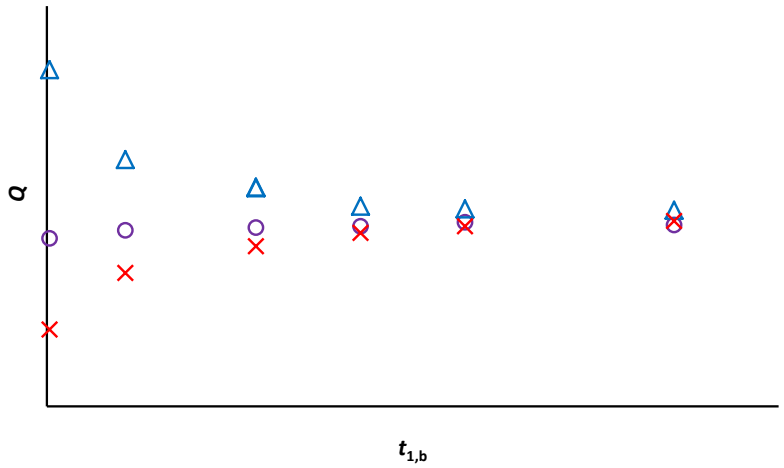

Figure 2-18: Schematic representation of possible situations for the first sub-stage of 2P experiments, as seen from the stripping charges (Q) in three series of experiments (each characterized by a given $t_{1,a}$) along increasingly long relaxation times ($t_{1,b}$). The markers triangle, circle and cross, exhibit overshoot, equilibrium and undershoot situations, respectively. The series indicated with triangle markers are associated to a $t_{1,a}$ larger than the optimum one (for the aimed gain), while the cross series are associated to a too short $t_{1,a}$.

2.3.1.1.2. *Second stage: quantification of the reduced indium inside the amalgam*

The goal of the second stage is to quantify how much In^0 has been accumulated in the amalgam during the first stage. There are different ways to achieve the goal of this second stage, which lead to the variants AGNES-I, AGNES-Q, AGNES-SCP and AGNE-LSV.[56,57]

In AGNES-I, the metal is reoxidized at a constant potential under diffusion limited conditions, then the current is measured and the calibration and measurement can use the equation below.

$$I = Y\eta\left[\mathrm{In}^{3+}\right] \tag{2-11}$$

Some irreversible systems (e.g. those with Zn) can also be analyzed with AGNES-I [33], because the reoxidation potential can be sufficiently more positive than the standard redox potential (to overcome the irreversibility and reach diffusion limited conditions), without reaching a potential where the reoxidation interference of other cations (e.g. Cd) occurs.

Also for studying indium we could use AGNES-I as well, by using a much more positive potential to prevent any irreversibility, but a problem might be the interference of Pb. The standard redox potential of Pb and In are very close to each other, in fact this value for Pb is -0.317 V and for In is -0.510 V.

Hence to prevent any interference from Pb [60–62] and from the slight irreversibility (more details about the semi irreversibility of indium can be found in section 3.4.1 of chapter 3) of the indium couple, we used a fixed reoxidation potential E_2= -0.450 V (vs. Ag/AgCl) in AGNES-Q (this value of E_2 was chosen from an ASV).

In AGNES-Q the stripped charge is measured during a very long stripping time (t_2) at constant re-oxidation potential (E_2). All accumulated moles of In^0 will be stripped out (full discharge of In^0) from the amalgam to have the total faradaic charge. This total charge cannot be affected by any kinetics because the stripped charge is the one that corresponds to the total number of moles of In^0 in the amalgam. When all this In^0 is stripped, the speed at which this stripping is happening is irrelevant (as long as we wait long enough for the complete stripping).

Once discounted the blank (i.e. the capacitive charge in an experiment with no analyte, just background electrolyte)[57] from the total charge, one obtains the faradaic charge (Q). According to Faraday's law, one can write:

$$Q = 3F(\text{moles in amalgam}) = 3FV_{\text{Hg}}\left[\text{In}^{\text{o}}\right] \tag{2-12}$$

By defining the proportionality factor as

$$\eta_{\text{Q}} = 3FV_{\text{Hg}} \tag{2-13}$$

and combining with equation (2-11)

$$Q = \eta_{\text{Q}} Y[\text{In}^{3+}] \tag{2-14}$$

This expression indicates the direct proportionality between faradaic charge and the free concentration of indium in the solution.

In AGNES-Q, during the second stage, the current is sampled at short time intervals (e.g. each 50 ms) and it is recorded into a file (see figure 2-19). The integration of these currents provides the charge. Because of the existence of traces of oxygen and other interferents we need to subtract I_∞ (which is taken from the average of the last 20 points of the stripping process).[57]

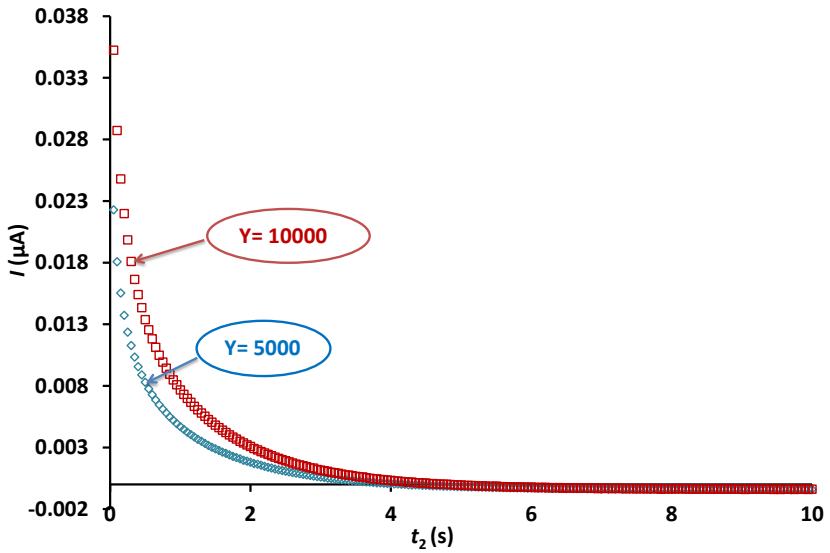

Figure 2-19: Stripping currents during the second stage. $c_{T,In}$ =10.3 µmol $L^{-1}$and $c_{T,NTA}$=12.2 µmol L^{-1}, square marker represents the results using higher gain while the diamond marker stands for the results using lower gain.

In practice, Q is just the summation of the cells containing the faradaic intensities I_j (once we have subtracted I_∞) multiplied by the fixed interval time (Δt) in an Excel file:[63]

$$Q = \int_0^t I\ dt\ \approx \Delta t\left(\sum_{j=1}^{n_{max}} I_j\right) \tag{2-15}$$

n_{max} is the number of intervals taken (usually 1000 intervals corresponding to the 50 s of t_2).

In AGNES-SCP, during the transition time τ (re-oxidation time), a constant oxidizing current I_s is being applied. In AGNES-SCP, electrons that result from the oxidation of M^0 and from the discharging process (of the electrode that functions as a capacitor), all can be consumed by oxidants such as oxygen molecules or any other interfering cations (also named the electroless effect) or provided as I_s (see equation (2-20)).[27]

$$I_s = I_{faradaic} + I_{Ox} + I_{cap} \tag{2-16}$$

Hence, as can be seen in the equation above, the imposed stripping current (I_s) can be calculated as the summation of the faradaic current ($I_{faradaic}$), the current due to oxidants (I_{ox}) and the capacitive current (I_{cap}).

The faradaic current will be calculated using the expression below:

$$Q = (I_s - I_{ox})\tau \tag{2-17}$$

So, this type of variant of AGNES is more useful when we cannot consider only our analyte. In another words, other electroactive metals also exist.

In AGNES-LSV, LSV stands for Linear Stripping Voltammetry. In this version of AGNES, the stripping current is recorded when the potential is being scanned at a constant rate.[57]

Complexation of the electroactive metal with ligands in the solution (including OH^-) does not impact on the equilibrium analytical response of AGNES, neither charge nor intensity, provided one is comparing solutions having the same free metal ion concentration. Moreover, the presence of ligands can only shorten the needed deposition time, as (if they are not totally inert) they might contribute to the flux that builds up the required amount of reduced metal in the amalgam.[33,58]

2.3.1.2. AGNES applications

In a recent review, it has been indicated that AGNES is a proper technique to determine free concentrations of amalgamating elements such as (Cd, Pb, Zn, Sn, Sb and Cu) and could be a good option for measuring free concentrations of other metals (eg. Tl and Ga). Additionally, there is a great potential to improve its application using solid electrodes (eg. Cu on gold electrode and Pb on BiFE, Bismuth Film Electrode).[56]

We can report that AGNES technique has been successfully applied for determining free concentrations of metals in a wide range of systems such as natural samples (seawater,[35] river water,[64,65] estuarine water,[36] solutions containing dissolved organic matter,[66,67] soil extracts)[64] and in systems containing nanoparticles.[57,68–75]

Also AGNES has been successfully applied to measure free metal ion concentrations in different systems. In a recent review, details on the applications of AGNES and its comparison with some other chemical methods have been presented.[56] Table 2-3 gives more information about some of the investigations that have been done using the technique AGNES in different systems.

Table 2-3: Some applications of AGNES.

Analyte	System	Type of electrode	Comments	source
Cd	NTA	HMDE	Basic principles of AGNES were described	58
Zn	NTA EDTA Oxalate	HMDE	AGNES 2P was developed. Irreversibility and precipitation did not affect AGNES results	33
Cd/ Zn	Aldrich Humic Acid	HMDE	AGNES results described with NICA Donnan model	34
Zn	Wine and synthetic solutions	HMDE	AGNES results were in agreement with DMT (Donnan Membrane Technique)	77
Zn	Coastal Mediterranean seawater	HMDE	First application of AGNES to seawater.	35
Zn	Rhine water and Dutch soil extracts	HMDE	AGNES results were in agreement with DMT results	64
Cu	Malonic and Iminodiacetic acids	VGME (Vibrating gold microwire electrode)	For the first time Au-electrode was used in AGNES.	78
Cd, Zn and Pb	Oxalate and NTA	HMDE and SPE (Screen Printed Electrode)	AGNES-SCP was developed.	27

2.3.2. ADLC

ADLC (Accumulation under Diffusion Limited Conditions) technique has been developed by our group and up to now has not been published.

In this technique, we apply an extremely negative potential during a time $t_{1,a}$ and then we measure the charge in the stripping stage. This charge is equal to the charge accumulated in the deposition stage and is proportional to the steady-state flux (under diffusion limited conditions) and $t_{1,a}$.

$$Q = nFAJt_{1,a} \tag{2-20}$$

(if we neglect the short transient).The negative potential that is used in ADLC corresponds to a huge gain, similar to the one ($Y_{1,a}$) applied during the first sub-stage of AGNES-2P. Figure 2-20 provides more details about the potential program of ADLC. As it is shown in this figure, a very negative potential is applied during the time $t_{1,a}$. Then the charge that we measure in the stripping step (Q_2) equals to the accumulated charge during

the deposition stage (Q_1), which is proportional to the steady-state flux (J) and the deposition time ($t_{1,a}$).

More details about ADLC will be discussed in chapter 4, section 4.3.2.

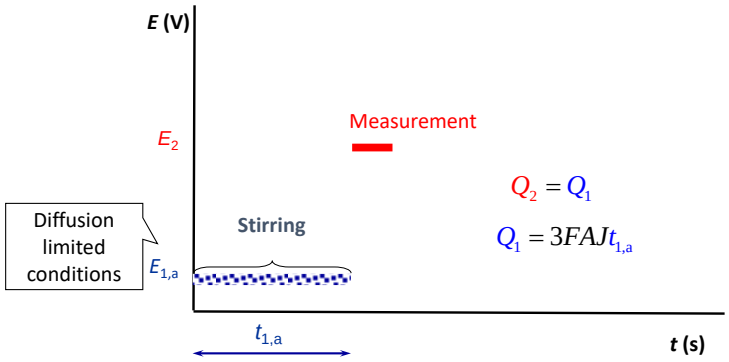

Figure 2-20: Potential program of ADLC, $t_{1,a}$ represents the needed deposition time during the stirring in the deposition stage and $E_{1,a}$ is the potential applied during the $t_{1,a}$.

2.4. Conclusions

The technique AGNES might be a proper technique to determine extremely low free concentrations of indium in different samples. The solubility of indium in mercury is very high (57%)[79] and the couple In^o/In^{3+} has a standard redox potential which is more negative than that of Hg, so such properties renders it a suitable candidate to be tackled with the technique AGNES.

The other techniques such as ASV, DPP, Cyclic voltammetry and ADLC might provide ancillary information about the behavior of indium in various samples. In the next chapters all of these aspects will be discussed more specifically.

2.5. References

(1) Tomaszewski, L.; Buffle, J.; Galceran, J. Theoretical and Analytical Characterization of a Flow through Permeation Liquid Membrane with Controlled Flux for Metal Speciation Measurement. *Anal Chem* **2003**, *75* (4), 893–900.

(2) Buffle, J.; Tercier-Waeber, M. L. Voltammetric Environmental Trace-Metal Analysis and Speciation: From Laboratory to in Situ Measurements. *TrAC - Trends Anal. Chem.* **2005**, *24* (3), 172–191.

(3) Anderson, M. .; Morel, F. M. .; Guillard, R. R. . Growth Limitation of a Coastal Diatom by Low Zinc Ion Activity. *Nature* **1978**, *276* (5683), 70.

(4) Paquin, P. R.; Gorsuch, J. W.; Apte, S.; Batley, G. E.; Bowles, K. C.; Campbell, P.

G. C.; Delos, C. G.; Di Toro, D. M.; Dwyer, R. L.; Galvez, F.; et al. The Biotic Ligand Model: A Historical Overview. *Comp. Biochem. Physiol. C. Toxicol. Pharmacol.* **2002**, *133* (1–2), 3–35.

(5) Zhao, C. M.; Campbell, P. G.; Wilkinson, K. J. When Are Metal Complexes Bioavailable ? *Environ. Chem.* **2016**, *13* (3), 425–433.

(6) Pesavento, M.; Profumo, A.; Biesuz, R.; Alberti, G. Ion Exchange Complexing Resins as Sensors for the Determination of Free Metal Ion Concentration at a Low Level. *Solvent Extr. Ion Exch.* **2008**, *26* (3), 301–320.

(7) Feldmann, J.; Salaün, P.; Lombi, E. Critical Review Perspective: Elemental Speciation Analysis Methods in Environmental Chemistry-Moving towards Methodological Integration. *Environ. Chem.* **2009**, *6* (4), 275–289.

(8) Filella, M. Food for Thought: A Critical Overview of Current Practical and Conceptual Challenges in Trace Element Analysis in Natural Waters. *Water* **2013**, *5* (3), 1152–1171.

(9) Hirose, K. Chemical Speciation of Trace Metals in Seawater: A Review. *Anal. Sci.* **2006**, *22* (8), 1055–1063.

(10) Hirata, S.; Hideki, T.; Masato, A. Determination of Arsenic Species in Marine Samples by HPLC-ICP-MS. *Anal. Sci.* **2006**, *22* (1), 39–43.

(11) Matsuura, H.; Hasegawa, T.; Nagata, H.; Takatani, K.; Asono, M.; Itoh, A.; Haragauchi, H. Speciation of Small Molecules and Inorganic Ions in Salmon Egg Cell Cytoplasm by Surfactant-Mediated HPLC/ICP-MS. *Anal. Sci.* **2003**, *19* (1), 117–121.

(12) Kim, J.-M.; Baars, O.; Morel, F. The Effect of Acidification on the Bioavailability and Electrochemical Lability of Zinc in Seawater. *Philos. Trans. R. Soc.* **2016**, *374* (2081), 20150296.

(13) Sánchez-Marín, P.; Slaveykova, V. I.; Beiras, R. Cu and Pb Accumulation by the Marine Diatom *Thalassiosira Weissflogii* in the Presence of Humic Acids. *Environ. Chem.* **2010**, *7* (3), 309–317.

(14) Harris, D. C. *Quantitative Chemical Analysis*, Seventh Ed.; Fiorillo, J., Anderson, V., Thorne, A., Eds.; W. H. Freeman and Company: New York, USA, 2007.

(15) Crow, D. R. *Principles and Applications of Electrochemistry*, Fourth Edi.; Chapman & Hall: Boca Raton, USA, 1994.

(16) Bühlmann, P.; Pretsch, E.; Bakker, E. Carrier-Based Ion-Selective Electrodes and Bulk Optodes. 2. Ionophores for Potentiometric and Optical Sensors. *Chem. Rev.* **1998**, *98* (4), 1593–1688.

(17) Pungor, E. The Theory of the Ion-Selective Electrodes. *PINSA* **1998**, *64* (1), 53–65.

(18) Covington, A. *Ion-Selective Electrodes*; Groves, P., Ed.; Educational techniques subject group, the royal society of chemisty: London, 1981.

(19) Dimeski, G.; Badrick, T.; John, A. S. Ion Selective Electrodes (ISEs) and Interferences-A Review. *Clin. Chim. Acta* **2010**, *411* (5–6), 309–317.

(20) Bakker, E.; Pretsch, E. Modern Potentiometry. *Angew. Chemie - Int. Ed.* **2007**, *46* (30), 5660–5668.

(21) Bakker, E.; Bühlmann, P.; Pretsch, E. Carrier-Based Ion-Selective Electrodes and Bulk Optodes. 1. General Characteristics. *Chem. Rev.* **1997**, *97* (8), 3083–3132.

(22) Bard, A.; Faulkner, L. *Electrochemical Methods: Fundamentals and Applications*, Second Edi.; Harris, D., Swain, E., Robey, C., Aiello, E., Eds.; John Wiley & sons, Inc.: New York, USA, 2001.

(23) Vanysek, P. The Glass pH Electrode. *Electrochem. Soc. Interface* **2004**, No. IF6-04, 19–20.

(24) Abbas, M. N.; Amer, H. S. A Solid-Contact indium(III) Sensor Based on a Thiosulfinate Ionophore Derived from Omeprazole. *Bull. Korean Chem. Soc.* **2013**, *34* (4), 1153–1159.

(25) Gupta, V. K.; Hamdan, A. J.; Pal, M. K. Comparative Study on 2-Amino-1,4-Naphthoquinone Derived Ligands as Indium (III) Selective PVC-Based Sensors. *Talanta* **2010**, *82* (1), 44–50.

(26) Town, R. M.; van Leeuwen, H. P. Fundamental Features of Metal Ion Determination by Stripping Chronopotentiometry. *Electroanal. Chem.* **2001**, *509* (1), 58–65.

(27) Parat, C.; Authier, L.; Aguilar, D.; Companys, E.; Puy, J.; Galceran, J.; Potin-Gautier, M. Direct Determination of Free Metal Concentration by Implementing Stripping Chronopotentiometry as the Second Stage of AGNES. *Analyst* **2011**, *136* (20), 4337–4343.

(28) Town, R. M.; van Leeuwen, H. P. Effects of Adsorption in Stripping

Chronopotentiometric Metal Speciation Analysis. *J. Electroanal. Chem.* **2002**, *523* (1–2), 1–15.

(29) Jagner, D. Potentiometric Stripping Analysis - A Review. *Analyst* **1982**, *107* (1275), 593–599.

(30) Kounaves, S. P. Voltammetric Techniques. In *Handbook of instrumental techniques for analytical chemistry*; Settle, F., Ed.; Tufts University, Department of Chemistry: Medford, Massachusetts, USA, 1997; pp 709–726.

(31) Ariño, C.; Serrano, N.; Díaz-Cruz, J. M.; Esteban, M. Voltammetric Determination of Metal Ions beyond Mercury Electrodes. A Review. *Anal. Chim. Acta* **2017**, *990*, 11–53.

(32) Protti, P. *Introduction to Modern Voltammetric and Polarographic Analisys Techniques*, Fourth Edi.; New York, USA, 2001.

(33) Companys, E.; Cecília, J.; Codina, G.; Puy, J.; Galceran, J. Determination of Zn^{2+} Concentration with AGNES Using Different Strategies to Reduce the Deposition Time. *Electroanal. Chem.* **2005**, *576* (1), 21–32.

(34) Companys, E.; Puy, J.; Galceran, J. Humic Acid Complexation to Zn and Cd Determined with the New Electroanalytical Technique AGNES. *Environ. Chem.* **2007**, *4* (5), 347–354.

(35) Galceran, J.; Huidobro, C.; Companys, E.; Alberti, G. AGNES: A Technique for Determining the Concentration of Free Metal Ions. The Case of Zn(II) in Coastal Mediterranean Seawater. *Talanta* **2007**, *71* (4), 1795–1803.

(36) Pearson, H. B.; Galceran, J.; Companys, E.; Braungardt, C.; Worsfold, P.; Puy, J.; Comber, S. Absence of Gradients and Nernstian Equilibrium Stripping (AGNES) for the Determination of [Zn^{2+}] in Estuarine Waters. *Anal. Chim. Acta* **2016**, *912*, 32–40.

(37) Pathiratne, K.; Skandaraja, S.; Jayasena, E. Linear Sweep Voltammetric Determination of Free Chlorine in Waters Using Graphite Working Electrodes. *J. Natl. Sci. Found. Sri Lanka* **2008**, *36* (1).

(38) Bruland, K. W.; Rue, E. L.; Donat, J. R.; Skrabal, S. A.; Moffett, J. W. Intercomparison of Voltammetric Techniques to Determine the Chemical Speciation of Dissolved Copper in a Coastal Seawater Sample. *Anal. Chim. Acta* **2000**, *405* (1–2), 99–113.

(39) Węgiel, K.; Robak, J.; Baś, B. Voltammetric Determination of Iron with Catalytic System at a Bismuth Bulk Annular Band Electrode Electrochemically Activated. *RSC Adv.* **2017**, *7*, 22027–22033.

(40) Puy-Llovera, J.; Pérez-Ràfols, C.; Serrano, N.; Díaz-Cruz, J. M.; Ariño, C.; Esteban, M. Selenocystine Modified Screen-Printed Electrode as an Alternative Sensor for the Voltammetric Determination of Metal Ions. *Talanta* **2017**, *175*, 501–506.

(41) Vestergaard, M.; Kerman, K.; Saito, M.; Nagatani, N.; Takamura, Y.; Tamiya, E. A Rapid Label-Free Electrochemical Detection and Kinetic Study of Alzheimer's Amyloid Beta Aggregation. *J. Am. Chem. Soc.* **2005**, *127* (34), 11892–11893.

(42) Ozkan, D.; Kara, P.; Kerman, K.; Meric, B.; Erdem, A.; Jelen, F.; Nielsen, P. E.; Ozsoz, M. DNA and PNA Sensing on Mercury and Carbon Electrodes by Using Methylene Blue as an Electrochemical Label. *Bioelectrochemistry* **2002**, *58* (1), 119–126.

(43) Hung, V. W. S.; Kerman, K. Gold Electrodeposition on Carbon Nanotubes for the Enhanced Electrochemical Detection of Homocysteine. *Electrochem. commun.* **2011**, *13* (4), 328–330.

(44) Aoki, K. Theory of Ultramicroelectrodes. *Electroanalysis* **1993**, *5* (8), 627–639.

(45) Ngamchuea, K.; Eloul, S.; Tschulik, K.; Compton, R. G. Planar Diffusion to Macro Disc Electrodes—what Electrode Size Is Required for the Cottrell and Randles-Sevcik Equations to Apply Quantitatively? *J. Solid State Electrochem.* **2014**, *18* (12), 3251–3257.

(46) Vyskočil, V.; Barek, J. Mercury Electrodes-Possibilities and Limitations in Environmental Electroanalysis. *Crit. Rev. Anal. Chem.* **2009**, *39* (3), 173–188.

(47) Wang, J. *Analytical Electrochemistry*, Third Edit.; John Wiley and Sons: Hoboken, New Jersey, United States of America, 2006.

(48) Ryan, T. H. *Electrochemical Detectors : Fundamental Aspects and Analytical Applications*; Plenum Press: London, England, 1984.

(49) A.Maclnnes, D.; Adler, L. Hydrogen Overvoltage. *Proc. Natl. Acad. Sci. U. S. A.* **1919**, *5* (5), 160–163.

(50) Galceran, J. *Electroanalisi de Complexos Labils Metall-Lligand Amb Adsorcio Induida*. PhD Thesis., Universitat de Barcelona, 1994.

(51) Arca, M.; Mirkin, M. V; Bard, A. J. Polymer Films on Electrodes. 26. Study of Ion Transport and Electron Transfer at Polypyrrole Films by Scanning Electrochemical Microscopy. *Phys. Chem.* **1995**, *99* (14), 5040–5050.

(52) Tehrani, M. H.; Companys, E.; Dago, A.; Puy, J.; Galceran, J. Free Indium Concentration Determined with AGNES. *Sci. Total Environ.* **2018**, *612*, 269–275.

(53) Brett, C.; Brett, O. *Electrochemistry: Principles, Methods, and Applications*; Oxford University Press: Oxford (UK), 1993.

(54) Aguilar, D.; Parat, C.; Galceran, J.; Companys, E.; Puy, J.; Authier, L.; Potin-Gautier, M. Determination of Free Metal Ion Concentrations with AGNES in Low Ionic Strength Media. *J. Electroanal. Chem.* **2013**, *689*, 276–283.

(55) Statsyuk VN, D. M. Change in pHs of near-Electrode Layer of the Dropping Mercury Electrode in the Course of Electrolytic Reduction of Molecular Oxygen in Polarographic Determination of Indium(III), Cadmium(II) and Thallium(I). *Russ J Gen Chem* **1998**, *68*, 691–693.

(56) Companys, E.; Galceran, J.; Pinheiro, J. P.; Puy, J.; Salaün, P. A Review on Electrochemical Methods for Trace Metal Speciation in Environmental Media. *Curr. Opin. Electrochem.* **2017**, *3*, 144–162.

(57) Galceran, J.; Lao, M.; David, C.; Companys, E.; Rey-Castro, C.; Salvador, J.; Puy, J. The Impact of Electrodic Adsorption on Zn, Cd and Pb Speciation Measurements with AGNES. *J. Electroanal. Chem.* **2014**, *722–723*, 110–118.

(58) Galceran, J.; Companys, E.; Puy, J.; Cecilia, J.; Garces, J. L. AGNES: A New Electroanalytical Technique for Measuring Free Metal Ion Concentration. *J. Electroanal. Chem.* **2004**, *566* (1), 95–109.

(59) Huidobro, C.; Companys, E.; Puy, J.; Galceran, J.; Pinheiro, J. P. The Use of Microelectrodes with AGNES. *J. Electroanal. Chem.* **2007**, *606* (2), 134–140.

(60) Pérez-Ràfols, C.; Serrano, N.; Díaz-Cruz, J. M.; Ariño, C.; Esteban, M. Simultaneous Determination of Tl(I) and In(III) Using a Voltammetric Sensor Array. *Sensors Actuators, B Chem.* **2017**, *245*, 18–24.

(61) Charalambous, A.; Economou, A. A Study on the Utility of Bismuth-Film Electrodes for the Determination of In(III) in the Presence of Pb(II) and Cd(II) by Square Wave Anodic Stripping Voltammetry. *Anal. Chim. Acta* **2005**, *547* (1), 53–58.

(62) Diaz-Cruz, M. S.; Diaz-Cruz, J. M.; Mendieta, J.; Tauler, R.; Esteban, M. Soft- and Hard-Modeling Approaches for the Determination of Stability Constants of Metal-Peptide Systems by Voltammetry. *Anal. Biochem.* **2000**, *279* (2), 189–201.

(63) Galceran, J.; Chito, D.; Martínez-Micaelo, N.; Companys, E.; David, C.; Puy, J. The Impact of High Zn^{2+} Concentrations on the Application of AGNES to Determine Free Zn(II) Concentration. *J. Electroanal. Chem.* **2010**, *638* (1), 131–142.

(64) Chito, D.; Weng, L.; Galceran, J.; Companys, E.; Puy, J.; van Riemsdijk, W. H.; van Leeuwen, H. P. Determination of Free Zn^{2+} Concentration in Synthetic and Natural Samples with AGNES (Absence of Gradients and Nernstian Equilibrium Stripping) and DMT (Donnan Membrane Technique). *Sci. Total Environ.* **2012**, *421–422*, 238–244.

(65) Zavarise, F.; Companys, E.; Galceran, J.; Alberti, G.; Profumo, A. Application of the New Electroanalytical Technique AGNES for the Determination of Free Zn Concentration in River Water. *Anal. Bioanal. Chem.* **2010**, *397* (1), 389–394.

(66) Pernet-Coudrier, B.; Companys, E.; Galceran, J.; Morey, M.; Mouchel, J. M.; Puy, J.; Ruiz, N.; Varrault, G. Pb-Binding to Various Dissolved Organic Matter in Urban Aquatic Systems: Key Role of the Most Hydrophilic Fraction. *Geochim. Cosmochim. Acta* **2011**, *75* (14), 4005–4019.

(67) Puy J, Galceran J, Huidobro C, Companys E, Samper N, Garcés JL, M. F. Conditional Affinity Spectra of Pb^{2+}-Humic Acid Complexation from Data Obtained with AGNES. *Env. Sci Technol* **2008**, *42* (42), 9289–9295.

(68) David, C.; Mongin, S.; Rey-Castro, C.; Galceran, J.; Companys, E.; Garcés, J. L.; Salvador, J.; Puy, J.; Cecilia, J.; Lodeiro, P.; et al. Competition Effects in Cation Binding to Humic Acid: Conditional Affinity Spectra for Fixed Total Metal Concentration Conditions. *Geochim. Cosmochim. Acta* **2010**, *74* (18), 5216–5227.

(69) Rotureau, E. Colloids and Surfaces A : Physicochemical and Engineering Aspects Analysis of Metal Speciation Dynamics in Clay Minerals Dispersion by Stripping Chronopotentiometry Techniques. *Colloids Surfaces A Physicochem. Eng. Asp.* **2014**, *441*, 291–297.

(70) Domingos, R. F.; Huidobro, C.; Companys, E.; Galceran, J.; Puy, J.; Pinheiro, J. P. Comparison of AGNES (Absence of Gradients and Nernstian Equilibrium

Stripping) and SSCP (Scanned Stripping Chronopotentiometry) for Trace Metal Speciation Analysis. *J. Electroanal. Chem.* **2008**, *617* (2), 141–148.

(71) Duval, J. F.; Farinha, J. P. S.; Pinheiro, J. P. Impact of Electrostatics on the Chemodynamics of Highly Charged Metal–polymer Nanoparticle Complexes. *Langmuir* **2013**, *29* (45), 13821–13835.

(72) Vale, G.; Franco, C.; Diniz, M. S.; Dos Santos, M. M. C.; Domingos, R. F. Bioavailability of Cadmium and Biochemical Responses on the Freshwater Bivalve *Corbicula Fluminea*- the Role of TiO2 Nanoparticles. *Ecotoxicol. Environ. Saf.* **2014**, *109*, 161–168.

(73) Vale, G.; Franco, C.; Brunnert, A. M.; Dos Santos, M. M. C. Adsorption of Cadmium on Titanium Dioxide Nanoparticles in Freshwater Conditions - a Chemodynamic Study. *Electroanalysis* **2015**, *27* (10), 2439–2447.

(74) Mu, Q.; Calin A, D.; Galceran, J.; Rey-Castro, C.; Krzemiński, Ł.; Wallace, R.; Bamiduro, F.; Milne, S.; Hondow, N.; Brydson, R.; et al. Systematic Investigation of the Physicochemical Factors That Contribute to the Toxicity of ZnO Nanoparticles. *Chem. Res. Toxicol.* **2014**, *27* (4), 558–567.

(75) Adam, N.; Schmitt, C.; Galceran, J.; Companys, E.; Vakurov, A.; Wallace, R.; Knapen, D.; Blust, R. The Chronic Toxicity of ZnO Nanoparticles and $ZnCl_2$ to Daphnia Magna and the Use of Different Methods to Assess Nanoparticle Aggregation and Dissolution. *Nanotoxicology* **2014**, *8* (7), 709–717.

(76) Alberti, G.; Biesuz, R.; Huidobro, C.; Companys, E.; Puy, J.; Galceran, J. A Comparison between the Determination of Free Pb(II) by Two Techniques: Absence of Gradients and Nernstian Equilibrium Stripping and Resin Titration. *Anal. Chim. Acta* **2007**, *599* (1), 41–50.

(77) Lao, M.; Companys, E.; Weng, L.; Puy, J.; Galceran, J. Speciation of Zn, Fe, Ca and Mg in Wine with the Donnan Membrane Technique. *Food Chem.* **2018**, *239*, 1143–1150.

(78) Domingos, R. F.; Carreira, S.; Galceran, J.; Salaün, P.; Pinheiro, J. P. AGNES at Vibrated Gold Microwire Electrode for the Direct Quantification of Free Copper Concentrations. *Anal. Chim. Acta* **2016**, *920*, 29–36.

(79) Habashi, F. Indium, Physical and Chemical Properties. In *Encyclopedia of Metalloproteins*; Kretsinger, R. H., Uversky, V. N., Permyakov, E. A., Eds.;

Springer New York: New York, USA, 2013; pp 981–982.

(80) Chester, M. A. IUPAC-IUB Joint Commission on Biochemical Nomenclature (JCBN) Nomenclature of Glycolipids: Recommendations 1997. *Mol. Biol.* **1999**, *286* (3), 963–970.

(81) Krizkova, S.; Fabrik, I.; Adam, V.; Kukacka, J.; Prusa, R.; Chavis, G. J.; Trnkova, L.; Strnadel, J.; Horak, V.; Kizek, R. Utilizing of Adsorptive Transfer Stripping Technique Brdicka Reaction for Determination of Metallothioneins Level in Melanoma Cells, Blood Serum and Tissues. *Sensors* **2008**, *8* (5), 3106–3122.

(82) Zhang, J.; Bond, A. Theoretical Studies of Large Amplitude Alternating Current Voltammetry for a Reversible Surface-Confined Electron Transfer Process Coupled to a Pseudo First-Order Electrocatalytic Process. *Electroanal. Chem.* **2007**, *600* (1), 23–34.

(83) Friedman, A.; Bostom, A.; Selhub, J.; Levey, A. .; Rosenberg, I. The Kidney and Homocysteine Metabolism. *Am. Soc. Nephrol.* **2001**, *12* (10), 2181–2189.

Chapter 3: Determination of free indium concentration in aquatic solutions using AGNES

Part of the material of this chapter has been published in:

Tehrani, M. H.; Companys, E.; Dago, A.; Puy, J.; Galceran, J. Free Indium Concentration Determined with AGNES. *Sci. Total Environ.* **2018**, *612*, 269–275

3.1. Abstract

Speciation of In in waters is important for its direct ecotoxicological effects, as well as for the fate of this element in the environment (e.g. fluxes from or towards sediments). Free indium concentrations in the environment can be extremely low due to hydrolysis, especially important in trivalent cations, to precipitation and to complexation with different ligands.

In this chapter, partially published recently,[1] the free indium concentration (which is a toxicologically and geochemically relevant fraction) in aqueous solutions at pH 3 has been measured with an adapted version of the electroanalytical technique AGNES (Absence of Gradients and Nernstian Equilibrium Stripping). Speciation measurements in mixtures of indium with the ligands NTA (nitrilotriacetic acid) and oxalate will be discussed.

3.2. Introduction

Indium is a critical element present in a huge number of electronic devices [2–4] from which it will eventually leach towards environmental waters and other compartments.[5,6] To understand fluxes of indium from the anthroposphere to the hydrosphere, lithosphere and biosphere, the relevant chemical properties of this poorly-studied element have to be adequately elucidated. For instance, the large hydrolysis processes of indium are key to explain the transfer from some natural waters to the sediments.[7,8] Moreover, hydrolysis also hinders the accurate study of its speciation with most conventional techniques and, so, there are many unresolved aspects of the behaviour of indium in a number of systems.[4,9] In particular, values of the reported stability constants of indium with most ligands are remarkably uncertain.[9]

Although solid electrodes of Bi and Au have been able to determine free concentrations of Pb[10] and Cu,[11] respectively, the typical implementation of AGNES with mercury electrodes requires amalgamating elements such as Zn, Cd, Pb or Sn. Given that indium is also an amalgamating element with a negative standard redox potential, it can be tackled with AGNES and conventional Hg electrodes.

This work is the first application of AGNES to a trivalent ion. pH 3 is chosen here to avoid any complication from hydrolysis,[7,8] for which conflicting formation constants have been reported.[9,12] This pH is also relevant for acid mine drainages where high In concentrations have been reported. [7,8] Speciation capability will be assessed with a ligand (NTA, nitrilotriacetic acid) forming a relatively inert complex and another one (oxalate) forming a labile one. In-NTA is also interesting for its application, in radiodiagnostic medicine,[13] as vector of isotopes In-111 and In-113 to transferrin (implying iron substitution).

3.3. Experimental

3.3.1. Reagents

Indium solutions were prepared by dilution from a 1000 mg L^{-1} stock solution (Fluka, indium standard for ICP, Fluka, St Louis, USA). NTA (p.a., Fluka, Buchs, Switzerland) and potassium oxalate monohydrate (both Fluka, analytical grade, Buchs, Switzerland) were used as ligands. Potassium nitrate was used as the inert supporting electrolyte at 0.1 mol L^{-1} (for all experiments) and prepared from solid KNO_3 (TraceSelect Fluka, St Louis, USA). KOH and HNO_3 0.1 mol L^{-1} (both Fluka, St Louis, USA) were used to adjust the pH of the solutions.

3.3.2. Procedures

Differential Pulse Polarography (DPP) was used to have an initial estimate of the potential to be applied in AGNES for a desired gain, compensating any drift from the reference electrode. For DPP experiments, the largest stand drop (labelled "3" which according to the catalogue corresponds to a radius r_0 = 203 μm) has been used in order to be able to apply an expression, valid for planar geometry, to the DPP peak potential.[14,15] For the "short" DPP variant, the drop lifetime was t_d=0.1 s, while for the "long" DPP was t_d=1 s; the scan rate was 4.5 mV/s and 0.45 mV/s, respectively. In both DPPs, the typical initial potential was -0.4 V and the final potential was -0.6 V; a modulation amplitude of 49.95 mV and a pulse time t_p=50 ms were applied.

To assess indium reversibility (i.e. the fast reaching of equilibrium conditions -ruled by Nernst equation- between In^0 and In^{3+} at the electrode surface) in the conditions of this work, Cyclic Voltammograms (CV) were performed between -0.1 V and -0.8 V with a scan rate of 10 mV/s. More details on the ancillary techniques (DPP and CV) and on

AGNES can be found in chapter 2, section 2.1.3.2.2 (DPP), 2.1.3.4. (CV) and 2.3.1. (AGNES).

We faced some difficulties while we were doing the speciation measurements with indium. The capillary of the mercury drop electrode was blocked more often than usual and we had also some irreproducibilities.

From Faraday's law and the equilibrium condition (3-1) reached by the end of the first stage:

$$Q = 3FV_{\mathrm{Hg}}[\mathrm{In}^{\mathrm{o}}] = 3FV_{\mathrm{Hg}}Y[\mathrm{In}^{3+}] \tag{3-1}$$

where V_{Hg} is the volume of the mercury electrode. The normalized proportionality factor (η_{Q}, obtained from a calibration in previous works with Zn, Cd and Pb)[16] can be defined as:

$$\eta_{\mathrm{Q}} = nFV_{\mathrm{Hg}} \tag{3-2}$$

Combining equations (3-1) and (3-2), one reaches the key equation for AGNES, which relates the analytical signal (faradaic charge in this case) with the free metal ion concentration

$$Q = \eta_{\mathrm{Q}}Y[\mathrm{In}^{3+}] \tag{3-3}$$

The faradaic charge can be obtained by subtracting a synthetic blank (i.e. the solution with just background electrolyte) to the total charge.[17]

3.4. Results and discussion

3.4.1. Impact of irreversibility: specific calibration for In

For Zn, Cd or Pb, the potential (E_j) associated to a given gain (Y_j) can be computed from the peak potential of a Differential Pulse Polarogram (DPP) with the formula:

$$Y = \sqrt{\frac{D_{\mathrm{M}^{n+}}}{D_{\mathrm{M}^{0}}}}\exp\left[-\frac{nF}{RT}\left(E_1 - E_{\mathrm{peak}} - \frac{\Delta E}{2}\right)\right] \tag{3-4}$$

where $D_{\mathrm{M}^{0}}$ is the diffusion coefficient for the reduced metal inside the amalgam, $D_{\mathrm{M}^{n+}}$ is the diffusion coefficient for the free metal ion in the solution, E_{peak} is the potential of the maximum obtained in a typical DPP (with the largest drop) and ΔE is the modulation amplitude of the DPP experiment. More details can be found in chapter 2, section 2.1.3.2.2. The expression for DPP assumes no complexation of the metal, so

working at pH 3 limited the impact of the formation of hydroxocomplexes of indium on the DPP peak potential. However, this formula assumes that the couple In^0/In^{3+} is behaving reversibly at the mercury electrode, while conflicting reports on the irreversibility of In[7,18–23] are known. The Cyclic Voltammogram (CV) shown in figure 3-1exhibits its cathodic and anodic peaks at -0.502 and -0.479 V, respectively. So, their difference is 23 mV. According to the rule in,[14] the expected difference in a reversible system should be:

$$\left|E_{\mathrm{pa}} - E_{\mathrm{pc}}\right| = \frac{RT}{nF}\ln(10) \approx \frac{59}{3}\,\mathrm{mV} \approx 19\,\mathrm{mV} \tag{3-5}$$

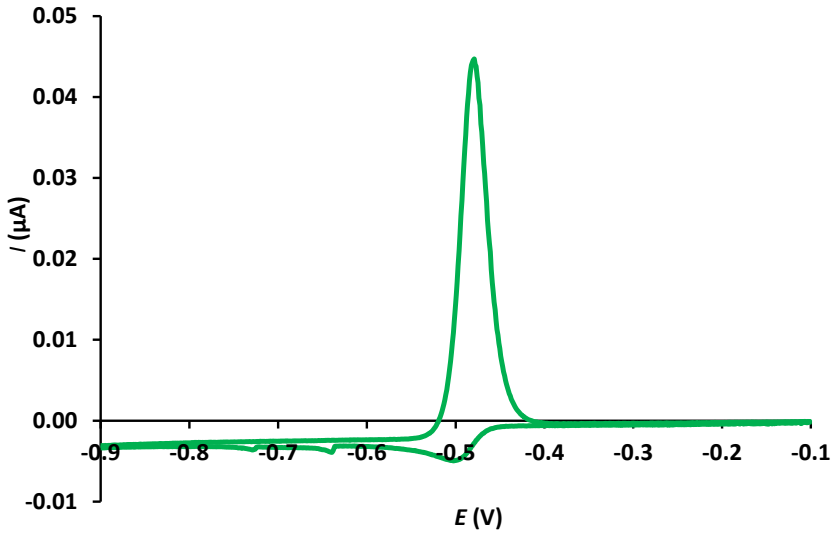

Figure 3-1: Cyclic voltammogram in $c_{T,In}$=4.98 µmol L^{-1} at pH=3 between -0.1V and -0.9V, scan rate 10 mV/s. Measured: E_c = -0.502 V, E_a = -0.479 V. The distance between the peaks is 23 mV.

This means that, in the CV timescale, the In couple is behaving quasi-reversibly. Thus, the (short term) irreversibility of indium prevents a direct accurate computation with the existing expression (3-4), so a new calibration procedure has been designed.

The key idea of the procedure is to fix η_Q according to equation (3-2) (instead of finding it as done with all other elements previously studied with AGNES). Using the radius of the drop 1 (which according to the catalogue corresponds to r_0= 141 µm), one obtains:

$$\eta_Q = 0.0034\ \mathrm{C\ L\ mol^{-1}} \tag{3-6}$$

One can calibrate the gain by measuring the charge with AGNES for known free indium solutions applying a (judiciously chosen) fixed potential (called E_{calib}). Figure 3-3 shows one of the calibrations used in this work. Taking into account equation (2-14) in

section 2.3.1.1.1 which is now written as equation (3-7), from the slope of the plot Q vs. $[In^{3+}]$ and the fixed value of η_Q given by (3-6), one can find the gain actually applied during the calibration (called Y_{calib}) associated to the used $E_1 = E_{calib}$.

$$Y = \frac{\left[In^{0}\right]}{\left[In^{3+}\right]} = \exp\left[-\frac{3F}{RT}\left(E_1 - E^{0'}\right)\right] \tag{3-7}$$

As a rough initial guideline, and to avoid a blind trial-and-error process when starting with a new reference electrode, E_{calib} can be computed from an aimed gain by using an empirically modified version of equation (3-4) suggested here:

$$Y_{estimated} = 2.11 \times \sqrt{\frac{D_{In^{3+}}}{D_{In^{0}}}} \exp\left[-\frac{3F}{RT}\left(E_1 - E_{peak} - \frac{\Delta E}{2}\right)\right] \tag{3-8}$$

where E_{peak} was determined from the "short" DPP (i.e. t_d=0.1s), see figure 3-2.

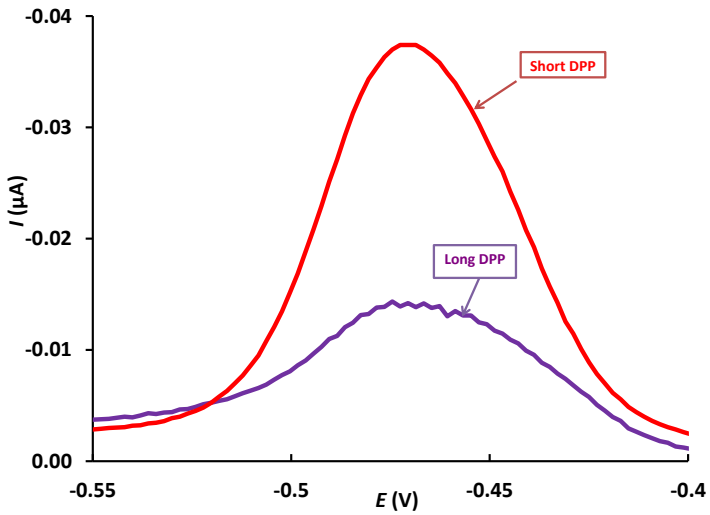

Figure 3-2: Differential Pulse Polarograms in an indium solution 4.90 µmol L^{-1} at pH=3. Purple line stands for the "long" or "standard" DPP (t_d=1s) while the red line stands for the "short" DPP (t_d=0.1s).

In this work, the used diffusion coefficients were $D_{In^0} = 1.38 \times 10^{-9}$ m^2 s^{-1} [24] and $D_{In^{3+}} = 4.363 \times 10^{-10}$ m^2 s^{-1} (taken from table 1 in,[25] who reported this value from a previous research).[26] Equation (3-8) provides a guideline (previous to the calibration) of the gain associated to a candidate E_{calib} because, from this gain, one can estimate the necessary deposition time (see section 3.3.2). After a succesful calibration, there is no longer need of any additional DPP run or use of equation (3-8), unless there is a dramatic change in the reference electrode, because (before a new calibration) one can use the estimate of the gain associated to the new E_{calib} from the previous calibration.

Figure 3-3 is an example of such kind of calibrations, where the free indium concentration in the abscissae is just a fraction of the total dissolved indium (e.g. around 82% at pH 3, see details in table 3-1).

Table 3-1: Computed free In concentrations (using NIST 46.7 database in VMINTEQ [27]) and percentages of the other main species in the solutions used for the calibration shown in figure 3-3.

Code	$c_{T,In}$ (µmol L^{-1})	pH	$[In^{3+}]_{VMINTEQ}$ (µmol L^{-1})	$\%In^{3+}$	$\%InNO_3^{2+}$	$\%In(OH)_2^{+}$	$\%InOH^{2+}$
M_1	0.85	2.997	0.70	82.5	14.4	0.18	2.86
M_2	1.67	3.002	1.38	82.6	14.3	0.19	2.91
M_3	3.26	3.000	2.70	82.7	14.1	0.19	2.93
M_4	6.24	3.002	5.18	83.0	13.8	0.20	3.00
M_5	8.94	3.002	7.44	83.2	13.5	0.20	3.06

Once the correspondence between E_{calib} and Y_{calib} is known, the necessary potential (E_j) to achieve any desired gain (Y_j) (and viceversa) can be computed with

$$E_j = E_{calib} - \frac{RT}{3F} \ln \frac{Y_j}{Y_{calib}} \tag{3-9}$$

Even though the true values of η_Q and/or Y_j might be away from the computed ones in a calibration, the correction factor would cancel out because the same offset applies to the calibration and to the measurement.

The slight irreversibility which affects CV and DPP signals does not impact on the achievement of Nernstian equilibrium by the end of the first stage of AGNES, just might delay it. Moreover, the timescale of the relevant redox processes in CV and DPP experiments is short (of the order of seconds), while the deposition stage of AGNES is of the order of hundreds of seconds. On the other hand, if any irreversibility still had an effect, one would just see (in 1P variant) that longer deposition times would lead to higher charges (because the response signal increases monotonously with t_1 as equilibrium is progressively approached as seen in figure 3-4 and one would just lengthen t_1 until the stabilization of the analytical response. The irreversibility cannot affect the second stage of AGNES, either, because of the long re-oxidation step (t_2=50 s, ample time for diffusion inside the drop) stripping off all the material at a potential far away from equilibrium.

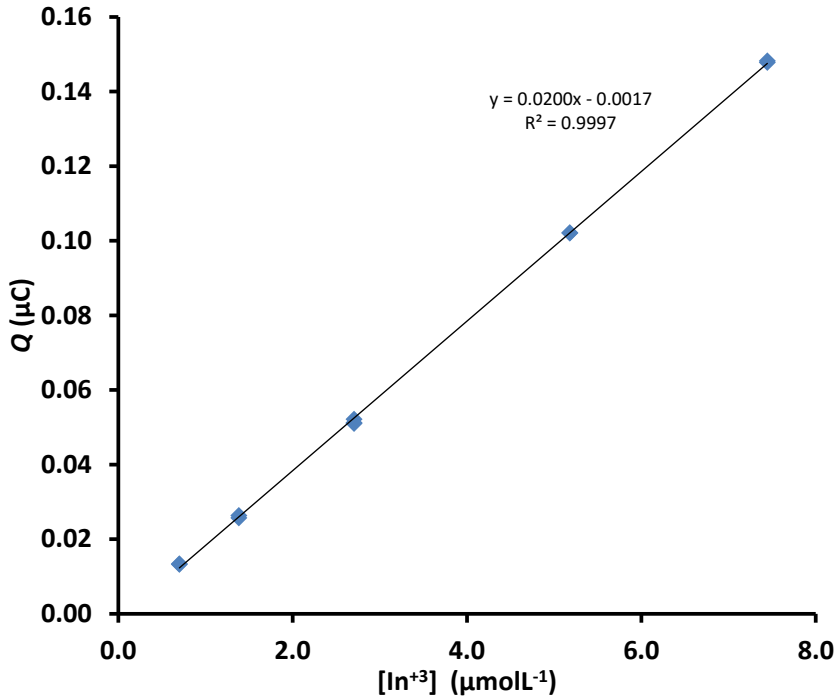

Figure 3-3: Calibration of In for faradaic charges (Q) at pH=3 using E_{calib}=-0.4996 V. From the slope, Y_{calib}=5.90 was derived. The free indium concentration in abscissae is computed with the speciation program VMINTEQ.

3.4.2. Time required to reach equilibrium

The attainment of equilibrium can be checked by performing a "trajectory" (time course or time profile): a set of experiments with a given gain and successively longer deposition times. When the charge stabilizes into a plateau or horizontal line (i.e. longer deposition times do not alter the measured charge), it is indicative of equilibrium. Before the plateau, lower values of charge are measured, which we term as undershoot values. Panel a) in figure 3-4 shows that the trajectories reach higher plateau values for higher gains, as expected from equation (3-7) (which only applies when equilibrium has been reached). Also, the time needed to reach the plateau increases with the gain. For previously studied divalent cations (Zn, Pb and Cd), the following rule [28], when using the smallest radius (drop 1) of the stand, for the deposition time (with stirring) needed to reach a certain gain had been suggested:

$$t_1 - t_w = 7Y \qquad (3\text{-}10)$$

(where the resulting time is expressed in seconds). Previous formula has proved useful when a standard stirring speed ("6" in the stand, corresponding to 3000 min^{-1}) is

in operation and when only the free metal contributes to the flux, i.e. for systems with just metal or with totally inert complexes.

The trajectories in panel a) of figure 3-4 have been plotted in panel b) in terms of a normalized charge, Q/Y, *vs.* a normalized deposition time with stirring $(t_1\text{-}t_w)/Y$.

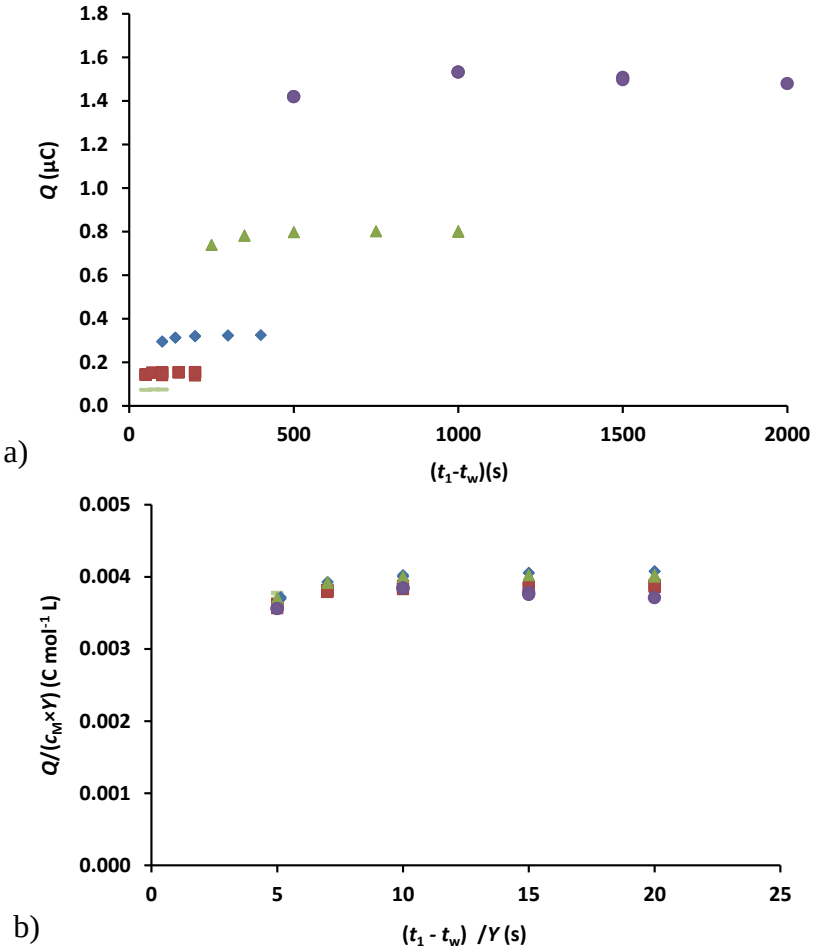

Figure 3-4: Trajectories at different gains in a solution $c_{T,In}$=5.00 µmol L^{-1} at pH=3. For both panels, purple circles, green triangles, blue diamonds, red squares and green horizontal lines stand for Y=100, 50, 20, 10 and 5, respectively. Panel a) Charge vs. deposition time with stirring; panel b) Collapse of the trajectories using normalized charge vs. normalized time.

The collapse of trajectories into practically one master curve demonstrates two conclusions:

i) The rule for the required deposition time can be re-formulated, for indium, as:

$$t_1 - t_w = 10Y \tag{3-11}$$

The slight increase in the deposition times required to reach AGNES equilibrium can be due to the described slight irreversibility of the In couple (as it is well known that

irreversibility is more critical close to equilibrium situations) and to the lower diffusion coefficient of indium.

ii) The collapse of the plateaus of the normalized trajectories confirms the Nernstian behaviour: there is a direct proportionality between the gain and the accumulated charge (as also indicated by equation (3-7)).

3.4.3. Speciation measurements

3.4.3.1. In+NTA

A first checking of AGNES measuring the free metal ion concentration, when complexes are present, involved a ligand (NTA) typically forming inert complexes in voltammetric experiments.[29] Markers in figure 3-5 show the experimental results of the evolution of free indium in several mixtures with NTA (see table 3-2), computing the plotted concentration from the average of the stabilized signals (typically at two different gains).

AGNES 1P strategy with gains from 2 to 50 and deposition times (t_1-t_w) up to 800 s was convenient until the total concentrations of NTA and indium were almost in the stoichiometric proportion 1:1. From this point of the titration onwards, the required deposition times with the 1P strategy were very long, so AGNES 2P has been used. The point at $c_{T,NTA}$=12.14 µmol L^{-1} applying $Y_{1,a}=10^{10}$ produced large overshoots, even with such a short $t_{1,a}$ as 1.5 s. It was observed that the accumulation rate during the first substage declined with decreasing $Y_{1,a}$, so -to avoid large overshoots- $Y_{1,a}=10^{8}$ was used for NTA concentrations higher than 12.14 µmol L^{-1}.

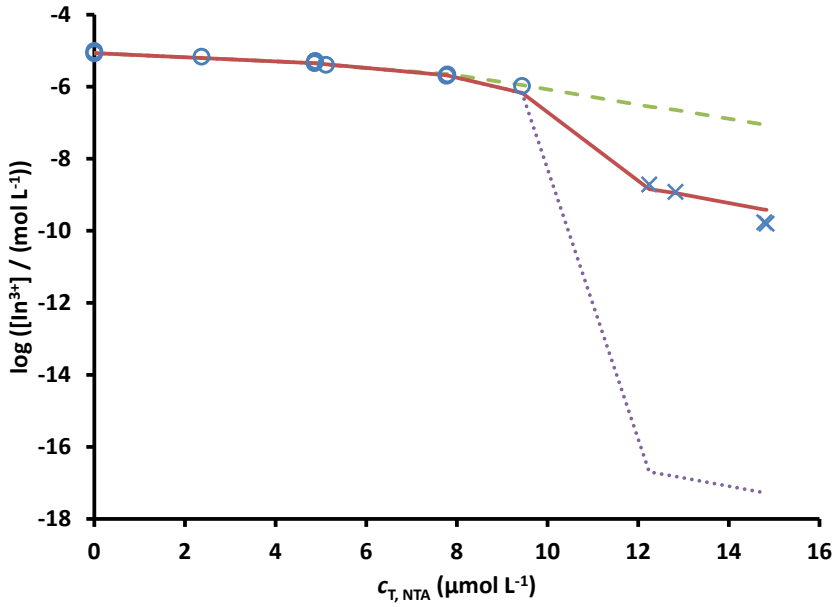

Figure 3-5: Free indium concentrations for several mixtures of In ($c_{T,In}$ around 10 µmol L^{-1}) with NTA at pH=3 (see table 3-2). Circle markers stand for AGNES 1 pulse measurements, while cross markers stand for AGNES 2 pulses measurements. Theoretical computations using VMINTEQ: Green dashed line for database NIST 46.7 (default in VMINTEQ); violet dotted line for values from Harris et al (1994),[30] and continuous red line for values from Biver et al (2008).[13]

These lowest free indium concentrations involved gains (Y) in the range 5000 to 10^5 and relaxation times ($t_{1,b}$) in the range 1000 to 2000 s (see table 3-2).

Table 3-2: Composition of the mixtures NTA+In and AGNES parameters applied at pH 3.00±0.03 ($t_{1,a}$=0 indicates a 1P strategy) with KNO_3 0.1 mol L^{-1} as supporting electrolyte.

pH	$c_{T,In}$ / µmol L^{-1}	$c_{T,NTA}$ / µmol L^{-1}	$[In^{3+}]$ AGNES / µmol L^{-1}	$[In^{3+}]$ VMINTEQ / µmol L^{-1}	$t_{1,a}$ / s	Y	t_1-t_w or $t_{1,b}$ / s	% $[In^{3+}]$ VMINTEQ
3.001	9.88	0.00	9.84	8.17	0	10, 20	200, 400	82.7
2.998	10.31	0.00	8.40	8.54	0	2, 5	100, 200	82.5
2.992	10.34	0.00	8.84	8.51	0	2, 5	100, 200	82.6
3.033	9.87	2.37	6.79	8.53	0	2,10,20	100, 200, 400	62.9
3.015	10.30	4.86	4.51	6.21	0	5, 10	200, 400	44.1
3.003	10.33	4.87	5.14	4.54	0	5, 10	200, 400	44.1
2.997	10.33	4.87	5.14	4.56	0	5, 10	100, 200	44.1
3.013	9.87	5.11	4.03	4.56	0	5,10	200, 400	40.5
3.014	10.29	7.77	2.01	3.99	0	10, 20	200, 400	21.9
2.999	10.32	7.79	2.11	2.26	0	10, 20	200, 400	22.0
3.005	10.32	7.79	2.18	2.27	0	10, 20	200, 400	22.0
2.997	10.31	9.44	0.632	2.27	0	15, 30	200, 400, 800	0.021

pH	$c_{T,In}$ / µmol L^{-1}	$c_{T,NTA}$ / µmol L^{-1}	$[In^{3+}]$ AGNES / µmol L^{-1}	$[In^{3+}]$ VMINTEQ / µmol L^{-1}	$t_{1,a}$ / s	Y	t_1-t_w or $t_{1,b}$ / s	% $[In^{3+}]$ VMINTEQ
3.007	10.26	9.44	1.05	1.14	0	20, 50	200, 400, 800 (for Y=20) 500, 1000, 2000 (for Y=50)	11.1
3.015	10.30	12.24	1.93×10^{-3}	1.11	1.5, 5	1×10^{4}	5000, 10000	2.72
3.000	10.20	12.82	1.20×10^{-3}	0.280	6, 10, 12, 20	1×10^{4}, 2×10^{4}	2000	2.23
3.004	8.56	14.78	1.72×10^{-4}	0.227	8, 9, 10	5×10^{4}, 5×10^{3}	1000, 2000	1.03
3.004	8.59	14.84	1.58×10^{-4}	0.0880	9, 18	1×10^{5}, 5×10^{4}	1000, 2000	1.02

As seen in table 3-2, at the first additions (say until $c_{T,NTA}$=9.46 µmol L^{-1}), the decrease in free In concentration measured with AGNES is practically equal to the amount of added ligand, indicating a strong complexation between one In atom and one NTA molecule (and perhaps other species such as H^+ or OH^-). When the stoichiometric proportion 1:1 is reached, there is a sudden drop in the free indium concentration (see figure 3-5). The use of NIST 46.7 (default database in the speciation program VMINTEQ [27]) for predicting the concentration is only acceptable below the proportion 1:1. Using the stability constants of Harris *et al*. (1994),[30] the agreement is practically the same as NIST46.7 for the first additions, but, for the values above the proportion 1:1, Harris' predicted free concentration is too low. The essential difference between NIST's and Harris *et al's* models is the value of the stability constant for $InH(NTA)_2$ (see table 3-3). In Harris *et al's* model this is the overwhelmingly principal species for In. On the other hand, the model of Biver *et al.*[13], which completely disregards the species $InH(NTA)_2^{2-}$, agrees much better with AGNES results in the probed conditions, albeit for the highest probed NTA concentration, Biver *et al's* predictions are somewhat higher than the free concentrations measured by AGNES. In summary, AGNES confirms the accuracy of Biver's constants in concentration regions of $[In^{3+}]$ spanning several orders of magnitude.

Table 3-3: Logarithm of the accumulated thermodynamic stability constants (β^0 or β^{th}) for In+NTA complexes from the literature

	log ßth		
Complex formed	**Default VMINTEQ database**	**Harris *et al.* [30]**	**Biver *et al.* [13]**
In NTA	15.73	15.74	18.39
In $(NTA)_2^{3-}$	25.62	25.63	27.99
$InH(NTA)_2^{2-}$	18.6	29.14	-

3.4.3.2. In+Oxalate

A second speciation experiment involved oxalate, which had been seen to form labile complexes with Zn.[31] A titration of a fixed amount of In with increasing amounts of oxalate is shown in figure 3-6). The green dashed line shows the expected concentration according to VMINTEQ 3.1 using its standard database, where the In-Oxalate constants are taken from NIST 46.7 (which, in turn, takes the stability constant values from Pingarron and coworkers[32]). The thermodynamic accumulative stability constants derived from the NIST values (i.e. extrapolating at zero ionic strength) are log β^0_{110}=7.3; log β^0_{120} =13.19; log β^0_{130}=15.82; log β^0_{111}=8.16 (where the subscripts indicate the metal, ligand and proton stoichiometry, respectively). AGNES results diverge from this standard prediction, with values very close to the predictions based on the constants more recently reported by Vasca *et al*. (2003)[33]: log β^0_{110}=7.95; log β^0_{120}=13.57; log β^0_{130}=15.5 (with the complex $InOxH^{2+}$ not being specifically considered). Notice the good agreement between AGNES and Vasca *et al*.'s prediction over five orders of magnitude variation in the free indium concentration (almost from millimolar to nanomolar). Due to the decreasing $[In^{3+}]$ at each oxalate addition, the gain had to be increased (see label close to each point in the figure 3-6)). However, the deposition time (t_1-t_w) could be kept to just 25 s and reached equilibrium (checked with longer times).

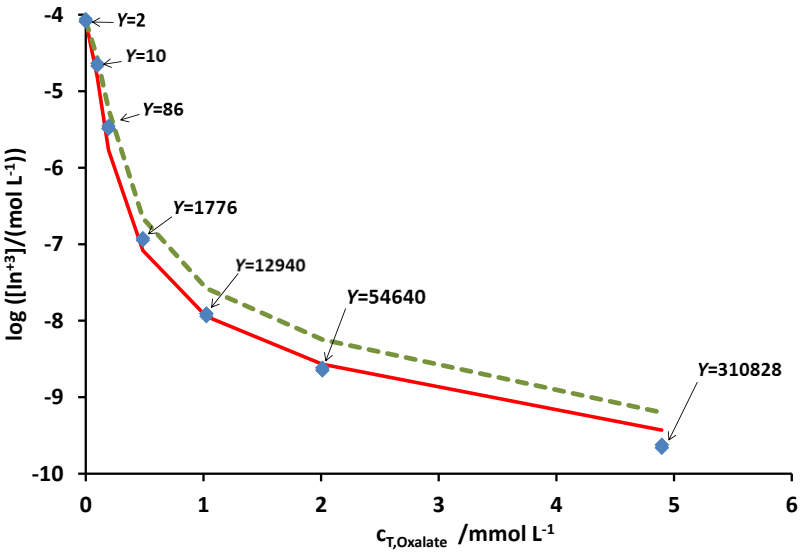

Figure 3-6: Free indium concentrations along a titration of an initial indium concentration of 5 µmol L^{-1} with increasing amounts of oxalate at pH 3. Dashed green line: theoretical expectation according to the stability constants in NIST 46.7. Continuous red line: theoretical expectations according to the stability constants of Vasca et al (2003).[33] *Diamond markers: experimental results obtained with AGNES. Gains are indicated with labels. Deposition time, t_1-t_w= 25 s.*

This is not contradictory with the time rule (3-11), because, in this case, the complexes of In with oxalates contribute to the flux.[31] We conclude that these complexes are very labile and mobile (i.e. diffusion coefficient similar to that of the free ion), because their contribution to the arrival of In^{3+} at the electrode surface is so large. Further exploitation of these properties is discussed in detail in chapter 4.

3.5. Conclusions

The determination of free In^{3+} concentration at pH 3 using the electroanalytical technique AGNES has been successfully achieved. The partial irreversibility of indium leads to inaccuracies in the computation of the gain from DPP peaks (as was the case for Zn and Cd at very low ionic strengths),[34] but they can be overcome by means of a new calibration strategy where the gain (rather than η_Q) is the calibrated parameter (see equation (2-14) in chapter 2, section 2.3.1.1.1, which in this chapter is written as equation (3-7) and see also equations (3-6) and (3-9)). The times required to attain equilibrium are slightly longer than the ones needed for reversible metals like Pb, Cd, and Zn, following the rule indicated in equation (3-11) rather than in equation. (3-10).

Speciation of indium at pH 3 in systems containing either inert (with NTA) or labile (with oxalate) complexes can be followed with AGNES which discriminates between

different published set of constants (models). Values reported in NIST 46.7 seems to be less accurate than other more recently published for In-NTA[13] and for In-oxalate.[33]

Very promising appears to be the application of AGNES in the presence of labile complexes, like In-oxalate complexes, where very short deposition times are enough, even for very low free concentrations, due to the contribution of the complexes to attain the equilibrium. Current assessments of the stability constants -for oxalate or NTA- at pH 3 do not rely on any particular set of In hydrolysis (contrarily to what happens in other methods such as the potentiometric titrations).[13] In the next chapter, with the help of our knowledge achieved in this chapter, not only more studies will be devoted to lability degree of indium complexes such as indium oxalate and indium hydroxides, but also the behaviour of indium in precipitated solutions at different pH values will be discussed.

3.6. References

(1) Tehrani, M. H.; Companys, E.; Dago, A.; Puy, J.; Galceran, J. Free Indium Concentration Determined with AGNES. *Sci. Total Environ.* **2018**, *612*, 269–275.

(2) Abbas, M. N.; Amer, H. S. A Solid-Contact indium(III) Sensor Based on a Thiosulfinate Ionophore Derived from Omeprazole. *Bull. Korean Chem. Soc.* **2013**, *34* (4), 1153–1159.

(3) Wood, S. A.; Samson, I. M. The Aqueous Geochemistry of Gallium, Germanium, Indium and Scandium. *Ore Geol. Rev.* **2006**, *28* (1), 57–102.

(4) Chung, Y. H.; Lee, C. W. Electrochemical Behaviors of Indium. *J. Electrochem. Sci. Technol.* **2012**, *3* (1), 1–13.

(5) White, S. J. O.; Hemond, H. F. The Anthrobiogeochemical Cycle of Indium: A Review of the Natural and Anthropogenic Cycling of Indium in the Environment. *Crit. Rev. Environ. Sci. Technol.* **2012**, *42* (2), 155–186.

(6) Zimmermann, Y. S.; Schäffer, A.; Corvini, P. F. X.; Lenz, M. Thin-Film Photovoltaic Cells: Long-Term Metal(loid) Leaching at Their End-of-Life. *Environ. Sci. Technol.* **2013**, *47* (22), 13151–13159.

(7) Nosal-Wiercińska, A. Catalytic Activity of Thiourea and Its Selected Derivatives on Electroreduction of In(III) in chlorates(VII). *Cent. Eur. J. Chem.* **2010**, *8* (1), 1–11.

(8) White, S. J. O.; Hussain, F. A.; Hemond, H. F.; Sacco, S. A.; Shine, J. P.; Runkel, R. L.; Walton-Day, K.; Kimball, B. A. The Precipitation of Indium at Elevated

pH in a Stream Influenced by Acid Mine Drainage. *Sci. Total Environ.* **2017**, *574*, 1484–1491.

(9) Tuck, D. G. Critical Evaluation of Equilibrium Constants in Solution Part A : Stability Constants of Metal Complexes. Critical Survey of Stability Constants of Complexes of Indium. *Int. Union Pure Appl. Chem.* **1983**, *54* (12).

(10) Rocha, L. S.; Galceran, J.; Puy, J.; Pinheiro, J. Determination of the Free Metal Ion Concentration Using AGNES Implemented with Environmentally Friendly Bismuth Film Electrodes. *Anal. Chem.* **2015**, *87* (12), 6071–6078.

(11) Domingos, R. F.; Carreira, S.; Galceran, J.; Salaün, P.; Pinheiro, J. P. AGNES at Vibrated Gold Microwire Electrode for the Direct Quantification of Free Copper Concentrations. *Anal. Chim. Acta* **2016**, *920*, 29–36.

(12) Alekseev, V. G.; Myasnikova, E. N.; Nikol'Skii, V. M. Hydrolysis Constants of Al^{3+}, Ga^{3+}, and In $^{3+}$ Ions in 0.1 M KNO_3 Solution. *Russ. J. Inorg. Chem.* **2013**, *58* (12), 1593–1596.

(13) Biver, T.; Friani, R.; Gattai, C.; Secco, F.; Tiné, M. R.; Venturini, M. Mechanism of indium(III) Exchange between NTA and Transferrin: A Kinetic Approach. *J. Phys. Chem. B* **2008**, *112* (38), 12168–12173.

(14) Bard, A.; Faulkner, L. *Electrochemical Methods: Fundamentals and Applications*, Second Edi.; Harris, D., Swain, E., Robey, C., Aiello, E., Eds.; John Wiley & sons, Inc.: New York, USA, 2001.

(15) Galceran, J.; Companys, E.; Puy, J.; Cecilia, J.; Garces, J. L. AGNES: A New Electroanalytical Technique for Measuring Free Metal Ion Concentration. *J. Electroanal. Chem.* **2004**, *566* (1), 95–109.

(16) Parat, C.; Authier, L.; Aguilar, D.; Companys, E.; Puy, J.; Galceran, J. Determination of Free Metal Concentration by Implementing Stripping Chronopotentiometry as Second Stage of AGNES. *Analyst* **2011**, *136*, 4337–4343.

(17) Galceran, J.; Lao, M.; David, C.; Companys, E.; Rey-Castro, C.; Salvador, J.; Puy, J. The Impact of Electrodic Adsorption on Zn, Cd and Pb Speciation Measurements with AGNES. *J. Electroanal. Chem.* **2014**, *722–723*, 110–118.

(18) Almagro V, Pena MJ, S. J. Polarographic Study on Reduction of In(III). *An. Quim.* **1977**, *73*, 1409–1414.

(19) Engblom, S. O.; Ivaska, A. U. Characteristic Criteria for A Reversible-Reaction in Ac Polarography. *J Electroanal Chem* **1987**, *222*, 11–20.

(20) Guru, A. K.; Mahaian, A. V. Polarographic Studies of Indium (III) Complex with Sodium Oxalate. *Curr. Sci.* **1976**, *45* (13), 492–494.

(21) Komatsu M. Potential-Step Anodic Stripping Voltammetry. *Bull Chem Soc Jpn* **1973**, *46*, 1670–1674.

(22) Taher MA. Differential Pulse Polarography Determination of Indium after Column Preconcentration with [1-(2-Pyridylazo)-2-Naphthol]-Naphthalene Adsorbent or Its Complex on Microcrystalline Naphthalene. *Talanta* **2000**, *52* (2), 301–309.

(23) Zelić, M.; Mlakar, M.; Branica, M. Influence of Perchlorates and Halides on the Electrochemical Properties of indium(III). *Anal. Chim. Acta* **1994**, *289* (3), 299–306.

(24) Galus Z. Diffusion-Coefficients of Metals in Mercury. *Pure Appl Chem* **1984**, *56*, 635–644.

(25) Kariuki S, D. H. Polarographic Determination of Diffusion Coefficient Values of In(III) in Potassium Chloride and Nitrate Supporting Electrolytes. *Talanta* **1997**, *44*, 1765–1771.

(26) Turnham, D. S. Polarographic Diffusion Coefficients of Some Simple Cations in Various Electrolytes, Calculated for Infinite Dilution and under Polarographic Conditions. *J. Electroanal. Chem.* **1965**, *10* (1), 19–27.

(27) Gustafsson, J. P. Visual MINTEQ https://vminteq.lwr.kth.se/download/ (accessed Sep 15, 2013).

(28) Galceran, J.; Chito, D.; Martínez-Micaelo, N.; Companys, E.; David, C.; Puy, J. The Impact of High Zn^{2+} Concentrations on the Application of AGNES to Determine Free Zn(II) Concentration. *J. Electroanal. Chem.* **2010**, *638* (1), 131–142.

(29) Alberti, G.; Biesuz, R.; Huidobro, C.; Companys, E.; Puy, J.; Galceran, J. A Comparison between the Determination of Free Pb(II) by Two Techniques: Absence of Gradients and Nernstian Equilibrium Stripping and Resin Titration. *Anal. Chim. Acta* **2007**, *599* (1), 41–50.

(30) Harris WR, Chen Y, W. K. Equilibrium-Constants for the Binding of Indium(Iii) to Human Serum Transferrin. *Inorg Chem* **1994**, *33*, 4991–4998.

(31) Companys, E.; Cecília, J.; Codina, G.; Puy, J.; Galceran, J. Determination of Zn2+ Concentration with AGNES Using Different Strategies to Reduce the Deposition Time. *J. Electroanal. Chem.* **2005**, *576* (1), 21–32.

(32) Pingarrón Carrazón, J. M.; Gallego Angreu, R.; Sánchez Batanero, P. *Détermination Potentiométrique Des Constantes de Stabilité Des Complexes Formés Par Indium (III) et Différents Agents Chélatants*. *Bull. Soc. Chim. Fr.* **1984**, *3–4*, 115–122.

(33) Vasca, E.; Ferri, D.; Manfredi, C.; Torello, L.; Fontanella, C.; Caruso, T.; Orru, S. Complex Formation Equilibria in the Binary Zn^{2+}-Oxalate and In^{3+}-Oxalate Systems. *Dalt. Trans.* **2003**, No. 13, 2698–2703.

(34) Aguilar, D.; Galceran, J.; Companys, E.; Puy, J.; Parat, C.; Authier, L.; Potin-Gautier, M. Non-Purged Voltammetry Explored with AGNES. *Phys. Chem. Chem. Phys.* **2013**, *15* (40), 17510.

Chapter 4: Lability degree of indium-oxalate complexes: determination and exploitation

4.1. Abstract

This Chapter investigates how the new technique ADLC (Accumulation under Diffusion Limited Conditions) can be used to calculate the lability degree of indium-oxalate complexes and hydroxides. It also inquires whether AGNES can be used in determining free concentrations of indium in precipitated solutions with the help of labile complexes such as indium-oxalate. With the term "precipitated solutions" we mean solutions that are in equilibrium with precipitated $In(OH)_3$.

Here, we hypothesized that the lability degree measured with ADLC is a guideline to estimate proper deposition times to be used in AGNES to determine low concentrations of free indium in precipitated solutions.

4.2. Introduction

To study the behaviour of indium in a wide variety of systems, it is crucial to check its solubility at different pH values. It is well known that if we increase the alkalinity, indium hydroxides start to precipitate. It was also indicated that studying the kinetics of the re-dissolved metastable precipitates of indium and its complexes was challenging and very difficult.[1] Additionally, due to the increased interest of using indium in modern technology, scientists have been attracted more than before to study not only the solubility of indium complexes, but also to study its cycling in the environment. Accordingly, some reports showed that low concentrations of indium and its compounds in the environment are related to the extremely low solubility of the hydroxides.[2]

Despite of many investigations that have been conducted, there is still a lack of certainty about the solubility product of indium and the mobility of its complexes. Also, it is crucial to find a proper technique to determine its free concentration in precipitated solutions. Therefore, this chapter is focused on using a technique named ADLC (Accumulation under Diffusion Limited Conditions) to calculate the lability degree of indium complexes such as indium-oxalate and indium-hydroxides. Additionally, it will present how ADLC can help in finding optimum deposition times under diffusion-limited conditions ($t_{1,a}$) for our measurements using the 2 Pulses strategy of AGNES, especially at very low free indium concentrations. Moreover it will cover our study on the evolution of precipitated solutions at different pH values through ADLC and AGNES measurements. Our claim is that AGNES can be utilized in determining free concentrations of indium in precipitated solutions and ADLC can be used to study the

rate of dissociation of the complex (by providing the lability degree). Hence the use of these two techniques might shed light on indium's behaviour in different solutions.

4.3. Experimental section

4.3.1. Reagents

Indium solutions (1000 mg L^{-1} indium standard for ICP, Fluka, St Louis, USA) and inert supporting electrolyte solutions were prepared in the same way as it is explained in chapter 3, section 3.3.1.

Potassium oxalate monohydrate (analytical grade, Fluka, Buchs, Switzerland) was used as a ligand. KOH 0.1 mol L^{-1} (Fluka, St Louis, USA) and HNO_3 0.1 mol L^{-1} (Fluka, St Louis, USA) were used to adjust the pH of the solutions. MES buffer (> 99%, Sigma, St Louis, USA) with the concentration of 0.1 mol L^{-1} was prepared and used to fix the pH of the solutions at 5.6 and 6.

4.3.2. Procedures

The ADLC technique (Accumulation Under Diffusion Limited Conditions) was used to determine the lability degree of indium hydroxides and indium oxalate complexes. A brief explanation about the principles of this technique has been presented in chapter 2, section 2.3.2.

Two strategies of AGNES, 1P at pH=4 and 2P at pH=5, 5.5, 5.6 and 6, were used to be able to determine free concentrations of indium in precipitated solutions. More details about both strategies can be found in chapter 2, section 2.3.1.1.

4.4. Lability degree of Indium complexes

4.4.1. The concept of lability degree

It is almost impossible to have a solution where 100% of the indium is in its free form with no complexes. Indeed, even at very low pH a certain fraction of In will be in the form of complexes such as hydroxides or ion pairs like $InNO_3^{2+}$. So, complexes are practically always present in indium solutions. AGNES measures directly the free form, but the presence of complexes can impact on the deposition time.

We start by considering the reaction of one generic metal (M) with just one ligand (L) to form one complex (ML):

$$M + L \rightleftharpoons ML \qquad (4\text{-}1)$$

The supply of a metal from the medium towards a consuming sensor or organism will result from the contributions of its free form plus the contributions of the complexed forms.

$$J = J_{\text{free}} + J_{\text{complex}} \tag{4-2}$$

The lability degree, ξ, is a quantification of the contribution of the complex to the flux. As can be seen in equation (4-3), ξ is defined as the ratio of the current complex contribution to the flux over the maximum possible contribution.[3,4]

$$\xi = \frac{J_{\text{complex}}}{J_{\text{complex, max}}} = \frac{J - J_{\text{inert}}}{J_{\text{labile}} - J_{\text{inert}}} \tag{4-3}$$

In the equation above J is the current flux, J_{labile} is the hypothetical flux if the complexes were fully labile and J_{inert} (sometimes also labelled J_{free}) is the hypothetical flux if the complexes were totally inert. The value of ξ lies between zero (totally inert) and 1 (fully labile).

From the previous definition, it follows that the total flux can be computed as the summation of the contribution of the free metal ion plus the maximum possible contribution of the complex multiplied by the lability degree. If we further assume a steady state where the species diffuse through a diffusion layer of thickness δ,

$$J = D_{\text{M}} \frac{c_{\text{M}}^{*}}{\delta} + D_{\text{ML}} \frac{c_{\text{ML}}^{*}}{\delta} \xi \tag{4-4}$$

The normalized diffusion coefficient, ε, is defined as

$$\varepsilon = \frac{D_{\text{ML}}}{D_{\text{M}}} \tag{4-5}$$

The conditional stability constant, K', associated to reaction (4-1), can be defined as the ratio between the concentration of the complex and the free concentration of the metal:

$$K' = \frac{c_{\text{ML}}^{*}}{c_{\text{M}}^{*}} \tag{4-6}$$

Then, finally, the expression of the total flux can be condensed into

$$J = \frac{D_{\text{M}} c_{\text{M}}^{*}}{\delta} + \xi \frac{D_{\text{ML}} c_{\text{ML}}^{*}}{\delta} = D_{\text{M}} \frac{c_{\text{M}}^{*}(1 + \varepsilon K' \xi)}{\delta} \tag{4-7}$$

If we have a collection of complexes, each one labelled with a subscript i,

$$J = D_{\mathrm{M}} \frac{c_{\mathrm{M}}^{*}(1+\sum_{i=1}^{numcomplex} \varepsilon_i K_i' \xi_i)}{\delta} \tag{4-8}$$

One alternative method to compute the lability degree is retrieving information from techniques such as SSCP (Scanned Stripping Chronopotentiometry) or SCP (Stripping Chronopotentiometry).[5] It has been indicated that, in systems with one complex ML, we can calculate the lability degreefrom $\tau^{*}_{\mathrm{M+L}}$ and τ^{*}_{M} (which represent the limiting deposition transition times in presence and absence of ligands, respectively):

$$\frac{\tau^{*}_{\mathrm{M+L}}}{\tau^{*}_{\mathrm{M}}} = 1 + \varepsilon K' \xi \tag{4-9}$$

But, in our experiments, we used the ADLC technique to calculate the lability degrees of hydroxides and oxalate indium complexes taking into account also the impact of the ion pair $InNO_3^{2+}$ and the case of multiple complexes.

4.4.2. Derivation of equations

As presented in chapter 2, the deposition program of ADLC consists just in a constant potential pulse under diffusion limited conditions, while the stripping step quantifies the accumulated amount (via the charge).

In ADLC our aim is not to reach equilibrium conditions. So, we can spare any waiting time and proceed immediately from the deposition stage to the stripping step.

Using expression (2-22),

$$Q = nFAJt_{1,\mathrm{a}} \tag{4-10}$$

and combining it with equation (4-8), the resulting expression will be:

$$Q^{\alpha} = nFAJt_{1,\mathrm{a}} = nFAD_{\mathrm{M}} \frac{\left[\mathrm{In}^{3+}\right]^{\alpha}(1+\sum \varepsilon_i \, K_i'^{,\alpha} \, \xi_i^{\alpha})}{\delta} t_{1,\mathrm{a}} = slope^{\alpha} \, t_{1,\mathrm{a}} \tag{4-11}$$

where the superscript α is a reminder of the parameters that are dependent of some conditions (e.g. pH or solution composition). $Slope^{\alpha}$ indicates the slope of the plot of charge versus deposition time at the conditions denoted by α and can be identified with

$$slope^{\alpha} = nFAD_{\mathrm{M}} \frac{\left[\mathrm{In}^{3+}\right]^{\alpha}(1+\sum \varepsilon_i \, K_i'^{,\alpha} \, \xi_i^{\alpha})}{\delta} \tag{4-12}$$

Since all here considered complexes (hydroxides and oxalates) are very small, we will assume

$$\varepsilon_{InNO_3} = \varepsilon_{In-oxalates} = \varepsilon_{In-hydroxides} = 1 \tag{4-13}$$

The lability degree of indium-nitrate can be taken as equal to one because one expects a weak binding in this ion pair:

$$\xi_{InNO_3} = 1 \tag{4-14}$$

Now we turn to consider the calculation of the lability degree with ADLC for the specific cases of hydroxides and, then, of oxalate indium complexes.

4.4.2.1. Lability degree of hydroxides in the absence of oxalates

Since there is a mixture of hydroxide complexes, we can define a global (conditional) stability constant at each pH. For instance, at pH 4:

$$K'^{\text{at pH=4}}_{hydroxides} \equiv \frac{\sum_{n=1}^{nmax}\left[\text{In}(\text{OH})_n\right]^{\text{at pH=4}}}{\left[\text{In}^{3+}\right]^{\text{at pH=4}}} = \frac{c_{T,M} - \left[\text{In}^{3+}\right]^{\text{at pH=4}}(1+K'_{InNO_3^{2+}})}{\left[\text{In}^{3+}\right]^{\text{at pH=4}}} \tag{4-15}$$

The last member of the equality relies on a mass balance, so that it only applies in non-precipitated conditions or understanding that $c_{T,M}$ is just the dissolved concentration (not including the precipitated amounts).

Extending eqn 20 in,[6] we can define the global lability degree of hydroxides as:

$$\xi^{\text{at pH=4}}_{hydroxides} \equiv \frac{\xi_{InOH^{2+}} \times K'^{\text{at pH=4}}_{InOH^{2+}} + \xi_{In(OH)_2^+} \times K'^{\text{at pH=4}}_{In(OH)_2^+} + \xi_{In(OH)_3} \times K'^{\text{at pH=4}}_{In(OH)_3}}{K'^{\text{at pH=4}}_{hydroxides}} \tag{4-16}$$

If -using eqn. (4-12)- we divide the ADLC slope at pH=3 by the one measured at pH=4, then the lability degree of hydroxides at pH=4 can be calculated as.

$$\xi^{\text{at pH=4}}_{hydroxides} = \left(\frac{slope^{\text{at pH=4}}\left[\text{In}^{3+}\right]^{\text{AGNES at pH=3}}}{slope^{\text{at pH=3}}\left[\text{In}^{3+}\right]^{\text{AGNES at pH=4}}}\left(1+K'_{InNO3^{2+}}\right) - 1 - K'_{InNO3^{2+}} \right) \times \frac{\left[\text{In}^{3+}\right]^{\text{AGNES at pH=4}}}{c_{T,M} - \left[\text{In}^{3+}\right]^{\text{AGNES at pH=4}}(1+K'_{InNO_3^{2+}})} \tag{4-17}$$

if we use the free indium concentrations measured with AGNES. Alternatively, we can use the free indium concentrations obtained from VMINTEQ calculations using NIST 46.7:

$$\xi_{hydroxides}^{\text{at pH=4}} = \frac{\dfrac{slope^{\text{at pH=4}}\left[\text{In}^{3+}\right]^{\text{NIST at pH=3}}}{slope^{\text{at pH=3}}\left[\text{In}^{3+}\right]^{\text{NIST at pH=4}}}(1+K'_{\text{InNO3}^{2+}})-1-K'_{\text{InNO3}^{2+}})}{K'^{\text{at pH=4}}_{hydroxides}} \quad (4\text{-}18)$$

4.4.2.2. Lability degree of oxalates in the presence of hydroxides

For the sake of simplicity in the notation, we specify now the treatment of just oxalate complexes (without concomitant hydroxides, which are negligible compared to oxalate complexes in the experimental conditions for determining the lability degrees). In this case, we can also define a global conditional stability constant as:

$$K'^{\alpha}_{oxalates} \equiv \frac{\sum_{n=1}^{nmax}\left[\text{In}(\text{Ox})_n\right]^{\alpha}}{\left[\text{In}^{3+}\right]^{\alpha}} = \sum_{n=1}^{nmax} K'^{\alpha}_{\text{In}(\text{Ox})_n} \quad (4\text{-}19)$$

(where the charges of the complexes are omitted for the sake of simplicity). Notice that this average conditional stability constant depends on the conditions of the experiments (indicated by the superscript α). Under ligand of excess conditions and constant ionic strength, $K'^{\alpha}_{oxalates}$ is a function of the free ligand concentration (in the conditions α):

$$K'^{\alpha}_{oxalates} = \sum_{n=1}^{nmax} K'^{\alpha}_{\text{In}(\text{Ox})_n} = \sum_{n=1}^{nmax} K_{\text{In}(\text{Ox})_n}\left(\left[\text{Ox}^{2-}\right]^{\alpha}\right)^n \quad (4\text{-}20)$$

As previously done for hydroxides in eqn(4-16), we can define a collective lability degree for oxalates

$$\xi_{oxalates} \equiv \frac{\sum_{n=1}^{nmax} \xi_{\text{In}(\text{Ox})_n} K'^{\alpha}_{\text{In}(\text{Ox})_n}}{K'_{oxalates}} \quad (4\text{-}21)$$

For determining the collective lability degree of oxalates, we compare ADLC slopes from two experiments with different composition, using equation (4-12) . One solution, which could be called the “reference solution”, contains just In and KNO_3 at pH 3 (indicated by superscript “R”, which replaces α), while the other solution has added oxalate (indicated by superscript “oxal”).

By dividing equation (4-12) applied to both solutions,

$$\frac{slope^{oxal}}{slope^{\mathrm{R}}}=\frac{\left[\mathrm{In}^{3+}\right]^{\mathrm{oxal}}\left(1+K'_{\mathrm{InNO_3^{2+}}}+\xi_{oxal}K'_{oxalates}\right)}{\left[\mathrm{In}^{3+}\right]^{\mathrm{R}}\left(1+K'_{\mathrm{InNO_3^{2+}}}\right)} \tag{4-22}$$

where $\varepsilon_{\mathrm{oxal}}=1$ in consistency with previous hypotheses and $K'_{\mathrm{InNO_3^{2+}}}$ is the same in both solutions as we are working with a fixed large concentration of background electrolyte (0.1 mol L^{-1}) so that the ionic strength is essentially constant.

Solving for the desired lability degree of the mixture of In-oxalate complexes:

$$\xi_{oxalates}^{\mathrm{Vasca}}=\frac{\dfrac{slope^{oxal}\left[\mathrm{In}^{3+}\right]^{\mathrm{R}}\left(1+K'_{\mathrm{InNO_3^{2+}}}\right)}{slope^{\mathrm{R}}\left[\mathrm{In}^{3+}\right]^{oxal}}-\left(1+K'_{\mathrm{InNO_3^{2+}}}\right)}{K'_{oxalates}}=\left(\frac{slope^{oxal}\left[\mathrm{In}^{3+}\right]^{\mathrm{R}}}{slope^{\mathrm{R}}\left[\mathrm{In}^{3+}\right]^{oxal}}-1\right)\frac{\left(1+K'_{\mathrm{InNO_3^{2+}}}\right)}{K'_{oxalates}} \tag{4-23}$$

Previous equation relies on the values of the stability constants of oxalates, because of the computation of K'_{oxalates}. As the values that we consider optimal are those from Vasca *et al.* (see previous chapter), we have replaced in VMINTEQ the existing values (which, previously, were taken from NIST 46.7) by those of Vasca *et al.*[7] So, we will label as "Vasca" (see superscript) the lability degrees computed with equation (4-23) together with Vasca *et al.*'s values of the stability constants for oxalate complexes.

In order not to depend on the accuracy of a given set of constants (such as those of Vasca *et al.*), we derive now an alternative expression where the knowledge of these constants is not needed. As the result will depend on AGNES measurements of the free concentration, we will label the lability degree computed in this manner as "AGNES". We start by replacing the summation in eqn. (4-19) by a balance of indium: the amount in oxalate complexes is the total one minus what is bound to nitrate or free:

$$K'_{oxalates}\equiv\frac{\sum_{n=1}^{nmax}\left[\mathrm{In}\left(\mathrm{Ox}\right)_n\right]^{\mathrm{oxal}}}{\left[\mathrm{In}^{3+}\right]^{\mathrm{oxal}}}=\frac{c_{\mathrm{T,In}}^{\mathrm{oxal}}-\left[\mathrm{In}^{3+}\right]^{\mathrm{oxal}}-\left[\mathrm{InNO_3^{2+}}\right]^{\mathrm{oxal}}}{\left[\mathrm{In}^{3+}\right]^{\mathrm{oxal}}} \tag{4-24}$$

Substitution in equation (4-23) and simple algebra, leads to

$$\xi_{oxalates}^{\mathrm{AGNES}}=\left(\frac{slope^{\mathrm{oxal}}\left[\mathrm{In}^{3+}\right]^{\mathrm{R}}}{slope^{\mathrm{R}}\left[\mathrm{In}^{3+}\right]^{\mathrm{oxal}}}-1\right)\frac{\left(1+K'_{\mathrm{InNO_3^{2+}}}\right)\left[\mathrm{In}^{3+}\right]^{\mathrm{oxal}}}{c_{\mathrm{T,In}}^{\mathrm{oxal}}-\left[\mathrm{In}^{3+}\right]^{\mathrm{oxal}}-\left[\mathrm{InNO_3^{2+}}\right]^{\mathrm{oxal}}} \tag{4-25}$$

4.4.2.3. Reduction of the deposition time due to the contribution of the complexes

The presence of complexes reduces the deposition time because they contribute to the flux.[8] In this section, we derive guidelines for the deposition times $t_{1,a}$ required in the 2 Pulse strategy if we take into account the help of complexes.

As in reference,[9] one can equate the number of moles of In^0 desired inside the amalgam by the end of the first substage computed from:

i) Multiplication of the area $\left(4\pi r_0^2\right)$ by the steady-state flux under diffusion-limited conditions (see equation (4-7)) and by the time of accumulation ($t_{1,a}$).

ii) Multiplication of the volume of the drop by [In^0] which is Y [In^{3+}].

So,

$$4\pi r_0^2 \frac{D_{In^{3+}}\left(1+\sum \varepsilon_i K_i' \xi_i\right)\left[In^{3+}\right]}{\delta} t_{1,a} = \frac{4}{3}\pi r_0^3 Y\left[In^{3+}\right] \quad (4\text{-}26)$$

Then, we can solve for $t_{1,a}$

$$t_{1,a} \approx \frac{\delta r_0 Y}{3D_{In^{3+}}\left(1+K'_{hydroxides}\xi_{hydroxides}+K'_{oxalates}\xi_{oxalates}+K'_{InNO_3}\xi_{InNO_3}+K'_{buffer}\xi_{buffer}+...\right)} \quad (4\text{-}27)$$

The particular case without help of any complex is included in previous equations by just taking all K'=0.

The numerical factors can be gathered in

$$\frac{\delta r_0}{3D_{In^{3+}}} \approx \frac{2.0\times10^{-5}\ m\times141\times10^{-6} m}{3\times4.363\times10^{-10}\ m^2 s^{-1}} \approx 2\ s \quad (4\text{-}28)$$

taking a value of 20 μm for δ.[10]

So, it turns out that a theoretical simple rule, when having no help from any complex, would be

$$t_{1,a}^{theoretical} = \frac{\delta r_0 Y}{3D_{In^{3+}}} \approx 2Y \quad (4\text{-}29)$$

However, we prefer to rely on the experimental result found in previous chapter for K'=0 (only metal), where we needed 10 Y for 1P (see eqn. 3-11) combined with the fact

that the rule for 2P had been found to be 10 times shorter than for 1P.[8,11] So, the practical rule, for a case without ligands, is:

$$t_{1,a}^{\text{practical}} \approx Y \tag{4-30}$$

For more details, see comments around eqn. (4-34), below.

So, in the case of 2P with contribution of oxalates and hydroxides, while neglecting the contribution of the ion pair with nitrate or from complexes with a buffer, the practical applicable rule is

$$t_{1,a} = \frac{Y}{\left(1 + K'_{hydroxides}\xi_{hydroxides} + K'_{oxalates}\xi_{oxalates}\right)} \tag{4-31}$$

We will refer to the product $K'_{hydroxides}\xi_{hydroxides}$ as "helping factor of hydroxides" and to $K'_{oxalates}\xi_{oxalates}$ as "helping factor of oxalates".

4.4.3. Determination of lability degrees

4.4.3.1. Lability degree of indium hydroxide complexes

Figure 4-1 shows an example of ADLC experiments at pH=3 with only indium, where we measured the total charge accumulated under diffusion limited conditions at different $t_{1,a}$. The linearity of the plot supports the hypothesis that the measurements are done under steady state.

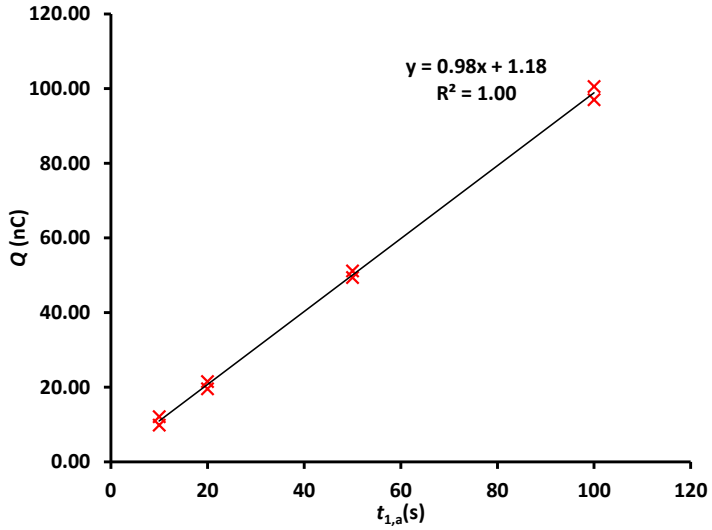

Figure 4-1: ADLC experiments at pH = 3.00 with $c_{T,In}$ = 0.600 µmol L^{-1}, $Y_1 = 1\times10^{10}$, $Y_2 = 1\times10^{-8}$ and t_2 = 50 s.

Table 4-1 shows details about the computation of the lability degree of indium-hydroxides at pH=4 in non-precipitated solutions. As can be seen here, all of the values of ξ resulting from AGNES measurements are between 0 and 1, but with some dispersion of values. So, we take the average of the obtained lability degrees. In any case, these values are to be considered as preliminary results which require further investigation.

Table 4-1: Lability degree of indium-hydroxides at pH=4 in non-precipitated solutions all including KNO_3 0.1 M. Lability degrees in column with heading "ξ^{AGNES}" are computed with eqn. (4-25) while those in column with heading "$\xi^{NIST\ 46.7}$" are computed with eqn. (4-23). Number within parentheses indicates standard deviation and refers to the last significant digit.

pH	$c_{T,In}$ (µmol L^{-1})	ADLC slope (nC s^{-1})	$[In^{3+}]^{AGNES}$ (µmol L^{-1})	$[In^{3+}]^{Vasca}$ (µmol L^{-1})	$\xi^{AGNES}_{hydroxides}$	$\xi^{NIST46.7}_{hydroxides}$
4.00	0.696	1.14	0.27 (1)	0.38	0.76	0.30
4.00	0.696	1.16	0.165 (7)	0.38	0.84	0.36
4.00	0.696	1.18	0.158 (6)	0.38	0.86	0.39
4.01	0.607	0.877	0.269 (6)	0.33	0.55	0.33
4.02	0.609	0.929	0.1700 (3)	0.33	0.75	0.48
4.03	0.609	1.05	0.230 (4)	0.32	0.89	0.82
4.00	0.605	0.940	0.10 (4)	0.33	0.67	0.68
4.02	0.609	0.718	0.180 (4)	0.33	0.58	0.11
4.03	0.609	0.795	0.160 (4)	0.33	0.44	0.35
4.04	0.600	0.816	0.107 (9)	0.31	0.50	0.72
4.00	0.603	0.937	0.189 (5)	0.34	0.78	0.57

According to the calculations mentioned above, the average $\xi_{hydroxides}^{AGNES}$ and $\xi_{hydroxides}^{NIST46.7}$, at pH=4 is 0.70 and 0.50, respectively. Also the standard deviation of the presented lability degrees calculated relying on AGNES measurements is 0.16 while the one relying on NIST predictions is 0.18.

In conclusion, for further calculations, we will take the average of $\xi_{hydroxides}^{AGNES}$ and $\xi_{hydroxides}^{NIST46.7}$ which is $\xi_{hydroxides}$ = 0.60 as a fixed value for the hydroxides contribution, even if - rigorously speaking- $\xi_{hydroxides}$ might change with changing pH (see eqn. (4-16).

4.4.3.2. Lability degree of indium oxalate complexes

Table 4-2 presents the lability degrees of indium-oxalate mixtures at pH=3 and pH=4 obtained from the free indium concentration measured with AGNES using the equation (4-25) and the lability degree obtained from the calculations taking into account the set of constants of Vasca *et al*. using equation (4-23).

Table 4-2: Lability degree of indium-oxalate complexes using the measurements of AGNES and predictions of Vasca. $\xi_{oxalates}^{AGNES}$ *refers to the lability degree calculated using equation (4-25), while* $\xi_{oxalates}^{Vasca}$ *is calculated using equation (4-23). Number within parentheses indicates standard deviation and refers to the last significant digit.*

pH	$c_{T,In}$ (µmol L^{-1})	$c_{T,\ oxalate}$ (µmol L^{-1})	log [Ox^{2-}] (mol L^{-1})	Slope ADLC (nC)	$[In^{3+}]^{AGNES}$ (µmol L^{-1})	$[In^{3+}]^{Vasca}$ (µmol L^{-1})	$\xi_{oxalates}^{AGNES}$	$\xi_{oxalates}^{Vasca}$
Ref pH=3	0.595	0.0	-	1.03	0.470(8)	0.49	-	-
3.99	0.545	1.94	-6.144	0.924	0.08(9)	0.092	1.07	1.0
4.00	0.543	18.8	-5.068	0.923	$5.74(3)\times10^{-3}$	5.2×10^{-3}	0.80	1.0
4.00	0.542	103	-4.314	0.943	$2.68(2)\times10^{-4}$	2.4×10^{-4}	0.92	0.96
Ref pH=3	0.597	0.0	-	0.977	0.396(6)	4.9×10^{-7}	-	-
3.99	0.542	101	-4.325	0.836	$2.43(4)\times10^{-4}$	2.6×10^{-4}	0.73	0.90
4.00	0.536	201	-4.021	0.838	$5.91(1)\times10^{-5}$	6.6×10^{-5}	0.73	0.91
Ref pH=3	0.586	0.00	-	0.988	0.480(8)	0.48	-	-
4.01	0.548	10.1	-5.350	0.880	0.0192(7)	0.013	0.93	1.0
4.00	0.533	20.4	-5.033	0.880	$6.30(2)\times10^{-3}$	4.3×10^{-3}	0.94	0.95
4.00	0.533	10.04	-5.354	0.775	0.016(1)	0.012	0.84	0.83
4.00	0.523	200	-4.021	0.794	$6.2(2)\times10^{-5}$	6.4×10^{-5}	0.86	0.87

pH	$c_{T,In}$ (µmol L^{-1})	$c_{T,oxalate}$ (µmol L^{-1})	log [Ox^{2-}] (mol L^{-1})	Slope ADLC (nC)	$[In^{3+}]^{AGNES}$ (µmol L^{-1})	$[In^{3+}]^{Vasca}$ (µmol L^{-1})	$\xi^{AGNES}_{oxalates}$	$\xi^{Vasca}_{oxalates}$
Ref pH=3	0.592	0.00	-	0.913	0.440(9)	0.49	-	-
3.99	0.548	20.1	-5.043	0.880	$7.09(4)\times10^{-3}$	4.7×10^{-3}	0.91	1.0
4.00	0.547	100	-4.325	0.799	$2.35(6)\times10^{-4}$	2.6×10^{-4}	0.82	0.91
4.00	0.545	100	-4.325	0.767	$2.8(3)\times10^{-4}$	2.6×10^{-4}	0.79	0.88
3.99	0.544	203	-4.021	0.766	$5.3(1)\times10^{-5}$	6.7×10^{-5}	0.79	0.88
Ref pH=3	0.598	0.00	-	0.00103	0.415(6)	0.49	-	-
3.00	0.600	10.9	-5.990	0.00108	0.100(1)	0.085	1.0	1.0
3.00	0.590	20.1	-5.715	0.00113	0.0479(9)	0.043	0.99	1.0
3.00	0.588	102	-5.001	0.973	$3.71(5)\times10^{-3}$	4.7×10^{-3}	0.78	0.91
2.99	0.585	203	-4.711	0.940	$1.16(6)\times10^{-3}$	1.5×10^{-3}	0.76	0.89
2.99	0.578	200	-4.714	0.998	$9.8(2)\times10^{-4}$	1.5×10^{-3}	0.81	0.95
Ref pH=3	0.600	0.00	-	1.075	0.420(6)	0.49	-	-
3.00	0.595	24.0	-5.641	1.04	0.037(8)	0.037	0.85	0.95
3.00	0.593	50.8	-5.310	1.01	0.011(2)	0.014	0.79	0.92
3.00	0.592	106	-4.983	1.11	$3.41(8)\times10^{-3}$	4.5×10^{-3}	0.86	1.0
3.00	0.591	208	-4.685	1.16	$9.9(4)\times10^{-4}$	1.4×10^{-3}	0.90	1.1
3.00	0.585	475	-4.332	1.062	$2.3(1)\times10^{-4}$	3.1×10^{-4}	0.83	0.98
2.99	0.571	986	-4.022	1.00	$4.8(3)\times10^{-5}$	7.5×10^{-5}	0.80	0.94
3.02	0.569	9.81×10^{-4}	-4.003	1.05	$5.8(1)\times10^{-5}$	6.8×10^{-5}	0.85	1.0

It can be shown that the lability degree is -among others- a function of the free ligand concentration.[12]

Figure 4-2 plots the lability degrees measured in front of the free ligand concentration of the solutions included in table representing both measurements at around pH=4 and pH=3 in the same plot. Results at pH=4 are shown with green diamonds, and the ones at pH=3 are denoted with the same symbol, but using blue colour. This figure suggests that the lability degree of indium-oxalate complexes slightly decreases when the free concentration of oxalate increases. No relevant difference is seen for pH 3 and pH 4, especially if we take into account the limited reproducibility for very similar conditions. The average of all these values of $\xi^{AGNES}_{oxalates}$ and $\xi^{Vasca}_{oxalates}$ is 0.86 and 0.97, so the average of all

will be 0.91, which will be the value used for further computations (even at higher pH values). Also the standard deviation for AGNES measurements is 0.21 and for Vasca predictions is 0.21.

The average value $\xi_{oxalates} = 0.91$ shows that indium oxalate complexes are very labile and this confirms results discussed in chapter 3, section 3.4.3.2. In fact in that experiment, as explained in chapter 3, the needed deposition time to reach equilibrium was very short (25 s). This is consistent with the high lability of indium oxalate complexes that we calculated here. Hence such a high lability of this complex helped to reach equilibrium in a much shorter times than those expected without the help of oxalate.

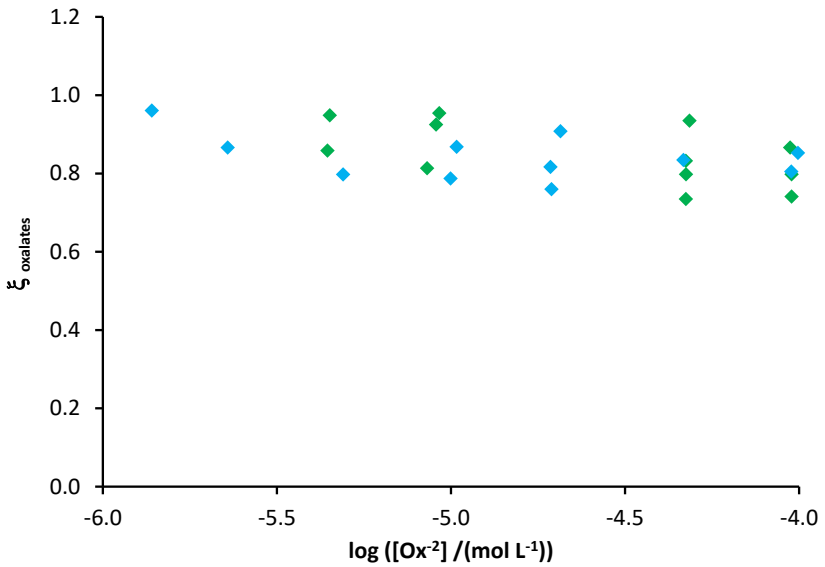

Figure 4-2: Lability degree of indium-oxalate complexes computed from the ADLC experiments specified in table 4-2. Green and blue diamond stand for pH=4 and pH=3, respectively.

4.5. Determining free concentrations of indium in precipitated indium hydroxide solutions

Increasing the alkalinity of the solutions in the absence of ligands can easily cause the precipitation of indium in the form of $In(OH)_3$. This happens even at relatively low total indium concentrations and pH values, in accordance with the very low solubility products that have been reported.

Tuck compiled values of the solubility product (K_{sp}) which corresponds to the equation

$$K_{sp} = \left\{In^{3+}\right\}\left\{OH^{-}\right\}^{3} \qquad (4\text{-}32)$$

Earlier investigators[13] reported a value of log K_{sp} = -33.2 at 25 ºC. Later on, in another exploration[1], it was found out that K_{sp} is temperature dependent and its log value is -33.1 at 25 ºC, but the values that he reported were not reliable because he did not wait enough to reach the equilibrium situation in complex formation. Akselrud *et al.*[1] reported that aging of the solution can impact on K_{sp}. Akselrud and co-workers found out that the K_{sp} of the aged solution (76 days) was completely different from that only after 1 day of preparation; in fact they calculated the difference in K_{sp} of 4 orders of magnitude between freshly prepared and aged solution. In case of aged solutions they reported a tentative value of log K_{sp} = -36.9±0.1 at 25 °C .[1]

Additionally another recent research done by Orlov *et al,*[14] reported that there is a significant difference between the K_{sp} of the aged and fresh precipitated solutions. Such log K_{sp} for fresh and aged precipitated solutions were -33 and -37, respectively

More over, Feitknecht and Schindler described difficulties in finding reliable values of solubility constants of $In(OH)_3$.[1]

Some years later, the values for the solubility product of $In(OH)_3$ (s) were reviewed[15] and the recommended value was log K_{sp} = -36.9 at 25°C taken from the database of NIST 46.7. In a recently published paper[15], it has been mentioned that hydroxide species tend to dominate indium precipitations in oxic waters. During their investigations,[15] they faced difficulties in determining solubility constants, while they were working with two different starting concentrations, 10^{-8} and 10^{-6} M in precipitated solutions. They thought that these two different concentrations should have resulted in the same kind of precipitated solid, but this prediction was in contradiction with their results. Therefore, they hypothesised that such problem might be due to the formation of a less crystalline phase when the lower concentration (10^{-8} M) is being examined.

Even today many unresolved questions still remain. So it is convenient to design more experiments to shed light on this area.

Here, several solutions were prepared at different pH values with known (relatively large) total concentrations of indium that were predicted to precipitate (according to VMINTEQ and NIST 46.7). When the precipitation process was evident at each fixed pH, AGNES was applied to determine the free concentration of indium.

One preliminary point is to check whether aging of the precipitates might have an effect on the free ion concentration in equilibrium with these precipitates. Hence, by

following the evolution of [In^{3+}] with time, we concluded that the precipitation process was completed, as we will show in the next paragraphs.

From figure 4-3 we see that, once the precipitation process is completed, the free concentration is essentially the same (and so K_{sp}) within the probed elapsed time (up to 6 days).

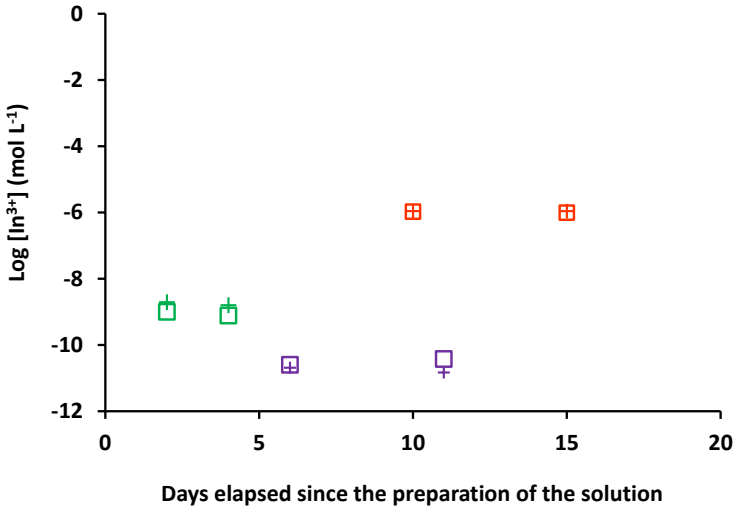

Figure 4-3: Free indium concentration measured during different days at different pH values in precipitated solutions. Square symbols stand for VMINTEQ predictions and cross symbols indicate AGNES measurements. Red symbols stand for the measurements at pH=4 (see figure4-5), the green ones represent the results at pH=5 (see figures 4-5, 4-6, 4-7) and purple colour corresponds to pH=5.5 (see figures 4-8 and 4-9).

In general, to be able to measure free concentrations of indium at each pH, we started calculating our required *Y* and deposition time.

Equation (4-33) estimates a minimum needed *Y*. For predicting this *Y*, despite the charge of the blank was mostly around 1×10^{-9} C, to be on the safe side and far away from the limit of detection, a fixed charge around 5×10^{-8} C or 3×10^{-8} C was used.

The free indium concentration predicted by NIST 46.7 was introduced in the following formula:

$$Y = \frac{Q_{\text{minimum}}}{\left[\text{In}^{3+}\right]\times\eta_Q} \tag{4-33}$$

For our experiments, 1P and 2P were used when we needed to apply low gains and high gains, respectively.

Using the standard variant 1P, a safe deposition time can be calculated applying the formula (4-34). In chapter 3 section 3.4.2 this formula and the experiments related supporting it are explained in detail.

$$t_1 - t_w = 10 \times Y \tag{4-34}$$

The rules for 1P and 2P differ by a factor of 10,[11,16] so when we apply the strategy of 2P, the needed times, even for the worst of scenarios when there are no contributions from complexes (see derivation of eqn (4-30) , above), are:

$$t_{1,a} = Y \tag{4-35}$$

This rule is also consistent with the rough theoretical estimated given by equation (4-29). The lower the free concentrations of indium, the higher the needed gain and the longer is the needed deposition time.

For instance, for pH 5.5, expected $[In^{3+}]$ around 3.74×10^{-11} mol L^{-1} leads, via equation (4-33), to a gain around 4×10^5. This gain, implies -in the strategy 2P- almost 4×10^5 s that is around 5 days, if there was no contribution from the complexes.

The equilibrium situation could be achieved faster by adding moderate amounts of oxalate. Indium-oxalate complexes are labile and can help in reducing the needed deposition time. In principle, adding oxalate does not change the free concentrations of indium in precipitated solutions.[17] Indeed, equation (4-32) can be written as

$$\left[In^{3+}\right] = \frac{K_{sp}}{\gamma_{In^{3+}} \left\{OH^-\right\}^3} \tag{4-36}$$

where $\gamma_{In^{3+}}$ is the activity coefficient of the cation In^{3+}. This equation will hold for any solution in equilibrium with precipitated $In(OH)_3$. K_{sp}, $\gamma_{In^{3+}}$ and $\left\{OH^-\right\}$ are fixed, if we work at constant temperature, ionic strength and pH. So, $[In^{3+}]$ will be fixed, even if there are complexes (and a different speciation).

Table 4-3 shows information about measurements at different pH values in precipitated solutions, which will be presented in detail in the next sections.

Table 4-3: Details about the experiments determining free indium concentrations at different pH values in precipitated solutions. Subtable a) shows the results using strategy of 1P, while Subtable b) shows the ones using strategy of 2P. When present, $c_{T,MES}$= 1.08×10^{-2} mol L^{-1} $c_{T,Ox}$=1.51×10^{-4} mol L^{-1}. Number within brackets indicates standard deviation and refers to the last significant digit.

a)

pH	**Oxalate/ MES**	**Strategy**	**t_1-t_w (s)**	***Y***	**[In^{3+}]^{AGNES} (nM)**	**[In^{3+}]$^{NIST\ 46.7}$ (nM)**
4.01	None	1P	500, 1000	50	1.10 (2)×10^3	1.0×10^3
4.01	None	1P	500, 1000	50	1.1 (2)×10^3	1.0×10^3

b)

pH	**Oxalate / MES**	**Strategy**	**$t_{1,a}$ (s)**	**$t_{1,b}$ (s)**	***Y***	**[In^{3+}]^{AGNES} (nM)**	**[In^{3+}]$^{NIST\ 46.7}$ (nM)**
5.05	None	2P	420	50, 400, 800	5000	1.60 (8)	0.77
5.00	None	2P	400, 800	600, 2000	10000	1.9 (2)	1.0
5.00	None	2P	*Y* 10000 $t_{1,a}$: 400,800 *Y* 20000 $t_{1,a}$: 800	600, 2000 800,2000, 2500	10000 and 20000	1.9 (2)	1.1
5.50	None	2P	1200	100, 500	5×10^5	0.015 (2)	0.037
5.55	None	2P	1000	100, 500	5×10^5	0.0206 (1)	0.025
5.60	MES and Oxalate	2P	500	200, 2000	5×10^6	0.0069 (2)	0.015
6.06	MES and Oxalate	2P	800	2000	5.69×10^7	0.00137 (2)	1.1

4.5.1. Determining [In^{3+}] in precipitated solutions at pH 4

Table 4-4 gathers details about the percentage of the different species in the precipitated studied solutions at pH=4. We can conclude that even at this relatively acidic pH, almost 40% of indium is in some hydroxide form. All percentages that are indicated are respect to the dissolved fraction of indium (not to its total amount).

Table 4-4: Free indium concentrations from AGNES results and predictions of VMINTEQ including percentage of other dissolved species in these precipitated solutions. Number within parentheses indicates standard deviation and refers to the last significant digit.

pH	$c_{T,In}$ (µmol L^{-1})	$[In^{3+}]^{AGNES}$ (nM)	$[In^{3+}]^{NIST\ 46.7}$ (nM)	$\%In^{3+}$	% $InNO_3^{2+}$	% $In(OH)_3$ (aq)	% $In(OH)^{2+}$	% $InOH^{2+}$
4.0	5.02	$1.10(2)\times10^{-3}$	1.0×10^{-6}	55.0	9.7	2.6	13	20
4.0	5.02	$1.1(2)\times10^{-3}$	9.8×10^{-7}	54.4	9.6	2.7	13	20

To measure free indium concentrations at pH 4, AGNES methodology 1P was followed. For this experiment, *Y*= 50 was applied and, as can be seen in figure 4-4, the assayed deposition times 500 and 1000 s were enough to reach the equilibrium situation. Table 4-4 shows that the difference between AGNES measurements and the predictions of VMINTEQ is almost negligible: in logarithmic scale, free indium concentration measured by AGNES is -5.97 and the predictions of NIST 46.7 (VMINTEQ) is almost -6.00, which is in very good agreement.

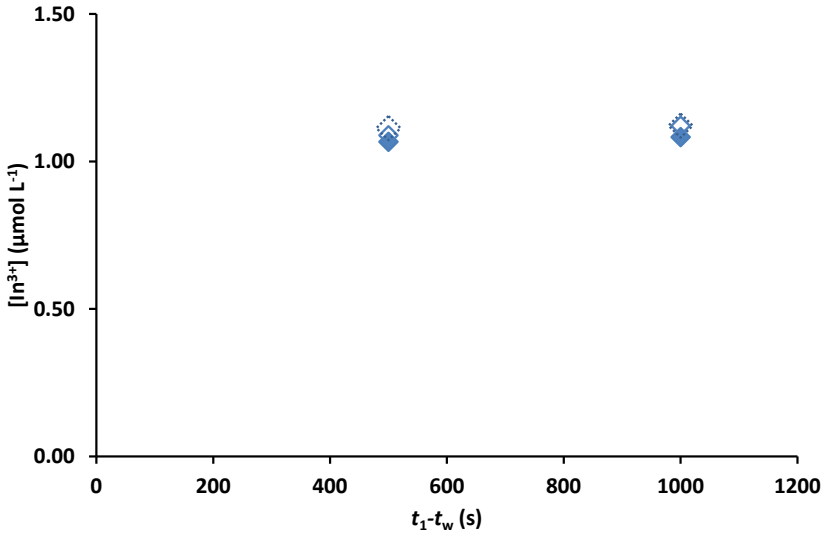

Figure 4-4: 1P-trajectory at Y=50 showing the stabilization of retrieved concentrations for deposition times 500 and 1000 s at pH= 4.0 and $c_{T,In}$ =5.01 µmol L^{-1} (62.2% precipitated, according to VMINTEQ). Replicates in full or empty markers.

4.5.2. Determining $[In^{3+}]$ in precipitated solutions at pH 5

At pH values above 5, our strategy was changed to 2P to be able to keep a reasonable deposition time. If we take the minimum acceptable *Q* as 30 nC, the application of formula (4-33), leads to a gain around 8000. We used two different gains such as 5000 and 10000 to be able to find the equilibrium position by overshoot and undershoot. Using

Y=5000, $K'_{hydroxide} = 77$ and $\xi_{hydroxide} = 0.60$, applying (4-31) a theoretical candidate $t_{1,a}$ was 105 s. And also using Y=10000 provided a theoretical candidate time be around 211 s.

Fig 4-5 shows a first set of AGNES measurements at Y= 5000 and Y=10000, both with the same $t_{1,a}$= 420 s, that converged satisfactorily. The ones that stand for Y=10000 show a slight undershoot, while the ones at Y= 5000 show a slight overshoot and both almost reached equilibrium for $t_{1,b} > 400$s.

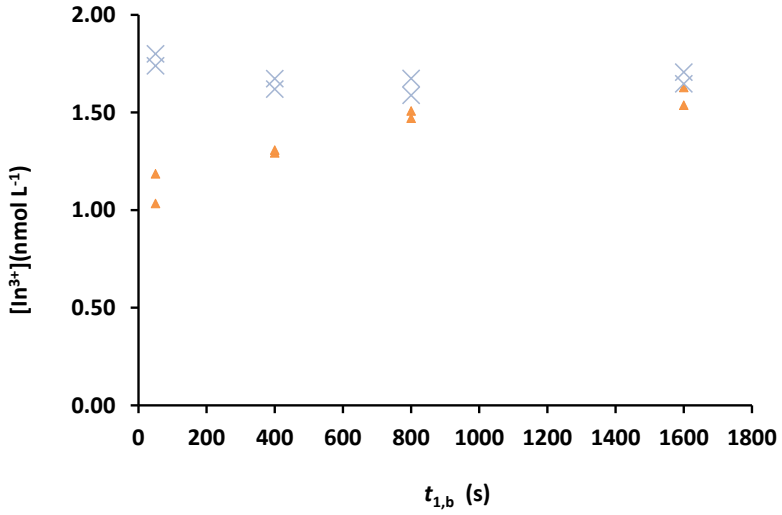

Figure 4-5: 2P-trajectory revealing stabilization of retrieved concentration for $t_{1,b}$ 800 s and longer. pH= 5.05, $c_{T,In}$ =20.6 µmol L^{-1} and $c_{T,MES}$ =1.08×10^{-2} mol L^{-1}. The blue × symbols stand for Y=5×10^3 , $t_{1,a}$ =420s, while orange triangles Y = 10^4, $t_{1,a}$ =420s.

Corresponding to a second set of experiments at pH close to 5, figure 4-6 shows convergence (at equilibrium) of the two series at gain 1×10^4 with $t_{1,a}$ 400s and 800s for $t_{1,b}$ =2000 s.

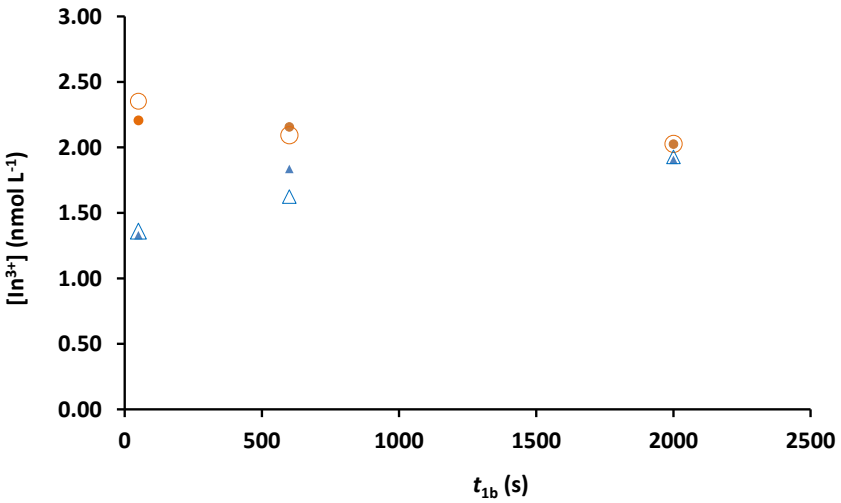

Figure 4-6: 2P-trajectory showing stabilization of retrieved concentrations for pH=5.01 and $c_{T,In}$ *=100 µmol L⁻¹. Symbols that are filled denote first measurements, while the empty ones stand for their replicates. The orange circles stand for Y=1×10⁴, $t_{1,a}$ =800s, blue triangles correspond to Y = 1×10⁴, $t_{1,a}$ =400s.*

For a third set of experiments close to pH 5, figure 4-7 shows that both gains were already in equilibrium at $t_{1,b}$= 2000s.

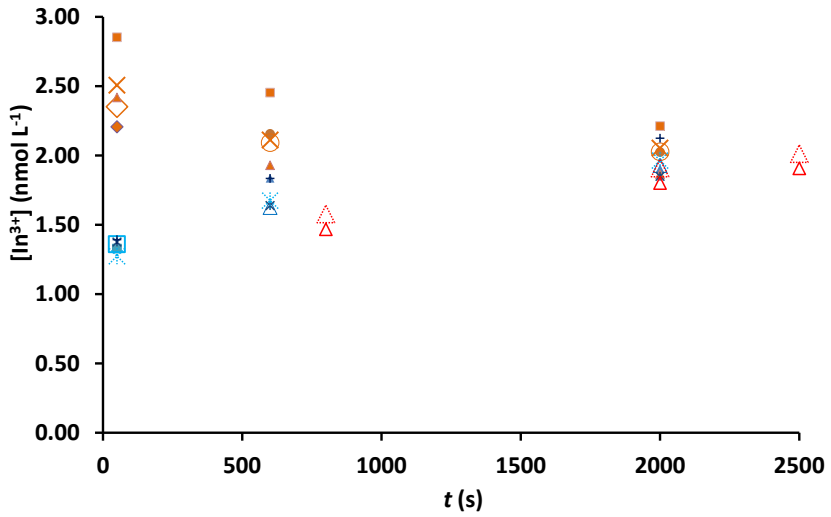

Figure 4-7: 2P-trajectory showing stabilization of the retrieved concentration for pH= 5.00 and $c_{T,In}$ *=100 µmol L⁻¹. Different shapes of the same colour mean that they are replicates. All orange symbols stand for Y=1×10⁴ with $t_{1,a}$= 800 s, and all blue symbols show the ones using Y=1×10⁴ with $t_{1,a}$= 400s and all red triangles stand for Y=2×10⁴ with $t_{1,a}$= 800s.*

Table 4-5 shows that at pH 5 AGNES measurements were very close to the predictions of NIST 46.7. We highlight that in all cases $C_{T,In}$ is the total concentration (i.e. the dissolved concentration and the precipitated amounts). The comparison between AGNES measurements with MES (figure 4-5) and without MES (figures 4-6 and 4-7), confirms that in precipitated solution the free ion concentration is fixed regardless of the amount of ligands (such as MES in this case).

Table 4-5: Free indium concentrations from AGNES results and predictions of NIST 46.7 at pH close to 5.

pH	$c_{T,In}$ (µM)	$c_{T,MES}$ (M)	$[In^{3+}]^{AGNES}$ (nM)	$[In^{3+}]^{NIST\ 46.7}$ (nM)	log $[In^{3+}]^{AGNES}$	Log $[In^{3+}]^{NIST\ 46.7}$	*Number of the related figure*
5.05	20.6	0.0108	1.65 (8)	0.77	-8.798	-9.11	Fig 4-5
5.01	100	0.00	1.95 (2)	1.0	-8.709	-9.00	Fig 4-6
4.95	100	0.00	1.9 (2)	1.1	-8.73	-8.96	Fig 4-7

4.5.3. Determining $[In^{3+}]$ in precipitated solutions at pH 5.5

Figures 4-8 and 4-9 represent two different sets of experiments at pH close to 5.5 using the 2P strategy and applying $Y = 5\times10^5$. The rule for 2P strategy without contribution of any complexes would require $t_{1,a}=5\times10^5$ seconds. However, the high lability of the hydroxides suggested to try with a shorter time such as $t_{1,a}=1000$s.

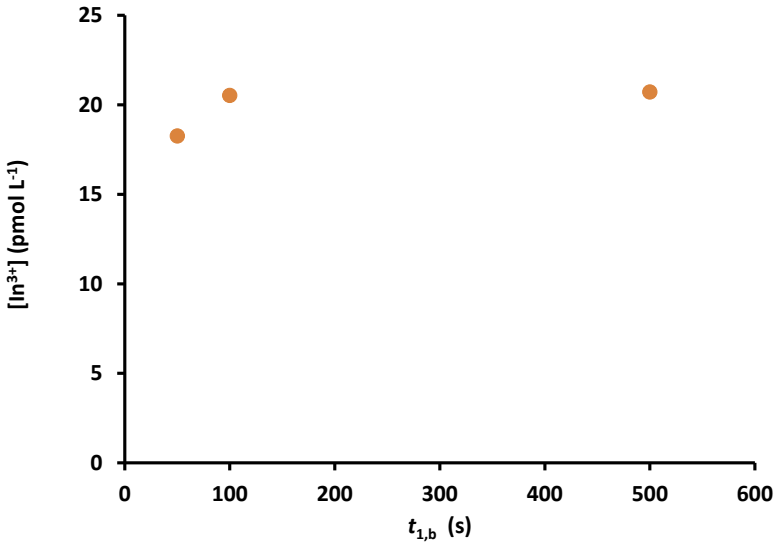

Figure 4-8: 2P-trajectory showing equilibrium situation at pH=5.55 with $c_{T,In}$*=960 µmol* L^{-1}*. Orange circles stand for* $Y = 5\times10^5$*,* $t_{1,a}$*=1000 s.*

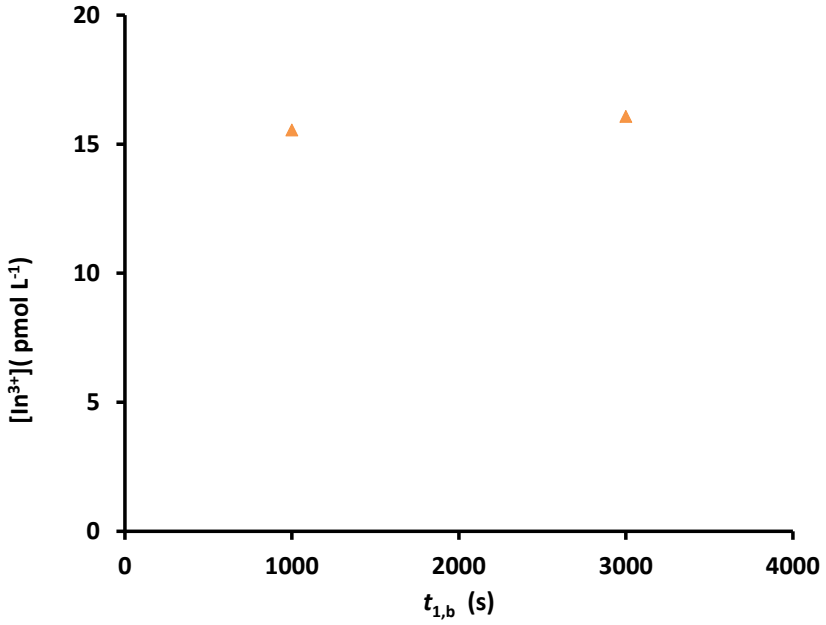

Figure 4-9:2P-trajectory showing stabilized situation at pH=5.50, $c_{T,In}$*=960 µmol* L^{-1} *and applying* $Y = 5\times10^5$ *with* $t_{1,a}$*=1000 s.*

Table 4-6 shows the comparison between the AGNES free concentrations of indium and NIST 46.7.

Table 4-6: Free indium concentrations from AGNES results and predictions of NIST 46.7 at pH around 5.5. Number within parentheses indicates standard deviation and refers to the last significant digit.

pH	$K'_{hydroxides}$	$c_{T,In}$ (µmol L^{-1})	$[In^{3+}]^{AGNES}$ (pmol L^{-1})	$[In^{3+}]^{NIST\ 46.7}$ (pmol L^{-1})	log $[In^{3+}]^{AGNES}$ (mol L^{-1})	Log $[In^{3+}]^{NIST\ 46.7}$ (mol L^{-1})
5.50	1530	9.60×10^{-2}	15 (2)	37.5	-10.83	-10.43
5.55	2239	9.60×10^{-2}	20.6 (1)	25.1	-10.686	-10.60

We conclude that the hydroxides do contribute considerably to the faster reaching of equilibrium at this pH. More precisely, to estimate the expected deposition times taking into account the hydroxide contribution, equation () was used. If we take into account that the average value of $\xi_{hydroxides}$ equals to 0.60 (see section 4.4.2.1), the expected $t_{1,a}$ at pH=5.5 ($K'_{hydroxide} = 1530$) and pH=5.55 ($K'_{hydroxide} = 2239$), using the Y=5×10^5 at both mentioned pH values, will be around 544 s and 372 s, respectively. These rough estimations are within the order of magnitude of the acceptable $t_{1,a}$= 1000 s (see Figures 4-8 and 4-9).

4.5.4. Determining [In^{3+}] in precipitated solutions at pH 5.6

At pH=5.6, using the free concentration 1.47×10^{-11} mol L^{-1} predicted by NIST 46.7 in equation (4-33), the needed Y would be around 1×10^{6}, but to be on the safe side we used $Y=5\times10^{6}$. If we applied 1P in absence of the complex contribution, the needed deposition time calculated applying the formula (4-34) yields a deposition time around 5×10^{7} s. This means we need to wait more than 578 days to be able to measure free indium concentration.

At this pH, we combined two strategies to reduce the deposition time:

1. Using 2P.
2. Adding oxalate to form labile complexes.

For cases where we added oxalate and applied 2P, the required deposition times were calculated using equation (4-31).

If we apply 2P, at pH=5.6 the predicted needed deposition time without the help of oxalate and hydroxide is estimated to be around 5×10^{6} s which is more than about 58 days, but by adding oxalate with a concentration of 140 µmol L^{-1} the needed deposition time can be decreased dramatically.

In this case, one can find a guideline about the required $t_{1,a}$ from the computed lability degrees obtained with ADLC (see section 4.4.2.3). Table 4-7 gives information about the speciation of the components related to the measurements shown in figure 4-10 of a precipitated indium solution, containing oxalate and at a pH 5.61. Through the informations from this table and using the equation (4-6) we were able to calculate the helping factors of oxalate and hydroxides which were 11032 and 2252, respectively:

$$K'_{\text{oxalates}}\xi_{\text{oxalates}} = 12123\times0.91 \approx 11032 > 3752\times0.60 \approx 2252 = K'_{\text{hydroxides}}\xi_{\text{hydroxides}}$$

We are neglecting the possible contribution of indium complexes with the MES buffer.

So, using data from table 4-7 to compute conditional stability constants, possible deposition times along the diffusion-limited step should be approximately

$$t_{1,a} \approx \frac{Y}{K'_{oxalates}\xi_{oxalates} + K'_{hydroxide}\xi_{hydroxide}} \approx \frac{5\times10^{6}}{(11032+2252)} = 376\,\text{s} \qquad (4\text{-}37)$$

Table 4-7. Speciation of a precipitated solution of $In(OH)_3$ with KNO_3 0.1 M, $c_{T,In}$= 37.08 µmol L^{-1}, $c_{T,Ox}$ =142.0 µmol L^{-1}, $c_{T,MES}$ = 1.00×10^{-2} mol L^{-1} at pH=5.61.

Major species	Concentration (mol L^{-1})	% (dissolved) indium complexes
H_2-Oxalate	8.42×10^{-11}	-
H-Oxalate$^-$	2.52×10^{-6}	-
$In(OH)_3$ (aq)	4.90×10^{-8}	-
$In(OH)_2^+$	6.07×10^{-9}	2.60
$In(OH)_4^-$	5.23×10^{-12}	-
In-$(Oxalate)_2^-$	1.65×10^{-7}	70.8
In-$(Oxalate)_3^{-3}$	4.16×10^{-9}	1.78
In^{+3}	1.47×10^{-11}	0.63
InH-Oxalate^{+2}	4.90×10^{-32}	-
$InNO_3^{+2}$	2.33×10^{-12}	-
$InOH^{+2}$	2.20×10^{-10}	0.09
In-Oxalate$^+$	8.88×10^{-9}	3.80
Oxalate^{-2}	1.14×10^{-4}	-

Trajectories for the lowest gain in figure 4-10 indicate undershoot for $t_{1,a}$=300 s and a clear overshoot for $t_{1,a}$=800 s. This suggests an experimentally optimum $t_{1,a}$ value of 500 s (blue squares) quite close to the predicted one of 376 s (arising from $K'_{hydroxide} = 3752$, $K'_{oxalate} = 12123$).

Figure 4-11 uses the same data as in figure 4-10, but representing concentrations instead of charges. This allows to evidence the collapse of the trajectories when equilibrium is achieved.

As can be seen in table 4-10 free indium concentrations measured by AGNES are acceptably close to the predictions of NIST 46.7. AGNES measured value is 6.9×10^{-12} mol L^{-1} and the predicted free indium concentration by NIST 46.7 is 1.4×10^{-11} mol L^{-1}.

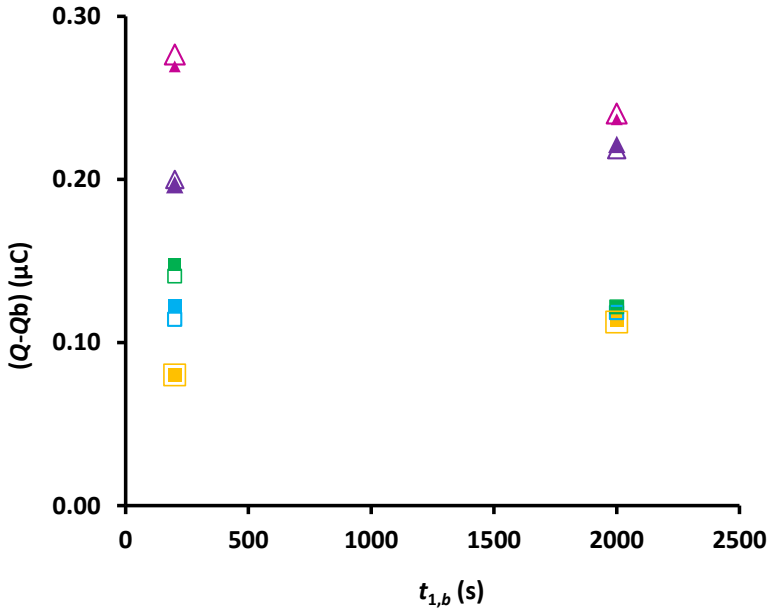

Figure 4-10: 2P charge trajectories showing the achievement of equilibrium situations when using optimized $t_{1,a}$-values close to the guideline obtained using the lability degree determined with ADLC. Dark purple triangle stands for Y=1×10⁷ with $t_{1,a}$= 1000 s, light purple triangle shows the ones using Y= 1×10⁷ with $t_{1,a}$= 1500 s. Square symbols with colour yellow, blue and green stand for Y= 5×10⁶ with t1,a=300 s, 500 s and 800 s, respectively. pH= 5.61, $c_{T,In}$ =37.1 µmol L⁻¹, $c_{T,Ox}$ =142 µmol L⁻¹ and $c_{T,MES}$ =0.0100 mol L⁻¹.

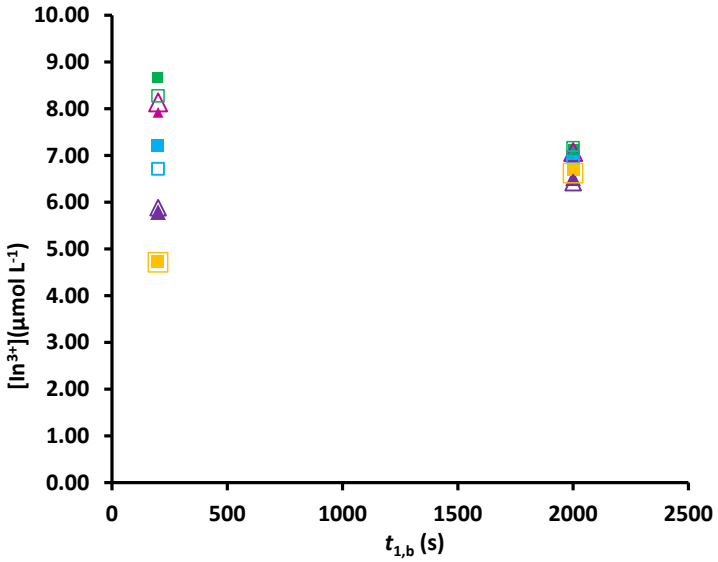

Figure 4-11: Re-plot of figure 4-10 in terms of concentration instead of charge with the same conditions and markers as in previous figure.

4.5.5. Determining [In^{3+}] in precipitated solutions at pH 6

Figure 4-12 shows that, at pH=6.06, adding oxalate helped to determine free concentrations of indium very fast, just with using $t_{1,a}$=800s. The improvement is remarkable: without the contribution of the complexes, the needed deposition time with 2P was calculated to be around 6×10⁷ s.

If we take into account the helping factor of just oxalate and calculate the needed $t_{1,a}$ using equation 4-37 (with values $K'_{Oxalate}$ = 13930 and $\xi_{oxalate}$ =0.91), the required $t_{1,a}$ would be equal to 4496 s and, taking into account the helping factors of both hydroxide (with values $K'_{hydroxide}$ = 48791 and $\xi_{hydroxide}$ =0.60) and oxalate, the needed $t_{1,a}$ would be around 908 s. So, our results might suggest that reaching equilibrium in 800 s is due to the help of the contributions of complexes with oxalate, hydroxide and MES. Probably, we can attribute to the complexes with MES the reduction from 900 s to 800 s, but current uncertainties preclude a clear elucidation of this issue. Free indium measured with AGNES is around 1.37 pmol L^{-1} and the predicted value of NIST 46.7 is 1.06 pmol L^{-1}.

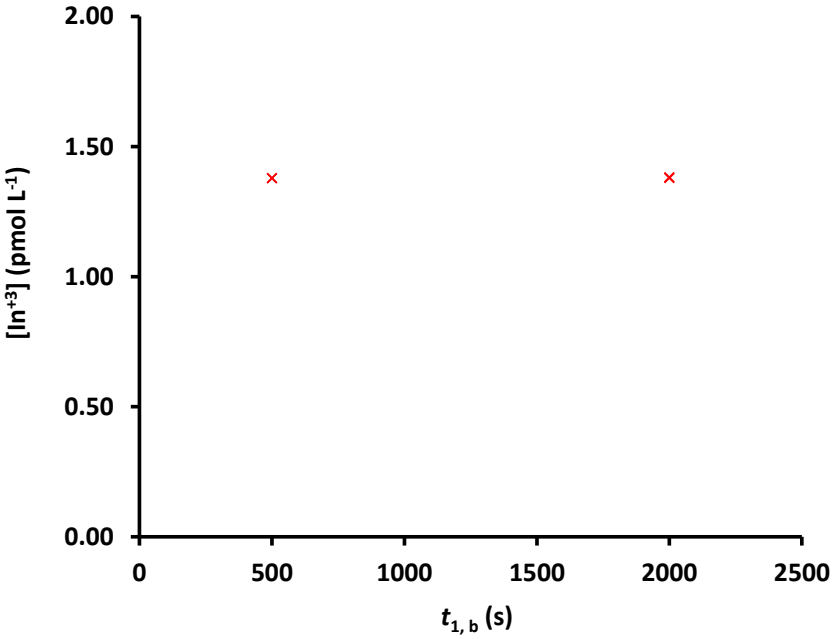

Figure 4-12: 2P-trajectory showing the stabilized situation for pH=6.06 with $c_{T,In}$ =140 µmol L^{-1}, $c_{T,Ox}$ =151 µmol $L^{-1}$and $c_{T,MES}$ =0.0100 mol L^{-1} applying Y=5.7×10^7 with $t_{1,a}$=800s.

4.5.6. General discussion of precipitated solutions

Figure 4-13 gathers all previously presented measurements at different pH values. As can be seen in this figure, the free concentrations of indium measured by AGNES reasonably agree with NIST predictions (see proximity of blue markers to the orange line that passes through the predictions of NIST 46.7 using VMINTEQ). The separations of the experimental values from the theoretical ones are not systematic, so that these differences can be attributed to experimental inaccuracies. Small variations in pH have a dramatic impact of the free concentration. Indeed, in precipitated solutions, the free concentration of indium decreases by a factor of 2 if the pH of a solution in equilibrium

with precipitated $In(OH)_3$ increases by 0.1 units. This can be explained by taking logarithms in the equation of the solubility product, eqn. (4-32)

$$\log\left\{In^{3+}\right\} = \log\left(K_{sp}\right) + 3\,pOH \tag{4-38}$$

If we split the activity as a product of concentration times activity coefficient and we recall that pH+pOH=14 at 25ºC,

$$\log\left[In^{3+}\right] = -\log\left(\gamma_{In^{3+}}\right) + \log\left(K_{sp}\right) + 3\left(14 - pH\right) = ct. - 3\,pH \tag{4-39}$$

So, assuming an uncontrolled oscillation in pH by 0.1 units, 3 multiplied by 0.1 equals to 0.3. In logarithmic scale this value (0.3) corresponds to a variation by a factor of 2 in the non-logarithmic scale.

The strategy of adding oxalate (used for pH 5.6 and 6) is faster and yielded consistent results with VMINTEQ and with the rest of experimental points, especially with those at pH 5.5.

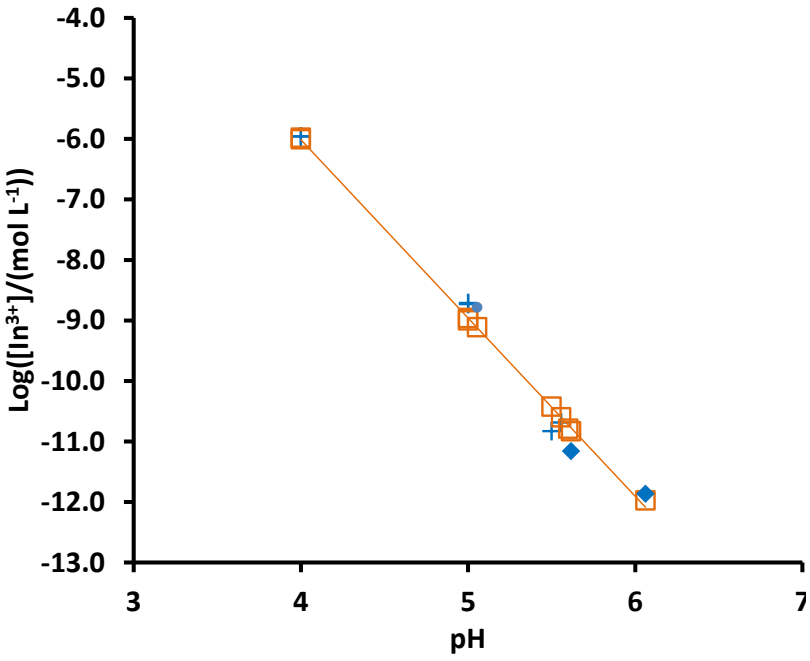

Figure 4-13: Free indium concentrations in precipitated solutions at different pH values. Blue markers stand for experimental determinations discussed in sections 4.5.1 to 4.5.5, while orange colour indicates the prediction of VMINTEQ using the database NIST 46.7. Blue cross shows the results of AGNES without added oxalate, while the diamond markers show the results with oxalate and MES at pH=5.6 and 6 and blue circle stands for AGNES measurement at pH=5.

4.6. Conclusions

Performing ADLC experiments provided an adequate way to calculate the lability degree of indium-oxalate and indium-hydroxide in our solutions and, thus, find proper $t_{1,a}$ for our AGNES measurements. The mobility of these complexes and their capability in shortening the predicted deposition times were remarkable. When the pH values were above 5.6, we took advantage of the high lability and mobility of In-Oxalate complexes to decrease the needed deposition times. Our experiments confirmed that in Indium-Hydroxide precipitated solutions, adding oxalate caused the complexes to contribute to the flux enabling a dramatic decrease in the needed deposition time. In our conditions, the helping factor of the indium-oxalate complexes was larger than that of indium-hydroxide. Moreover our results revealed that probably the difference between the K_{sp} of indium for the fresh and aged precipitated solutions which was reported in the work of Akselrud *et al*, could be due to the fact that waiting only one day was not enough for the precipitation process to be completed. Additionally the results demonstrated that AGNES measurements of precipitated solutions were very close to the predictions of the NIST 46.7. Finally, we were able to successfully determine picomolar concentrations of free indium in precipitated solutions.

4.7. References

(1) Tuck, D. G. Critical Evaluation of Equilibrium Constants in Solution Part A : Stability Constants of Metal Complexes. Critical Survey of Stability Constants of Complexes of Indium. *Int. Union Pure Appl. Chem.* **1983**, *54* (12).

(2) White, S. J. O.; Hemond, H. F. The Anthrobiogeochemical Cycle of Indium: A Review of the Natural and Anthropogenic Cycling of Indium in the Environment. *Crit. Rev. Environ. Sci. Technol.* **2012**, *42* (2), 155–186.

(3) Galceran, J.; Puy, J.; Salvador, J.; Cecília, J.; Van Leeuwen, H. P. Voltammetric Lability of Metal Complexes at Spherical Microelectrodes with Various Radii. *J. Electroanal. Chem.* **2001**, *505* (1–2), 85–94.

(4) Puy, J.; Galceran, J. Theoretical Aspects of Dynamic Metal Speciation with Electrochemical Techniques. *Curr. Opin. Electrochem.* **2017**, *1* (1), 80–87.

(5) Pinheiro, J. P.; Salvador, J.; Companys, E.; Galceran, J.; Puy, J. Experimental Verification of the Metal Flux Enhancement in a Mixture of Two Metal

Complexes: The Cd/NTA/glycine and Cd/NTA/citric Acid Systems. *Phys. Chem. Chem. Phys.* **2010**, *12*, 1131–1138.

(6) Salvador, J.; Puy, J.; Galceran, J.; Cecília, J.; Town, R. M.; Van Leeuwen, H. P. Lability Criteria for Successive Metal Complexes in Steady-State Planar Diffusion. *J. Phys. Chem. B* **2006**, *110* (2), 891–899.

(7) Vasca, E.; Ferri, D.; Manfredi, C.; Torello, L.; Fontanella, C.; Caruso, T.; Orrù, S. Complex Formation Equilibria in the Binary Zn^{2+}oxalate and In $^{3+}$ –oxalate Systems. *Dalt. Trans.* **2003**, No. 13, 2698–2703.

(8) Companys, E.; Cecília, J.; Codina, G.; Puy, J.; Galceran, J. Determination of Zn^{2+}concentration with AGNES Using Different Strategies to Reduce the Deposition Time. *J. Electroanal. Chem.* **2005**, *576* (1), 21–32.

(9) Alberti, G.; Biesuz, R.; Huidobro, C.; Companys, E.; Puy, J.; Galceran, J. A Comparison between the Determination of Free Pb(II) by Two Techniques: Absence of Gradients and Nernstian Equilibrium Stripping and Resin Titration. *Anal. Chim. Acta* **2007**, *599* (1), 41–50.

(10) Galceran, J.; Companys, E.; Puy, J.; Cecilia, J.; Garces, J. L. AGNES: A New Electroanalytical Technique for Measuring Free Metal Ion Concentration. *J. Electroanal. Chem.* **2004**, *566* (1), 95–109.

(11) Galceran, J.; Lao, M.; David, C.; Companys, E.; Rey-Castro, C.; Salvador, J.; Puy, J. The Impact of Electrodic Adsorption on Zn, Cd and Pb Speciation Measurements with AGNES. *J. Electroanal. Chem.* **2014**, *722–723*, 110–118.

(12) Jiménez-Piedrahita, M.; Altier, A.; Cecilia, J.; Rey-Castro, C.; Galceran, J.; Puy, J. Influence of the Settling of the Resin Beads on Diffusion Gradients in Thin Films Measurements. *Anal. Chim. Acta* **2015**, *885*, 148–155.

(13) T. Moeller, J. A. Contributions to the Chemistry of Indium. III. An Electrometric Study of the Precipitation of Hydrous Indium Hydroxide. *Am. Chem. Soc.* **1941**, *63* (10), 2625–2628.

(14) Orlov, Y. F.; Maslov, E. I.; Belkina, E. I. Solubilities of Metal Hydroxides. *Russ. J. Inorg. Chem.* **2013**, *58* (11), 1306–1314.

(15) White, S. J. O.; Hussain, F. A.; Hemond, H. F.; Sacco, S. A.; Shine, J. P.; Runkel, R. L.; Walton-Day, K.; Kimball, B. A. The Precipitation of Indium at Elevated pH in a Stream Influenced by Acid Mine Drainage. *Sci. Total Environ.* **2017**, *574*,

1484–1491.

(16) Chito, D.; Galceran, J.; Companys, E. The Impact of Intermetallic Compounds CuxZn in the Determination of Free Zn^{2+} concentration with AGNES. *Electroanalysis* **2010**, *22* (17–18), 2024–2033.

(17) David, C. A.; Galceran, J.; Rey-Castro, C.; Puy, J.; Companys, E.; Salvador, J.; Monné, J.; Wallace, R.; Vakourov, A. Dissolution Kinetics and Solubility of ZnO Nanoparticles Followed by AGNES. *J. Phys. Chem. C* **2012**, *116* (21), 11758–11767.

Chapter 5: Dissolution of indium (III) oxide nanoparticles

5.1. Abstract

This chapter investigates how AGNES can be used to study kinetic and thermodynamic features of the dissolution of indium nanoparticles in dispersions that contain KNO_3 0.1 mol L^{-1} at different pH values and in synthetic seawater solution at pH around 8.

Our initial hypothesis was that free indium measured in an equilibrated dispersion (with excess of nanoparticles) would have the same value as the free concentration found in equilibrium with precipitated $In(OH)_3$ at the same pH value. Another hypothesis was that the high concentration of chloride anions in the seawater media might help in the dissolution of the nanoparticles.

5.2. Introduction

In_2O_3 is one of the important materials for microelectronic applications and has been widely applied in engineering and in the electronic industry. For instance, it has been used in solar cells[1–3] and in opto-electronic equipments,[4] such as infrared reflectors, lasers, etc., since it has high optical transparency and reflectivity in the visible and IR regions respectively.[5] In_2O_3 can be used as catalyst material[6] and in gas sensing devices because of its good conductivity.[7–9]

Due to their vast applications, many investigations have focused on synthesizing In_2O_3 nanoparticles (NP) applying techniques such as evaporation,[5,9] sol gel process,[10] calcination process,[11] laser ablation in liquid techniques,[12] etc.

In_2O_3 appears in two types of crystal structure: bixbyite (of cubic unit cell) and corundum (structure of rhombohedral or hexagonal unit cell). It has been reported that most of the pure In_2O_3 has the structure of bixbyite cubic cell.[13] It was confirmed that during the transition from cubic $In(OH)_3$ to bixbyite type In_2O_3, no intermediate phase can be formed. So, it was concluded that orthorhombic InOOH does not form as a result of dehydroxilation of cubic $In(OH)_3$.[14]

Three possibilities have been suggested by researchers for the origin of the toxicity of NPs.[14,15] In some cases, it has been indicated that this toxicity comes from the dissolved free ion in solution, in some others it has been demonstrated that it is the nature of the NPs that causes such health problems, while another group of researchers suggest that NPs and dissolved free ions in the solution are both important factors.[16]

As it was discussed in chapter 1, section 1.3, indium NPs are toxic and their toxicity might cause several health problems.[14,17–19] Hence, it is crucial to study the process of dissolution of In_2O_3 NPs in various samples using a proper technique. The electroanalytical technique AGNES not only was used for determining free concentrations of amalgamating elements such as Zn, Cd, Pb and In (discussed in previous chapters) in various matrices, but also it was successfully applied to study the dissolution of ZnO NPs,[20,21] Cd-based NPs,[22,23] Cd and Pb NPs,[24] Pb NPs[25] and adsorption of cadmium on titanium dioxide NPs.[26]

Our claim is that it might be possible to study the dissolution of In_2O_3 NPs at various pH and media. Therefore, in this chapter it will be discussed how ASV and AGNES can be used for this aim.

5.3. Experimental

5.3.1. Reagents

Indium (III) oxide was bought from Sigma-Aldrich (Sant Louis, USA), and according to the manufacturer it was a nanopowder with particle size < 100 nm (TEM) 99.9% trace metal basis. Indium dispersions were prepared by dispersing around 10 mg of In_2O_3 NPs in 100 mL of KNO_3 0.1 mol L^{-1} at different pH values.

Synthetic seawater solution was prepared by dissolving known amounts of inorganic salts such as NaCl (TraceSelect, Fluka, St Louis, USA), $MgCl_2.6H_2O$ (p.a., Merck, Dramstadt, Germany), Na_2SO_4 (p.a., Prolado, Fontenay), $CaCl_2.2H_2O$ (reagent grade, Scharlau, Sentmenat, Spain), KCl (trace select, Fluka, St Louis, USA), $NaHCO_3$ (p.a., Merck, Darmstadt, Germany), KBr (ACS reagent, ACROS, New Jersey, USA), H_3BO_3 (p.a., Merck, Darmstadt, Germany), $SrCl_2.6H_2O$ (p.a., Merck, Darmstadt, Germany) and NaF (98%, Panreac, Barcelona). 1L of stock solution of sea water was prepared as follows: 0.410 mol L^{-1} NaCl, 0.053 mol L^{-1} $MgCl_2.6H_2O$, 0.028 mol L^{-1} Na_2SO_4, 0.014 mol L^{-1} $CaCl_2.2H_2O$, 9.08×10^{-3} mol L^{-1} KCl, 2.33×10^{-3} M $NaHCO_3$, 8.24×10^{-4} mol L^{-1} KBr, 4.37×10^{-4} mol L^{-1} H_3BO_3, 9.00×10^{-5} mol L^{-1} $SrCl_2.6H_2O$ and 7.14×10^{-5} mol L^{-1} NaF. 10 mg of In_2O_3 NPs were added to 100 mL of this solution and the pH of this synthetic seawater solution was checked and adjusted at pH=8.

Potassium nitrate was used as the inert supporting electrolyte at 0.1 mol L^{-1} (for all experiments except for the one of seawater) and prepared from solid KNO_3 (TraceSelect, Fluka, St Louis, USA). KOH and HNO_3 0.1 mol L^{-1} (Fluka standard solutions) were used

to adjust the pH of the solutions. Ultrapure water (Synergy UV purification system Millipore) was used in all experiments. Purified water saturated N_2 (purity ≥ 99.999%) was used for deaeration and blanketing the solutions. Solutions that only included In_2O_3 and KNO_3 0.1 mol L^{-1} after the preparation at each specific pH were kept in closable plastic cells stirred at 1300 rpm.

5.3.2. Instrumentation

All experiments were performed using NOVA 1.11 software. Voltammetric measurements were carried out with Autolab μAUTOLAB type III and PGSTAT101 potentiostats (Utrecht, Netherlands) attached to Metrohm 663 VA Stands.

The working electrode was a Metrohm Hanging Mercury Drop Electrode (HMDE). Glassy carbon was used as the auxiliary electrode and the reference electrode was protected with double-junction Ag/AgCl/3 mol L^{-1} KCl with KNO_3 0.1 mol L^{-1} in the salt bridge. A glass jacketed cell was used in all the experiments and thermostated at 25.0°C. A glass combined electrode (5209, Crison, Alella, Spain) was attached to an Orion Dual Star ion analyzer (Thermo, Singapore) and introduced in the cell to measure and, accordingly, control the pH.

Solutions were purged with N_2 before each experiment to avoid O_2 interference (e.g. so that pH was more stable close to the surface of the electrode).

A magnetic stirrer COLOR SQUID (IKA, Germany) was used to keep the solutions under stirring at a fixed speed during some days to favour dissolution.

5.3.3. Procedures

ASV (Anodic Stripping Voltammetry) was applied to explore whether there is a possibility to detect any peak of indium. In ASV the smallest size of the drop (labelled "1" which according to the catalogue corresponds to a radius r_0 = 141 μm) was utilized and, in the procedures, the waiting time was 5 s, the number of new drops before starting the ASV was fixed to be 5, the interval time was 1 s and the scan rate was 0.005 V/s. More details about this technique have been given in chapter 2, section 2.1.3.1.5.

For measurements with AGNES, two strategies, 1P and 2P, were applied using drop size"1". Specific details about these two AGNES variants have been discussed in detail in chapter 2, section 2.3.1.

5.4. Results

5.4.1. Performing ASV (Anodic Stripping Voltammetry) at pH=2

A preliminary trial was an ASV applied to check whether we could detect indium in a solution with NPs that only contained KNO_3 0.1 mol L^{-1} at pH=2 after 17 days of contact. If we had been unable to detect any peak of In with ASV in these conditions (favourable for dissolution), it would have meant that further [In^{3+}] determinations would have been very difficult or not possible.

Two deposition times were used: *t*= 30 and 300 s. Figure 5-1 shows that deposition time 30 s was enough to see the signal of indium at around -0.51 V.

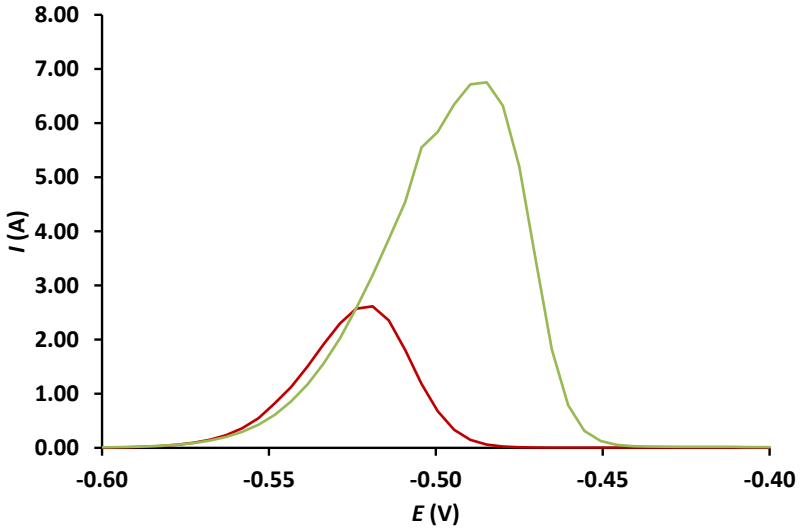

Figure 5-1: Anodic Stripping Voltammogram in a dispersion that contained 10 mg of In_2O_3 in 100 mL of KNO_3 0.1 mol L^{-1} at pH=2 using two deposition times, 30 and 300 s. Green line stands for deposition time 300 s, while red line shows the signal corresponding to deposition time 30 s.

5.4.2. Determining [In^{3+}] in solutions of In_2O_3 at pH=2

As it was explained in section 5.3.1, dispersions of around 10 mg of In_2O_3 in 100 mL were used for our measurements. If we assume equilibrium with only one solid phase, the total amount of In_2O_3 is irrelevant for the equilibrium free indium concentration, because the solubility product can only imply the activities of In^{3+} and OH^- (which is fixed via the pH). It is also important to indicate that even at such acidic pH full dissolution of the NPs was not observed.

The solubility product of $In(OH)_3$ (equation (4-36) discussed in section 4.5) with log K_{sp}= -36.92 taken from database of NIST 46.7[27] was used to estimate a rough possible value of [In^{3+}] around 1.15 mol L^{-1} in solutions at pH=2, provided an infinite amount of

$In(OH)_3(s)$ was present. If -on the contrary- there was the finite initial amount of indium from the 100 mg In_2O_3 NP in a liter, with $In(OH)_3(s)$ as the only possible solid phase, then one would expect total indium dissolution yielding a free indium concentration of 720 μmol L^{-1}. Hence, given that we saw most of particles not having been dissolved, we conclude that indium is in another type of precipitate, different from $In(OH)_3$. However, equation 4-32, $Y = \frac{Q}{\left[In^{3+}\right] \times \eta_Q}$ was used to calculate the needed Y taking a free concentration 5.21×10^{-4} mol L^{-1}. Our calculations predicted that the needed Y should be around 0.024, but we applied a higher Y (Y=2) to start the experiment given that even a deposition time of 20 s with AGNES 1P should be enough to reach equilibrium.

Figure 5-2 represents the same experimental data as in figure 5-3, with the difference that figure 5-2 shows the measured charge, while figure 5-3 represents the concentration of In^{3+} in dispersions of NPs which had been in contact with the medium for 17 days. From figure 5-2, we can see that the equilibrium situation has been almost reached at each specific Y. For Y=2, t_1-t_w= 20, 50, 100 and 200 s were used, then for Y=5, t_1-t_w = 50, 100 and 200 s were applied. As can be seen from figures 5-2 and 5-3, t_1-t_w= 100 s can be taken as a deposition time suitable for both gains to reach the equilibrium situation.

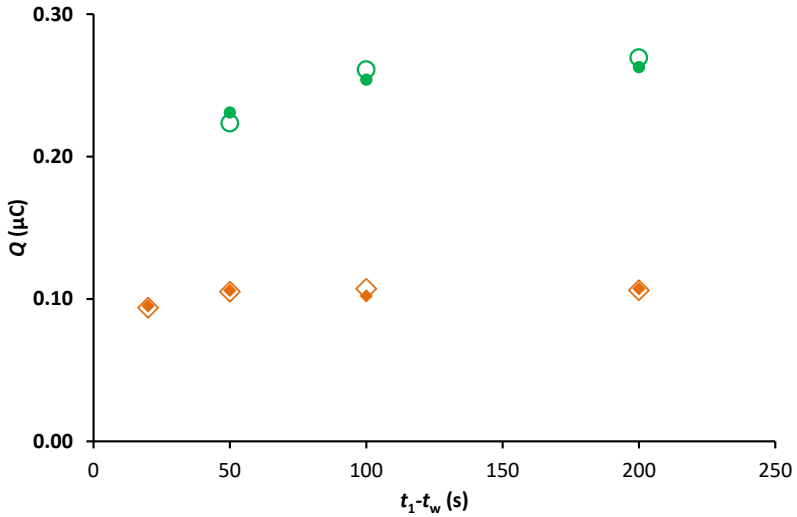

Figure 5-2: 1P trajectories showing the measured charge versus deposition time, in solutions that contained 10 mg of In_2O_3 NP in 100 mL of KNO_3 0.1 mol L^{-1}, at pH=2.00, after being in contact with NPs for 17 days. Filled symbols are first measurements, while their replicates are not filled. Orange diamonds and green circles stand for Y=2 and Y=5, respectively.

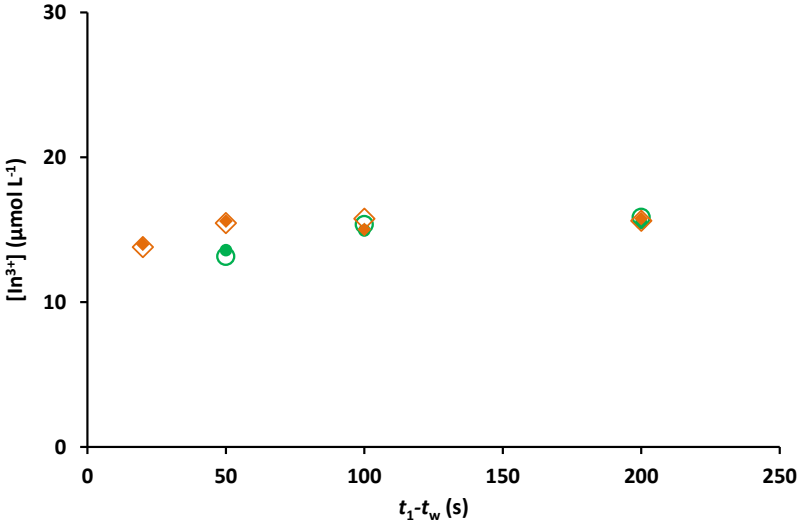

Figure 5-3: 1P trajectories of figure 5-2 re-plotted in terms of free concentration of In^{3+} versus deposition time. Markers as in previous figure.

Our experiments were designed to do some repetitions after some days, to check whether we might face further dissolution of indium NPs.

Figure 5-4 (for charge) and figure 5-5 (for concentration) both use the same data for a solution that was in contact with NPs for 49 days.

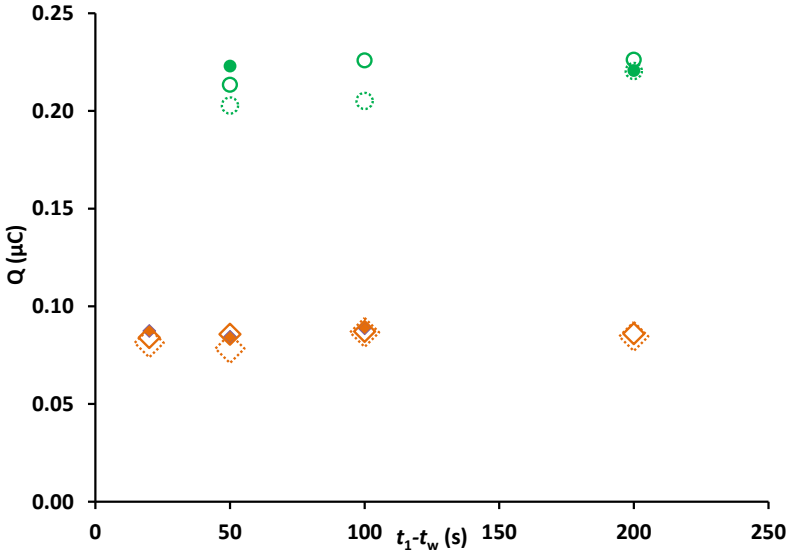

Figure 5-4: Trajectory of charge versus deposition time, in solutions that contained 10 mg of In_2O_3 NP in 100 mL of KNO_3 0.1 mol L^{-1}, at pH=2.00, being in contact with NPs for 49 days. Filled symbols are first measurements, while their replicates are not filled. Orange diamonds and Green circles stand for Y=2 and Y=5, respectively.

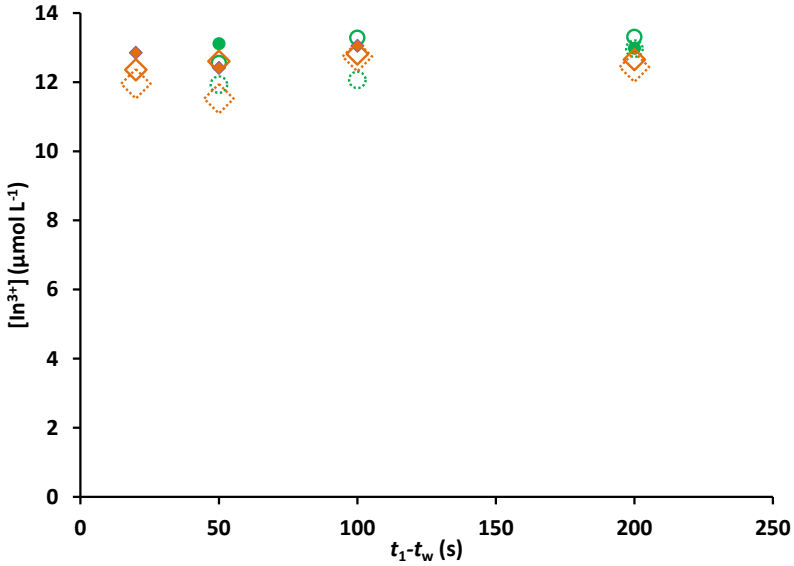

Figure 5-5: Re-plot of figure 5-4 in terms of free concentration of In^{3+} versus deposition time. Same markers as in previous figure.

Table 5-1 shows AGNES measurements and the predictions of NIST 46.7 at this pH (assuming, as VMINTEQ 3.1 by default does, just one possible solid phase: $In(OH)_3$).

Table 5-1: Details about the experiments determining free indium concentrations at pH=2 in NP dispersions that contain KNO_3 0.1 mol L^{-1}. Log $[In^{3+}]^{NIST\ 46.7}$ corresponds to the predicted value assuming full dissolution. Number in between parenthesis indicates standard deviation and refers to the last significant digit.

pH	Days in contact	$[In^{3+}]^{NIST46.7}$ (mol L^{-1})	$[In^{3+}]^{AGNES}$ (mol L^{-1})	*Number of the related figures*
2.00	17	5.21×10^{-4}	$1.461(3)\times10^{-5}$	5-2 and 5-3
2.00	49	5.22×10^{-4}	$1.25(1)\times10^{-5}$	5-4 and 5-5

Although the predictions suggested that at such pH and conditions we should have full dissolution, experimentally just a low proportion of In NPs was seen to be dissolved.

Figure 5-6 shows the effect of contact time on the free concentration of indium. From Figure 5-6 and table 5-1 it can be concluded that at pH=2, a partial (around 0.0012%) dissolution of the NPs was reached within 17 contact days, with negligible variation in 32 more contact days. The measured concentration values were almost 45 times lower than that predicted by VMINTEQ for the dissolution of $In(OH)_3$.

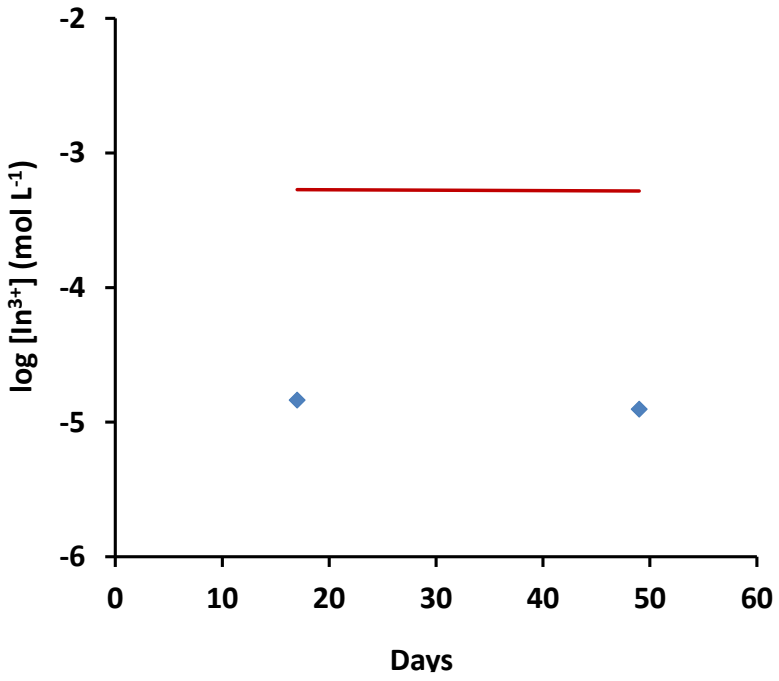

Figure 5-6: Effect of elapsed time in contact with In_2O_3 on the free indium concentration at pH=2. Blue diamonds stand for free indium concentration measured by AGNES, red line is the prediction of NIST 46.7 (full dissolution). Values are detailed in table 5-1.

5.4.3. Determining $[In^{3+}]$ in solutions of In_2O_3 at pH=3

Figure 5-7 (charges) and figure 5-8 (concentrations) use the same data of dissolution (10 mg of Indium NPs in 100 ml KNO_3 0.1 M) at pH 3 after 7 contact days with NPs.

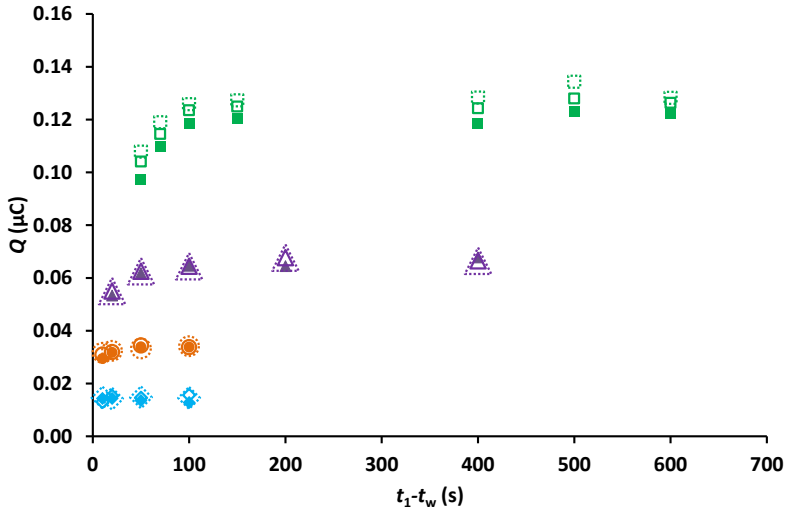

Figure 5-7: Trajectory of charge versus deposition time in dispersions that contained 10 mg of In_2O_3 NP in 100 mL of KNO_3 0.1 mol L^{-1}, at pH=3.00, being in contact with the NPs for 7 days. Filled symbols are first measurements, while their replicates are not filled. Symbols blue diamond, orange circle, purple triangles and green square stand for Y=2, 5, 10 and 20, respectively.

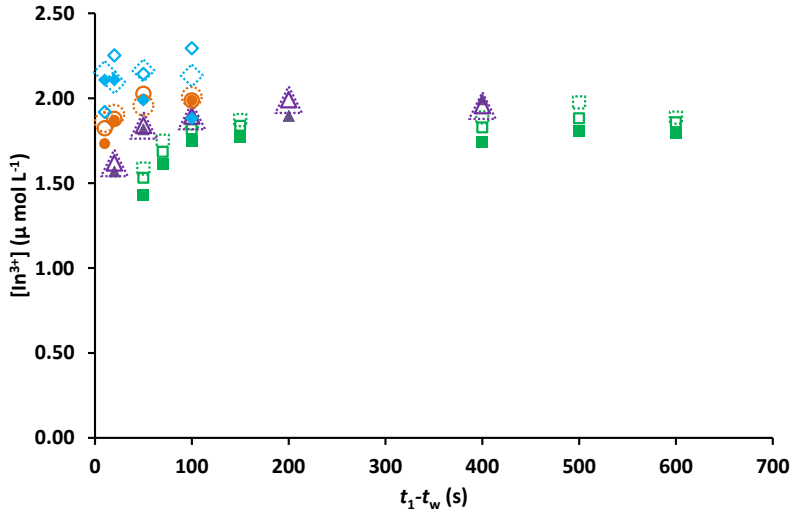

Figure 5-8: Re-plot of figure 5-7 in terms of free concentration of In^{3+} versus deposition time in solutions that contained 10 mg of In_2O_3 NP in 100 mL of KNO_3 0.1 mol L^{-1}, at pH=3.00, being in contact with NPs for 7 days. Symbols blue diamonds, orange circle, purple triangles and green square stand for Y=2, 5, 10 and 20, respectively.

The expected free concentration at this pH (assuming a solid phase of $In(OH)_3$ in equilibrium with In^{3+}) is 1.17×10^{-3} mol L^{-1}. Figure 5-9 and figure 5-10 represent the same data (taken after 29 days of being in contact with In_2O_3 NPs), with the difference that figure 5-9 shows trajectories of charge, while figure 5-10 shows the trajectories of concentrations versus the deposition time.

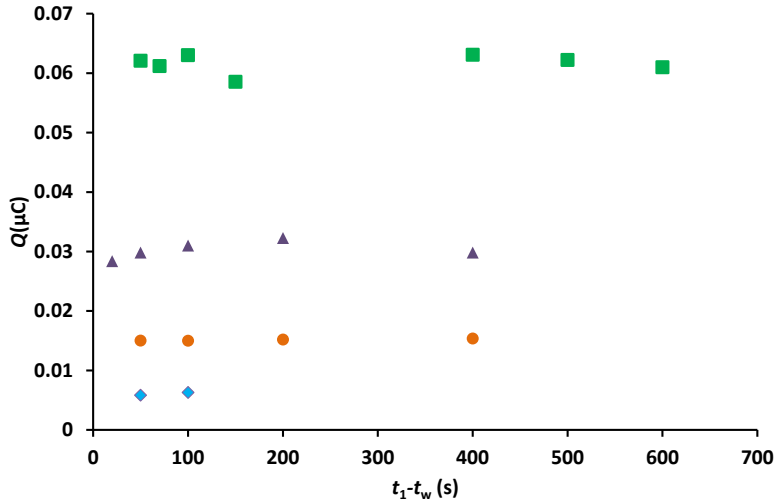

Figure 5-9: Trajectories of charge versus deposition time in solutions that contained 10 mg of In_2O_3 NP in 100 mL of KNO_3 0.1 mol L^{-1}, at pH=3.00, being in contact with NPs for 29 days. Blue diamonds, orange circles, purple triangles and green squares stand for Y=2, 5, 10 and 20, respectively.

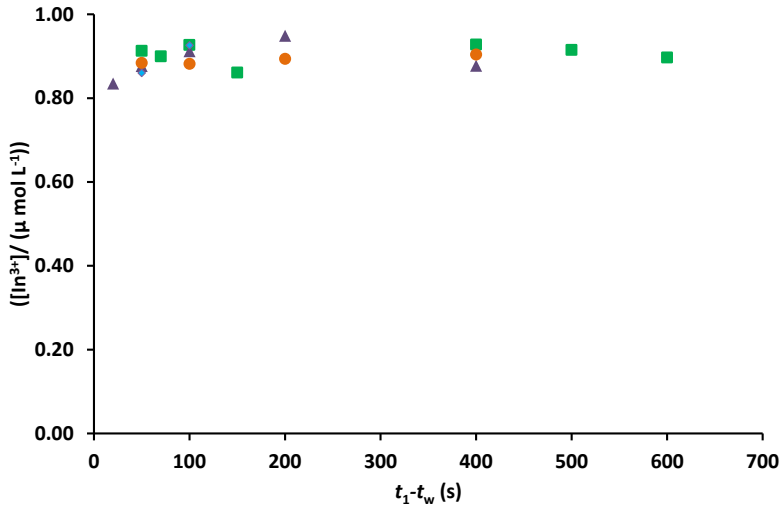

Figure 5-10: Re-plot of the figure 5-9, with the difference of representing trajectories of concentration versus deposition time in solutions that contained 10 mg of In_2O_3 NP in 100 mL of KNO_3 0.1 mol L^{-1} at pH=3.00, being in contact with NPs for 29 days. Markers are the same as in previous figure.

Table 5-2 gives more information about species distribution at pH=3 and provides more information about AGNES measurements and predictions of NIST 46.7

Table 5-2: Indium concentrations in dispersions of nanoparticles at pH=3.

pH	Days in contact	$[In^{3+}]^{NIST\ 46.7}$ (mol L^{-1})	$[In^{3+}]^{AGNES}$ (mol L^{-1})	*Number of the related figures*
2.99	7	5.85×10^{-4}	$1.89\ (2)\times10^{-6}$	5-7 and 5-8
2.99	29	5.88×10^{-4}	$9.1\ (2)\times10^{-7}$	5-9 and 5-10

Figure 5-11 is related to the data mentioned in table 5-2 and shows that the solubility of indium oxide NPs almost remained constant during 22 days.

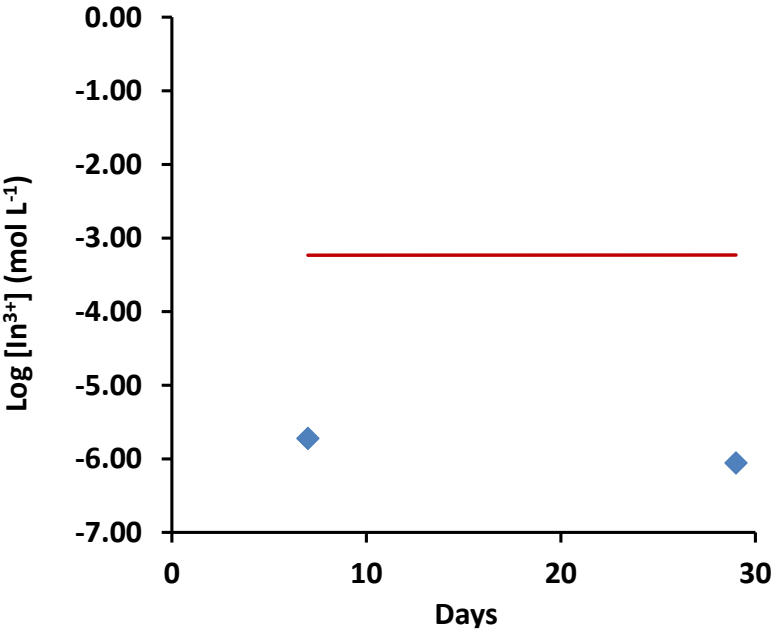

Figure 5-11: Effect of elapsed contact time on the free indium concentration at pH 3. Blue diamond's stand for free indium concentration measured by AGNES, red line shows the predictions of NIST 46.7. Values are related to table 5-2.

5.4.4. Determining $[In^{3+}]$ in solutions of In_2O_3 at pH=4

Figure 5-12 shows the measured charge versus the deposition time at pH around 4 in a dispersion (10 mg of indium NPs in 100 mL of KNO_3 0.1 M) in contact with NPs for 4 days. Figure 5-13 represents the measured free indium concentration using the same data as in figure 5-12.

From figure 5-12 one can see the measured charges at different *Y*. Also it can be observed that, from the applied gains (*Y*=800, 400 and 200), only for *Y*=200 have the measured charges reached clearly the constant situation (stabilized around 0.02 µC).

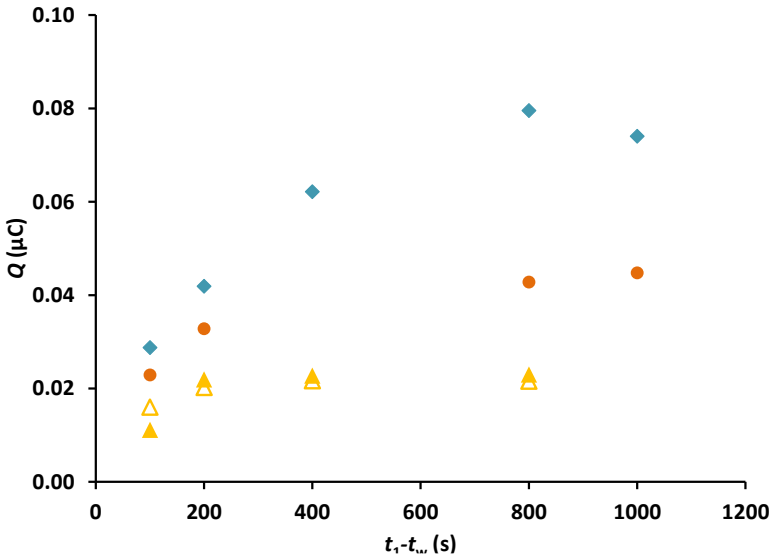

Figure 5-12: Charges measured at different deposition times, in solutions that contained 10 mg of In_2O_3 NP in 100 mL of KNO_3 0.1 mol $^{-1}$, at pH=4.06, after being in contact with NPs for 4 days. Filled yellow symbol correspond to first measurements, while the replicate markers are not filled. Yellow triangles stand for Y=200, orange circles represent Y= 400 and blue diamond's stand for Y= 800.

In figure 5-13, the series for *Y*=200 (yellow triangle) has reached the equilibrium situation from a deposition time 200 up to 800 s.

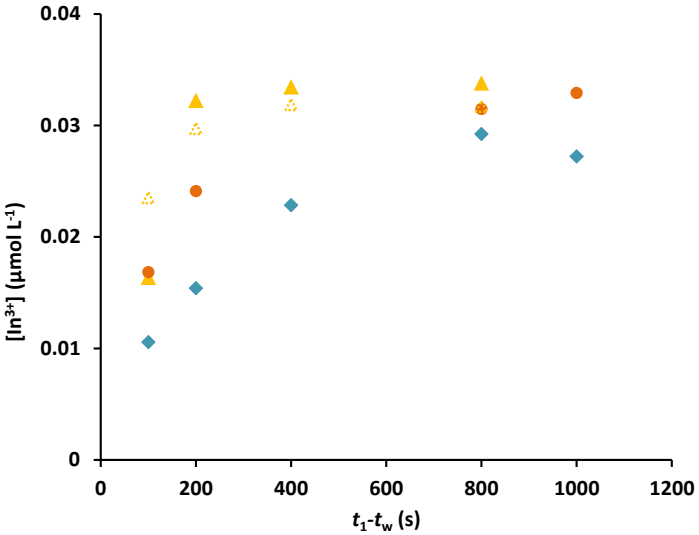

Figure 5-13: Re-plot of figure 5-12, with the difference of representing trajectories of concentration versus deposition time, in solutions that contained 10 mg of In_2O_3 NP in 100 mL of KNO_3 0.1 mol^{-1}, at pH=4.06, after being in contact with NPs for 4 days. Filled yellow symbol for first measurements and not filled for replicates. Yellow triangles stand for Y=200, orange circles show Y= 400 and blue diamond demonstrate Y=800.

After 13 days another measurement was applied with the strategy 2P. Figure 5-14 shows that for a Y = 1000 using a $t_{1,a}$ =300 s caused a slight overshoot at the beginning, then it reached the equilibrium situation above $t_{1,b}$= 800 s. Moreover, using $t_{1,a}$= 100 s

made a sharp undershoot in the begining, then it became constant when $t_{1,b}$ was almost more than 800 s.

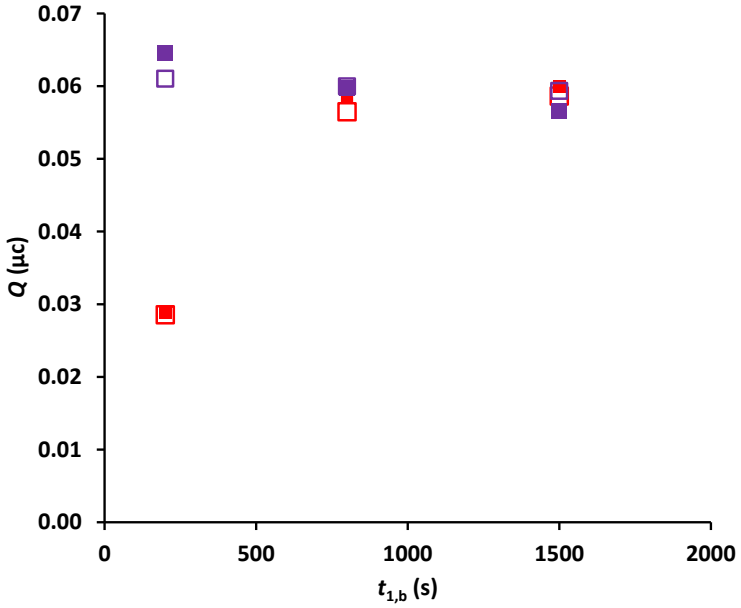

Figure 5-14: Trajectory of concentration versus deposition time in solutions that contained 10mg of In_2O_3 NP in 100 mL of KNO_3 0.1 mol $^{-1}$, at pH=4.06, after being in contact with NPs for 13 days. Filled symbols for first measurements and not filled for replicates. Purple squares stand for Y=1000 using $t_{1,a}$=300 s, while red squares show the same Y but with $t_{1,a}$= 100 s.

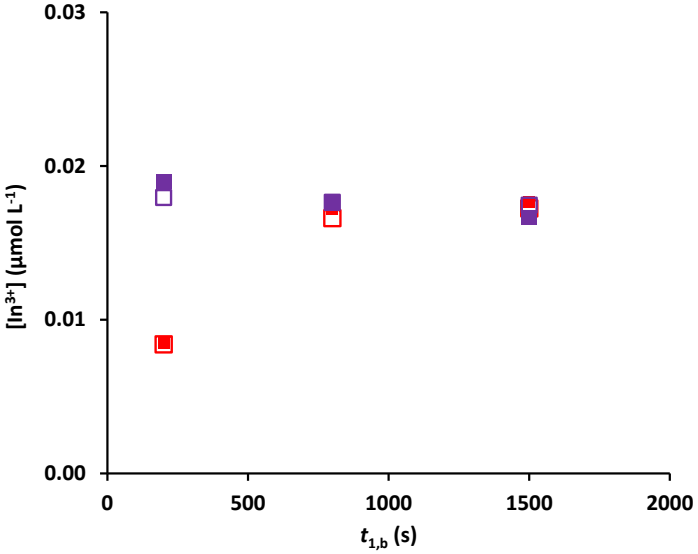

Figure 5-15: Re-plot of figure 5-14 with the difference of representing trajectories of concentration versus deposition time in solutions that contained 10 mg of In_2O_3 NP in 100 mL of KNO_3 0.1 mol L $^{-1}$, at pH=4.06, after being in contact with NPs for 13 days. Filled symbols are first measurements, while their replicates are not filled. Purple squares stand for Y=1000 using $t_{1,a}$=300 s, while red squares show the same Y but with $t_{1,a}$= 100 s.

Table 5-3 gives more information about direct measurements at pH=4 and compares AGNES measurements with NIST 46.7 predictions assuming equilibrium with $In(OH)_3$.

Table 5-3: Indium concentrations in dispersions of nanoparticles at pH around 4. Number in parenthesis indicates standard deviation and refers to the last significant digit.

pH	Days in contact	$[In^{3+}]^{NIST\ 46.7}$ (mol L^{-1})	$[In^{3+}]^{AGNES}$ (mol L^{-1})	*Number fo the related figures*
4.06	4	7.10×10^{-7}	$3.2\ (1)\times10^{-8}$	5-12 and 5-13
4.06	13	7.10×10^{-7}	$1.77\ (7)\times10^{-8}$	5-14 and 5-15

To check the solubility of In_2O_3 NPs in our solutions at around pH=4, we studied the effect of the days elapsed (see figure 5-16) since the day that the solution was prepared. During all these days the solution was kept in a closed plastic tube with stirring rate 1300 rpm.

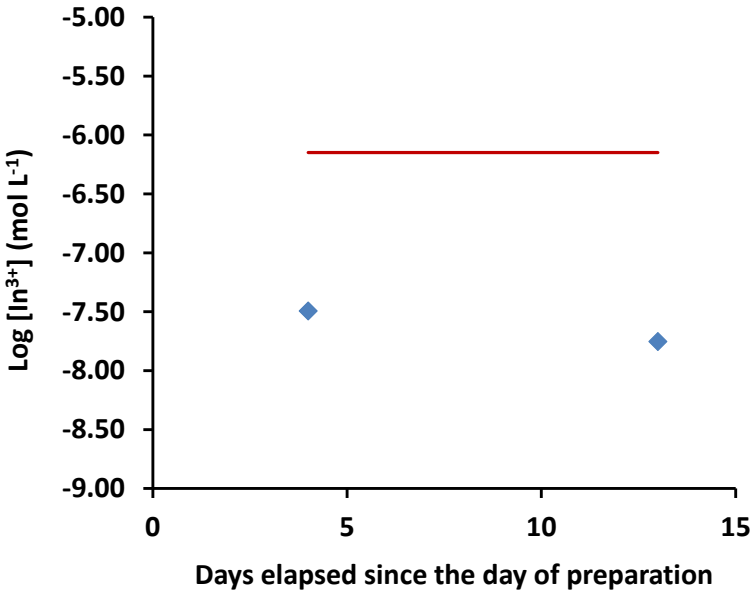

Figure 5-16: Logarithm of free indium concentration determined with AGNES versus days of the solution being in contact with the NPs. The solution contained 10 mg of In_2O_3 NP in 100 mL of KNO_3 0.1 mol L^{-1} at pH=4.06. Blue diamond's show AGNES measurements, while the red line shows the predictions of VMINTEQ.

5.4.5. Determining $[In^{3+}]$ in solutions of In_2O_3 when pH is re-adjusted from pH= 3 to pH= 4

In this section we discuss a new kind of experiments where we measured the evolving free indium concentration in a dispersion which, after being previously equilibrated (for 29 days) at pH 3, was moved to pH 4.

Figure 5-17 shows the collapse of the trajectories using 2P, applying Y=1000 with $t_{1,a}$=100 and $t_{1,a}$=300 s, this solution had been at pH=4 for one day.

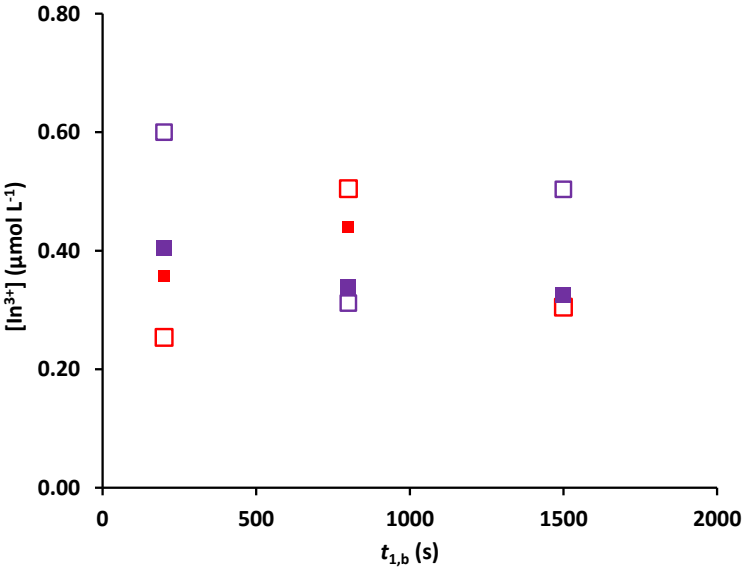

Figure 5-17: Trajectory of concentration versus deposition time in solutions that contained 10 mg of In_2O_3 NP in 100 mL of KNO_3 0.1 mol L^{-1}, when the solution -initially stabilized at pH=3 for 29 days- was moved to pH=4.006 and the measurement was done after 1 day of being at the higher pH. Open markers represent replicates. Purple squares stand for Y=1000 using $t_{1,a}$=300 s, while red squares show the same Y, but with $t_{1,a}$= 100 s.

Figure 5-18 presents the collapse of the trajectories at the different gains after 2-day contact at pH=4.

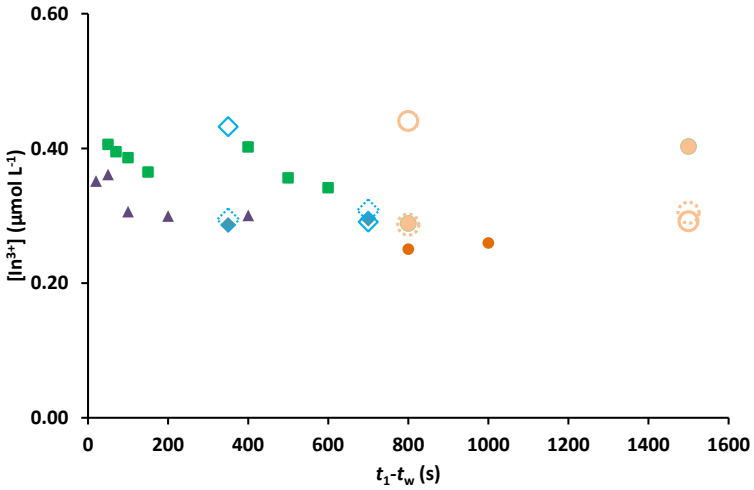

Figure 5-18: Trajectory of concentration versus deposition time in solutions that contained 10 mg of In_2O_3 NP in 100 mL of KNO_3 0.1 mol L^{-1}, where the solution- initially at pH=3 for 29 days- was moved to pH=3.986, and measurement was done after being 2 days at the higher pH. Open markers represent a replicate. Purple triangles, green square, blue diamonds and orange circles stand for Y=10, 20, 50 and 100, respectively.

Then, almost 16 days later, another experiment was performed to check the evolution of the free concentration (see figure 5-19). Through this figure one can also see the collapse of the trajectories.

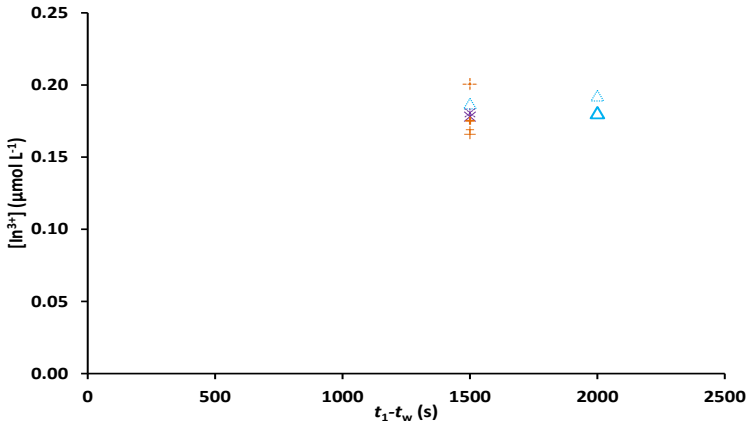

Figure 5-19: Trajectory of concentration versus deposition time, in solutions that contained 10 mg of In_2O_3 NP in 100 mL of KNO_3 0.1 mol L^{-1}, where the solution – initially at pH=3 for 29 days- was moved to pH=4.005, and the measurements were done after 16 days at high pH. Cross symbols, orange crosses and blue diamond's stand for Y=100, 150 and 200, respectively.

Table 5-4 presents more details about these AGNES measurements and NIST 46.7 predictions.

Table 5-4: Indium concentrations at pH=4 in a dispersion of In_2O_3 previously equilibrated at pH 3. Number within parenthesis indicates standard deviation and refers to the last significant digit.

pH	**Days in contact**	**$[In^{3+}]^{NIST\ 46.7}$ (mol L^{-1})**	**$[In^{3+}]^{AGNES}$ (mol L^{-1})**	***Number of the related figure***
4.006	1	1.08×10^{-6}	$3.7\ (8)\times10^{-7}$	5-17
3.986	2	1.24×10^{-6}	$3.4\ (6)\times10^{-7}$	5-18
4.005	16	1.09×10^{-6}	$1.6\ (3)\times10^{-7}$	5-19

Figure 5-20 shows the effect of days being elapsed with indium NPs at this re-adjusted pH. From this figure, it can be noticed that there was a very slight decrease in the free indium concentration measured after 16 days waiting with stirring.

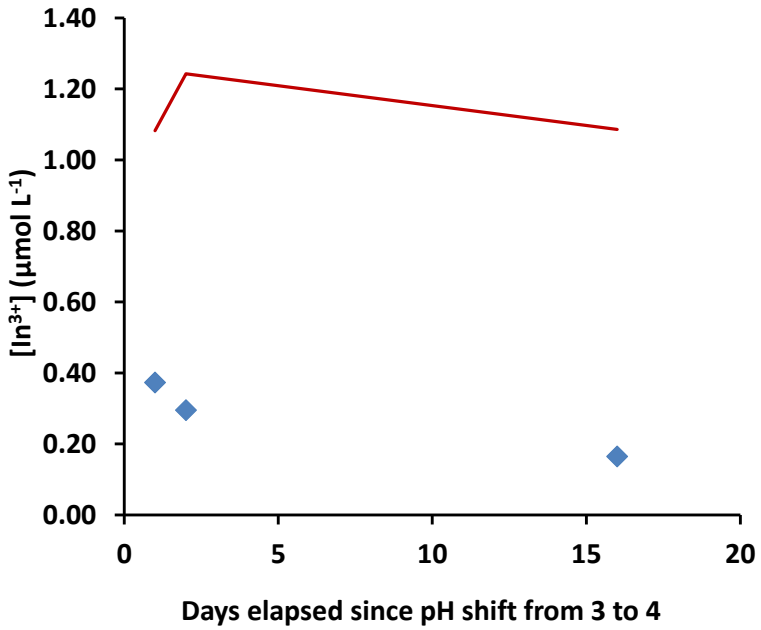

Figure 5-20: Free indium concentrations determined with AGNES versus days of the solutions being in contact with the NPs at the new pH 4 (pH 4.006, 3.986 and 4.000 are values related to first, second and third blue diamond). The solutions contained 10 mg of In_2O_3 NP in 100 mL of KNO_3 0.1 mol L^{-1}.

5.4.6. Determining $[In^{3+}]$ in solutions of In_2O_3 at pH=5

To determine free concentrations of indium at such high pH, an experiment of ASV was performed. From figure 5-21 one can see that even with two different deposition times, 30 s and 800 s, there was no detectable peak of indium around its usual potential at -0.60 V. Hence, not detecting any peak of indium in ASV (that measures free and labile metal) for a long deposition time of 800 s, led us to conclude that the free concentration was probably too low to be quantified with AGNES in a reasonable time.

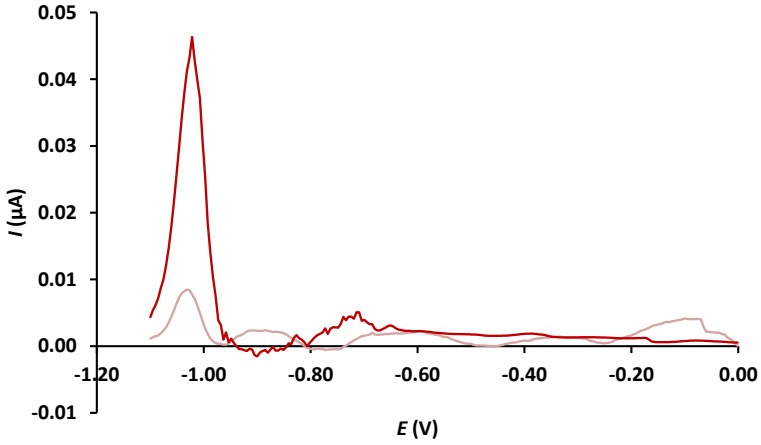

Figure 5-21: Anodic Stripping Voltammogram in a dispersion of 10 mg of In_2O_3 NP in 100 mL of KNO_3 0.1 mol L^{-1} at pH=5.00, being in contact with NPs for eight days, using two deposition times, 30 and 800 s. Pink line stands for deposition time 30 s, while red line shows signals corresponding to deposition time 800 s.

5.4.7. Free concentration of indium in synthetic seawater solutions

Synthetic seawater solution was prepared as has been described in this chapter in section 5.3.1.[14] 10 mg of In_2O_3 NP were added to 100 mL of synthetic seawater. The dispersion was stirred during 16 days. After this period, ASV experiments were performed using three deposition times: 30, 300 and 600 s. As can be seen in figure 5-22 around the potential -0.6 V there was no peak of indium. Thus, we were not able to perform further experiments and measure free indium concentrations in our synthetic seawater solutions at pH=8. We concluded that the free indium concentration in this solution was too low to be measured with AGNES in a reasonable time.

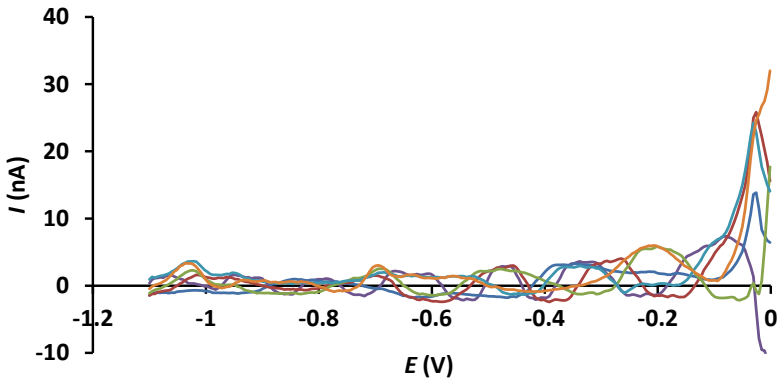

Figure 5-22: ASV of seawater solutions (10 mg of In_2O_3 in 100 mL of seawater solution) at pH=8.00 for 16 days. Lines with colours purple, dark blue and red are ASV results using deposition time 30 s. Lines with colours green and light blue are ASV results using deposition time 300 s and orange line represents ASV results using deposition time 600 s.

5.4.8. General discussion

Figure 5-23 represents all previous results presented in sections 5.4.3, 5.4.4, 5.4.5 and 5.4.6 at different pH values. The blue line is a guide to the eye about the direct measurements of free indium in contact with In_2O_3 NPs at each specific pH. The orange markers represent NIST 46.7 (VMINTEQ) expectations if the solubility was ruled by the solubility product of $In(OH)_3$. One can see that free indium concentration determined at re-adjusted pH (pink cross symbol) was very close to the predictions of NIST 46.7. As can be observed in this figure, the blue line that passes through the direct measurements at each pH is almost linear with a slope close to -1.34.

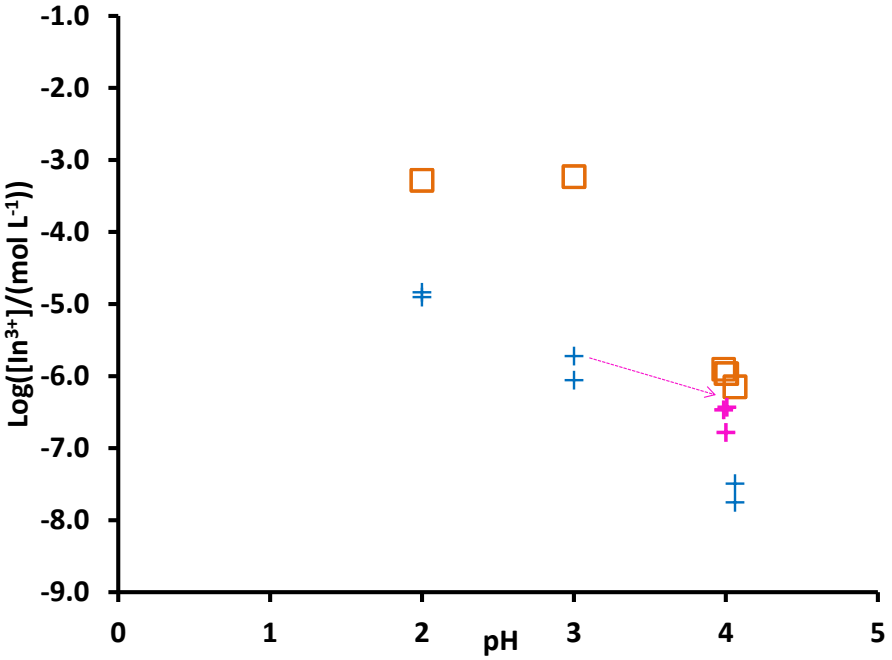

Figure 5-23: Free indium concentration measured in the solution that contained 10 mg of In_2O_3 NP in 100 mL of KNO_3 0.1 mol L^{-1}. Blue and purple cross symbols represent AGNES measurements discussed in sections 5.4.1 to 5.4.6, while the orange squares represent predictions of VMINTEQ assuming equilibrium with $In(OH)_3$ or full dissolution (pH 2 and 3). The predicted concentration of free indium using NIST 46.7 at pH 2, equals to 5.21×10^{-4} mol L^{-1}. Among AGNES results, symbols with the colour pink refer to the measurements achieved by re-adjusting the pH from 3 to 4 discussed in section 5.4.5, while the blue ones stem from direct measurements at each specific pH.

One interesting study, that was done some years ago, revealed that changing the pH of the solution generated a metastable phase of a Zn species around the existing ZnO NPs.[5] Figure 5-24 illustrates a possible hypothesis to explain the difference in free indium concentration at pH 4 depending on whether one has passed through pH 3 or not. The hypothesis is that a shell of indium hydroxide tend to cover the In_2O_3 NPs. This is roughly depicted in figure 5-24. Hence according to the equation for the solubility product of $In(OH)_3$:

$$K_{sp} = \left\{In^{3+}\right\}\left\{OH^{-}\right\}^{3} \qquad (5\text{-}1)$$

(see also eqn. (4-27)), the free indium concentration, determined at this re-adjusted pH, corresponds to the equilibrium value of the hydroxides.

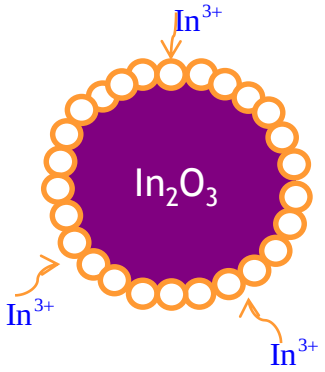

Figure 5-24: Schematic representation of the hypothesis of coverage of In_2O_3 NP by $In(OH)_3$ (phase depicted as orange circles) when determining free indium at re-adjusted pH=4.

We suggest that one way of testing our hypothesis would be to increase the number of (solid) NPs, then, in such a case, there might be a larger area so that the amount of precipitated $In(OH)_3$ would be insufficient to cover all the NPs.

5.5. Conclusions

AGNES was a proper method for determining free indium concentration in dispersions that only contained In_2O_3 NP in contact with KNO_3 0.1 mol L^{-1} from pH=2 up to pH=4. Our results demonstrated that once the measurements are done directly at each pH, they remain stable (i.e. the free concentration in equilibrium does not change with elapsed time since preparation). There was a significant difference between AGNES measurements at each pH with the ones of NIST 46.7 (VMINTEQ) expectations assuming that the solubility was ruled by $In(OH)_3$. This is consistent with many literature reports where the less hydrated phase exhibits a lower solubility, e.g. according to NIST 46.7, log K_{sp} of $CaCO_3$ (Aragonite) is -8.336, while for $CaCO_3$.2 H_2O is -7.144. The same thing happens in the case of $CaHPO_4$ and $CaHPO_4.2H_2O$, for instance log K_{sp} of $CaHPO_4$ is -19.275 and for $CaHPO_4.2H_2O$ is -18.995. On the other hand, when the measurements were performed on the re-adjusted solution at pH=4, free indium concentration determined was mostly close to the predictions of VMINTEQ. Hence, we speculate that, when the alkalinity of the solution is high and it is readjusted from acidic pH, the free indium that is measured arises from its indium hydroxides equilibrium value. Additionally our results demonstrated that the percentage of dissolved In_2O_3 NPs in the solutions containing KNO_3 0.1 mol L^{-1} were very low (0.0012%- 28.7%). Moreover in dispersions that contained KNO_3 0.1 mol L^{-1} at pH 5 and in synthetic seawater solutions

at pH=8 no ASV peak of indium appeared, therefore we were not able to determine free concentrations of indium, this indicating an extremely low solubility in these media.

5.6. References

(1) Takeda, Y.; Kato, N.; Higuchi, K.; Takeichi, A.; Motohiro, T.; Fukumoto, S.; Sano, T.; Toyoda, T. Monolithically Series-Interconnected Transparent Modules of Dye-Sensitized Solar Cells. *Sol. Energy Mater. Sol. Cells* **2009**, *93* (6–7), 808–811.

(2) Chen, S. Y.; Wu, M. C.; Lee, C. S.; Lin, M. C. Synthesis of $In(OH)_3$ and In_2O_3nanomaterials Incorporating Au. *J. Mater. Sci.* **2009**, *44* (3), 794–798.

(3) Granqvist, C. G. Transparent Conductive Electrodes for Electrochromic Devices: A Review. *Appl. Phys. A Solids Surfaces* **1993**, *57* (1), 19–24.

(4) Wang, C.; Chen, D.; Jiao, X. Flower-like In_2O_3 Nanostructures Derived from Novel Precursor: Synthesis, Characterization, and Formation Mechanism. *J. Phys. Chem. C* **2009**, *113* (18), 7714–7718.

(5) Islam, M. A.; Nuruzzaman, M.; Roy, R. C.; Hossain, J.; Khan, K. A. Investigation of Electrical and Optical Transport Properties of N-Type Indium Oxide Thin Film. *Am. J. Eng. Res.* **2015**, *4* (7), 62–67.

(6) Siedl, N.; Gügel, P.; Diwald, O. Synthesis and Aggregation of In_2O_3 Nanoparticles: Impact of Process Parameters on Stoichiometry Changes and Optical Properties. *Langmuir* **2013**, *29* (20), 6077–6083.

(7) Bielz, T.; Lorenz, H.; Jochum, W.; Kaindl, R.; Klauser, F.; Klötzer, B.; Penner, S. Hydrogen on In_2O_3: Reducibility, Bonding, Defect Formation, and Reactivity. *J. Phys. Chem. C* **2010**, *114* (19), 9022–9029.

(8) Himmerlich, M.; Wang, C. Y.; Cimalla, V.; Ambacher, O.; Krischok, S. Surface Properties of Stoichiometric and Defect-Rich Indium Oxide Films Grown by MOCVD. *J. Appl. Phys.* **2012**, *111* (9).

(9) Naseem, S.; Iqbal, M.; Hussain, K. Optoelectrical and Structural Properties of Evaporated Indium Oxide Thin Films. *Sol. Energy Mater. Sol. Cells* **1993**, *31* (2), 155–162.

(10) Naseem, S.; Rauf, I. A.; Hussain, K.; Malik, N. A. Effects of Oxygen Partial Pressure on the Properties of Reactively Evaporated Thin Films of Indium Oxide. *Thin Solid Films* **1988**, *156* (1), 161–171.

(11) Askarinejad, A.; Iranpour, M.; Bahramifar, N.; Morsali, A. Synthesis and Characterisation of $In(OH)_3$ and In_2O_3 Nanoparticles by Sol-Gel and Solvothermal Methods. *J. Exp. Nanosci.* **2010**, *5* (4), 294–301.

(12) Acacia, N.; Barreca, F.; Barletta, E.; Spadaro, D.; Curr, G.; Neri, F. Laser Ablation Synthesis of Indium Oxide Nanoparticles in Water. *Appl. Surf. Sci.* **2010**, *256* (22), 6918–6922.

(13) Schlicker, L.; Riedel, R.; Gurlo, A. Indium Hydroxide to Bixbyite-Type Indium Oxide Transition Probed in Situ by Time Resolved Synchrotron Radiation. *Nanotechnology* **2009**, *20* (49), 495702.

(14) David, C. A.; Galceran, J.; Rey-Castro, C.; Puy, J.; Companys, E.; Salvador, J.; Monné, J.; Wallace, R.; Vakourov, A. Dissolution Kinetics and Solubility of ZnO Nanoparticles Followed by AGNES. *J. Phys. Chem. C* **2012**, *116* (21), 11758–11767.

(15) Kahru, A.; Dubourguier, H. C.; Blinova, I.; Ivask, A.; Kasemets, K. Biotests and Biosensors for Ecotoxicology of Metal Oxide Nanoparticles: A Minireview. *Sensors*. 2008, pp 5153–5170.

(16) Castronovo, F. P. J.; Wagner, H. N. J. Comparative Toxicity and Pharmacodynamics of Ionic Indium Chloride and Hydrated Indium Oxide. *J. Nucl. Med.* **1973**, *14* (9), 677–682.

(17) Andersen, J. C. Ø.; Cropp, A.; Paradise, D. C. Solubility of Indium-Tin Oxide in Simulated Lung and Gastric Fluids: Pathways for Human Intake. *Sci. Total Environ.* **2017**, *579*, 628–636.

(18) Ahamed, M.; Akhtar, M. J.; Khan, M. A. M.; Alhadlaq, H. A.; Aldalbahi, A. Nanocubes of Indium Oxide Induce Cytotoxicity and Apoptosis through Oxidative Stress in Human Lung Epithelial Cells. *Colloids Surfaces B Biointerfaces* **2017**, *156*, 157–164.

(19) Amiri, A. Comparative Toxicity and Distribution of $InCl_3$ and In_2O_3 Nanoparticles in Rats. *Toxin Rev.* **2016**, *35* (3–4), 116–120.

(20) Galceran, J.; Lao, M.; David, C.; Companys, E.; Rey-Castro, C.; Salvador, J.; Puy, J. The Impact of Electrodic Adsorption on Zn, Cd and Pb Speciation Measurements with AGNES. *J. Electroanal. Chem.* **2014**, *722–723*, 110–118.

(21) Mu, Q.; Calin A, D.; Galceran, J.; Rey-Castro, C.; Krzemiński, Ł.; Wallace, R.;

Bamiduro, F.; Milne, S.; Hondow, N.; Brydson, R.; et al. Systematic Investigation of the Physicochemical Factors That Contribute to the Toxicity of ZnO Nanoparticles. *Chem. Res. Toxicol.* **2014**, *27* (4), 558–567.

(22) Domingos, R. F.; Franco, C.; Pinheiro, J. P. Stability of Core/shell Quantum Dots-Role of pH and Small Organic Ligands. *Environ. Sci. Pollut. Res.* **2013**, *20* (7), 4872–4880.

(23) Vale, G.; Franco, C.; Diniz, M. S.; Dos Santos, M. M. C.; Domingos, R. F. Bioavailability of Cadmium and Biochemical Responses on the Freshwater Bivalve *Corbicula Fluminea*- the Role of TiO2 Nanoparticles. *Ecotoxicol. Environ. Saf.* **2014**, *109*, 161–168.

(24) Duval, J. F. L.; Farinha, J. P. S.; Pinheiro, J. P. Impact of Electrostatics on the Chemodynamics of Highly Charged Metal-Polymer Nanoparticle Complexes. *Langmuir* **2013**, *29* (45), 13821–13835.

(25) Rocha, L. S.; Companys, E.; Galceran, J.; Carapuça, H. M.; Pinheiro, J. P. Evaluation of Thin Mercury Film Rotating Disk Electrode to Perform Absence of Gradients and Nernstian Equilibrium Stripping (AGNES) Measurements. *Talanta* **2010**, *80* (5), 1881–1887.

(26) Vale, G.; Franco, C.; Brunnert, A. M.; Dos Santos, M. M. C. Adsorption of Cadmium on Titanium Dioxide Nanoparticles in Freshwater Conditions - a Chemodynamic Study. *Electroanalysis* **2015**, *27* (10), 2439–2447.

(27) Díaz-De-Alba, M.; Galindo-Riaño, M. D.; Pinheiro, J. P. Lead Electrochemical Speciation Analysis in Seawater Media by Using AGNES and SSCP Techniques. *Environ. Chem.* **2014**, *11* (2), 137–149.

Chapter 6: Conclusions

This work has been mainly focused on determining free concentration of indium in different media and lability degree of indium complexes such as In-Oxalate and In-Hydroxide using the techniques Absence of Gradients and Nernstian Equilibrium Stripping (AGNES) and Accumulation under Diffusion Limited Conditions (ADLC), respectively. Additionally it has focused on the speciation of indium-nitrilotriacetic acid (In-NTA) and indium-oxalate complexes in aquatic solutions. Finally, the dissolution of In_2O_3 nanoparticles (NPs) in background electrolyte from pH 2 to 5 and in synthetic seawater solutions at pH 8 has been studied. The main conclusions of this thesis are:

- For the first time the Absence of Gradients and Nernstian Equilibrium Stripping technique (AGNES) has been applied to determine free concentrations of a trivalent ion, indium.
- To avoid any complication from hydrolysis, pH 3 has been chosen. This pH corresponds to acid drainages, where high indium concentrations have been reported in previous investigations. At higher pH values, free indium concentration could be decreased not only due to possible precipitation, but also due to the formation of hydroxocomplexes of indium.
- As a result of using Cyclic Voltammetry (CV), it has been revealed that indium couple is behaving quasi-irreversibly.
- Differential pulse polarography (DPP) could not be used to accurately compute the deposition potential for a given gain in AGNES measurements, because of the quasi-irreversibility behavior of indium couple. However, an empirical relationship has been derived to use the peak potential of a DPP (with short drop time) as a guideline.
- Although the slight irreversibility of indium has some effects on DPP and CV signals, AGNES equilibrium is not impacted by such irreversibility, because the deposition stage is much longer than the time scale redox process of DPP and CV. In fact, this irreversibility could just delay the achievement of Nernstian equilibrium by the end of the first stage of AGNES, but one can make the t_1 longer until the analytical response is stabilized and equilibrium situation is reached.
- To overcome any potential irreversibility of the indium couple on the stripping stage of AGNES, the variant AGNES-Q has been used. In AGNES-Q, the faradaic charge is measured using a constant reoxidation potential (E_2) during a long stripping time (t_2) which causes all In^0 to be stripped out from the amalgam and, accordingly, prevents effects that could arise from any possible kinetics on the faradaic charge. Also, to avoid

any interferences from Pb, taking into account the standard redox potentials of In and Pb, E_2 was fixed to -0.450 V.

- A new calibration method has been designed to overcome the impact of the irreversibility of the indium couple on DPP. In this new calibration, a fixed η_Q (0.0034 C L mol^{-1}) has been used from independent information (i.e. estimated from the volume of the mercury drop). One can calibrate the gain by measuring the charge with AGNES for solutions with known indium concentrations, when applying the fixed potential called E_{calib}. From the slope of the plot Q vs [In^{3+}] and assuming the fixed value of η_Q, one can find the applied gain, called Y_{calib}. With the correspondence between E_{calib} and Y_{calib}, one can compute any gain from a given deposition potential or conversely, any deposition potential from a given gain.

- Trajectories (or charges at various deposition times) at different gains have collapsed into one curve when representing Q/Y *vs.* a normalized deposition time with stirring, $(t_1-t_w)/Y$. It has been concluded that, in case of indium, the needed time to reach equilibrium is slightly longer (by a factor 10/7=1.43) than the time that is needed for reversible metals such as Pb, Cd and Zn. Such an increase in the deposition times could be due to the slight irreversibility of indium couple and to the lower diffusion coefficient of indium.

- Speciation measurements of indium at pH=3 have been done successfully using AGNES in either In-NTA or In-Oxalate solutions. Values reported in NIST 46.7 are less accurate than those more recently published for both In-NTA and In-Oxalate complexes.

- It has been revealed that In-Oxalate complexes are very labile. For instance, for a free concentration of 3.71×10^{-4} μmol L^{-1} and a total In concentration 93.2 μmol L^{-1}, the lability of the complexes has reduced the deposition time (initially estimated in 3000000 s) to just 25 s.

- A new technique Accumulation under Diffusion Limited Conditions (ADLC) has been used successfully to determine the lability degree of In-Oxalate and In-Hydroxide complexes in precipitated solutions and, hence, it has helped to find a proper $t_{1,a}$ to be used for AGNES 2P measurements.

- The found lability degree of In-Oxalate is higher ($\xi_{oxalates} = 0.91$) than that of In-Hydroxides ($\xi_{hydroxide} = 0.60$). The results have shown that the helping factors of both In-Oxalate and In-Hydroxides complexes can reduce the needed deposition time to reach to the equilibrium when determining free concentrations of indium using AGNES. Our

results have demonstrated that adding oxalate to In-hydroxide precipitated solutions cause the complexes to contribute to the flux enabling a dramatic decrease in the needed deposition time. Also it has been revealed that the helping factor depends on the amount of added ligand.

- AGNES has been successfully applied to determine picomolar concentrations of free indium in precipitated solutions and results of AGNES have been in good agreement with the predictions of NIST 46.7 in the pH range from 4 to 6.
- AGNES has been used to determine free concentrations of indium in dissolution experiments (at various exposure times) of dispersions of In_2O_3 NPs that only contained KNO_3 0.1 mol L^{-1} from pH=2 to pH=4. AGNES measurements in solutions that only contained KNO_3 0.1 mol L^{-1} have been significantly lower than the predictions of NIST 46.7 assuming that the solubility was ruled by $In(OH)_3$.
- Free indium concentrations determined at each specific pH in dispersions of In_2O_3 NPs that only contained KNO_3 0.1 mol L^{-1} have remained stable for elapsed period of times up to 32 days. No ageing effect has been observed.
- Free indium concentrations in dispersions of In_2O_3 NPs that only contained KNO_3 0.1 mol L^{-1} determined at re-adjusted pH 4 have been close to the indium hydroxide equilibrium values.
- Very small percentages of the total 10 mg of In_2O_3 NPs are dissolved in a volume of 100 mL, from pH=2 to pH=4 in solutions that only contained KNO_3 0.1 mol L^{-1}.
- AGNES could not be used for dispersions that contained KNO_3 0.1 mol L^{-1} at pH=5 or in synthetic seawater solutions at pH=8, as no anodic stripping voltammetry (ASV) peak of indium has been observed.